PEOPLE'S DEMOCRATIC REPUBLIC OF ALGERIA

ALGERIAN MINISTER OF HIGHER EDUCATION AND SCIENTIFIC RESEARCH

DJILALI LIABES UNIVERSITY OF SIDI BEL ABBES (UDL-SBA)
FACULTY OF TECHNOLOGY - DEPARTMENT OF ELECTRONICS

Doctoral Thesis intitled

Electronic and optical properties of the $Al_xGa_{1-x}As_{1-y}N_y$ materials, applied for vertical cavity surface emitting lasers (VCSELs) and solar cells

Submitted to obtain the degree of

DOCTOR IN SCIENCES

Option of Optoelectronic Materials and Components

Approved by

Prof. Bensaad Zouaoui, professor at the University of Djillali Liabes, S.B.A : President.

Dr. Djellouli Bouaza "Maitre de conférence A", University of Moulay Tahar, Saida: Examinator.

Dr. Berrah Smail "Maitre de conférence A", University Mira Abderahmane, Bedjaia: Examinator.

Prof. Abid Hamza professor at the University of Djillali Liabes, S.B.A: Supervisor.

Prepared at the Applied Materials Laboratory (Research Center), and presented by

Boualem MERABET

November xxth, **2012**

Contents

مختصر

إن الهدف المرجو من هذا العمل هو دراسة الخصائص الالكترونية و الضوئية لرقائق المواد$Al_xGa_{1-x}As_{1-y}N_y$، مستعملة كآبار كمية مبثوثة على أسسGaAs، و مطبقة لليزر التجويف العمودي المرسل عبر السطح (VCSEL) و للخلايا الشمسية. الخصائص الهيكلية (الثابت البلوري، مقياس الانضغاطية)، الالكترونية (فارق الطاقة، وطبيعة هذا الفارق)، و الضوئية (قرينة الانكسار، الانعكاسية) المراد دراستها هي من اجل تصور تراكيب ضوء-الكترونية ذات مجالات أطوال موجة أوسع مثل LW-VCSELs، وتطبيقات للخلايا الشمسية ذات أعلى مردود . طريقة الحساب المعتمدة هي Full Potential - Linear Augmented Plane Wavesباستعمال البرنامج Wien2k المشتغل في وسط النظام المعلوماتي Inux. تقارن هذه الدراسة و تقابل بمختلف البحوث النظرية و التجريبية (المتواجدة) في مجال أمثلية وتصميم LW-VCSELs و الخلايا الشمسية .

Abstract:

The aim of my study is to investigate electronic and optical proprieties of the $Al_xGa_{1-x}As_{1-y}N_y$ thin layers utilized as quantum wells (QW) grown on GaAs substrates, applied for solar cells and vertical cavity surface emitting lasers (VCSELs), in order to design high efficiency solar cell and long wavelength optoelectronic device applications. The method of calculations adopted is "Full Potential – Linear Augmented Plane Waves", using the Wien2k code under Inux environment. This study will confront the available theoretical and experimental works in the optimization and design of solar cells and LW-VCSELs research areas.

Résumé:

L'objectif de ce travail est d'étudier les propriétés électroniques et optiques des matériaux $Al_xGa_{1-x}As_{1-y}N_y$, utilisés en couches minces comme puits quantiques épitaxiés sur substrat GaAs et appliqués aux lasers à cavité verticale émettant par la surface (VCSELs) et aux cellules solaires. Les propriétés structurales (constante de réseau, module de compressibilité), électroniques (gap d'énergie et nature de gap) et optiques (indice de réfraction, réflectivité) à étudier sont dans le but de concevoir des dispositifs optoélectroniques à larges étendues de longueur d'onde (LW-VCSELs) et les applications des cellules solaires de haut rendement. La méthode de calcul adoptée est la FP-LAPW (Full Potential-Linear Augmented Plane Waves), utlisant le code Wien2k sous environnement Inux. Cette étude se confrontera aux différents travaux théoriques et expérimentaux (disponibles) dans le domaine d'optimisation et de conception des LW-VCSELs et des cellules solaires.

Keywords /Mots clés: **الكلمات المفتاحية**

AlGaAs, Nitrides, GaAsN, AlGaAsN, FP-LAPW, Wien2k, LW-VCSELs, solar cells, energy gap, dielectric constants, refractive index.

Preface

This thesis is written for the beginning student and user of optoelectronics and Wien 2k code, respectively. My purpose is as follows:

To introduce the basic concepts of VCSELs and solar optoelectronics cells as optoelectronic devices.

To describe the modeling technique for the AlGaAsN materials used in fiber-optic telecommunications and photovoltaics.

To provide the informations required to have a design of the above devices.

The thesis is intended to serve as reference for beginners in the optoelectronics field research. It starts with an introduction of general concepts including VCSELs, spin polarized VCSELs, and photovoltaic cells, involves the dilute nitrides and magnetic semiconductors III-As(N, Mn) used in these devices, and then gives an overview of the theoretical tool used to model these materials.

The thesis should also be useful as a textbook for optoelectronics courses designed for junior undergraduate and first-year graduate students. The listing of recent research papers should be useful for researchers using this thesis as a reference. At the same time, students can benefit from it if they are assigned problems requiring reading of the original research papers.

Aknowledgements

In the Name of Allah, the Most Beneficient, the Most Merciful.

All praises are due to Allah, the sustainer of the entire world, the origin of science and wisdom, and may Allah's peace and blessings be upon our leader and prophet Mohammad, his family and companions.

Words would not be sufficient to express my gratitude to everyone who contributed in completion of this thesis. I am deeply indebted to my supervisor Pr. Hamza Abid, professor at Djillali Liabes University, for its persistent guidance and encouragement, throughout the course of this dissertation.

I also appreciate the guidance of Pr. Nadir Sekkal while offring different computering codes during initial stage of the research. Special thanks and Pr. Ali Zaoui and Pr. Ahmed Hireche for sharing related information, and their valuable insights.

Thanks are due to all colleague from the modeling and simulation in materials science laboratory members including, especially my friend Mostefa Djermouni for its precious help.

Furthermore, I wish to thank Pr. Bensaad Zouaoui, my committee chairperson, Dr. Djellouli Bouaza and Dr. Berrah Smail from Moulay Tahar University and Abderahmane Mira, University, respectively, for serving on my advisory committee.

I acknowledge the moral support provided to me from every one. Last but not the least, I am thankful to all my family members for their affection and support without which I would not have been here.

Dedication

I dedicate this thesis in honor of my mother-sister.

Introduction:

Optoelectronics is a wide research field studying matter, light and their interactions [1], based on quantum mechanics of electron-photon interaction, quantization of the electromagnetic field, semiconductor (SC) properties, quantum theory of heterostructures, and non-linear optics, and describing the physics, properties, and performances of devices such as: photodetectors, quantum well infrared photodetectors, optical parametric oscillators and waveguides, optical frequency converters, light emitting diodes (LEDs), and quantum-well (QW) lasers and intersubband quantum cascade lasers [2]. These devices have received great attention in recent years, as they are key components of the Internet and other optical communication systems [3].

SC lasers have important applications in optical-fiber communications, signal processing and medicine, including optical interconnects, CD ROM, gyroscopes, surgery, printers, photocopying [1], high-resolution spectroscopy, and atmospheric pollution monitoring [4]. In spite of these significant potential of applications, the edge emitting SC lasers have some inconveniences: they tend to be multimodal, generate noise due to small thermal fluctuations, and their laser emission is divergent making efficient coupling to optical fibers a significant technological challenge. These disadvantages can be side-stepped by using a vertical-cavity surface-emitting lasers (VCSELs) [1], exhibiting low threshold currents, single mode operation, high coupling efficiencies into optical fibers, and high speed modulation [5].

In modern SC electronics, effort has been made to use spin (in addition to charge) of electrons degrees of freedom for information processing. This research field so-called spintronics, using the electron spin rather than the charge to make smaller, faster, and more versatile devices than those based solely on electron charge, is promising for the design of a new generation of SC storage units and signal processing devices based on new principles of operation [6-12], and have common applications with optoelectronics as the spin-polarized VCSEL that promises a number of advantages over the conventional VCSEL [13].

On the other hand and partially motivated by the increase in oil prices worldwide as a result of geopolitical and economic factors in recent years, there has been a significant, resurgent interest in renewable energy sources, including wind, fuel cells, solar cells, geothermal, biofuels, etc. Solar energy conversion is perhaps the most appealing of all these solutions, since the energy source is readily available [14]. Photovoltaic cells (PV) have become very

attractive as a truly clean, renewable energy source, but the biggest obstacle of the crystalline silicon-based PV is the high SC manufacturing cost [15].

The lack of III–Vs with band gaps near 1 eV that are lattice matched to GaAs has hampered the development of VCSELs for use in long haul optical communications as well as the development of very high efficiency solar cells [16]. Moreover, the cost of III–Vs (such as InP) -based material is still too high to meet the demands for designing a high volume modern data communication networks, although they have been the source for long reach application [5]. Among the III–Vs, the III nitride (InN, AlN and GaN) SCs are potentially useful at high frequency, microwave and short-wave-length electroluminescent devices. They are used for the fabrication of high speed heterojunction transistors [17], low cost solar cells with high effciency [18], visible light emitting diodes (LEDs) [19, 20], laser diodes (LDs) [20-24] for the amber, green, blue and UV regions of the spectrum and also as the basis for high power, high temperature electronic devices [25, 26].

Contrary to the general trends in the conventional III–V SCs, research on epitaxially grown dilute III-As-N/GaAs alloys, where the smaller covalent radius and larger electronegativity of Nitrogen (N) cause a very strong bowing parameter in the band gap (E_g) of the III-V-N materials, has revealed important electronic properties with many advantages over InP-based systems that could prove decisive in the race to cover the desired wavelength range and to meet the challenge for low-cost devices to be operated over a significant temperature range with moderate power [5]. For example, The Ga(In)AsN/GaAs system has been developed as an attractive alternative to the conventional InGaAsP/InP system for the fabrication of emission devices for fiber-optical telecommunications at 1.3 μm [27]. Dilute nitrides, like $GaAs_{1-x}N_x$ and $In_xGa_{1-x}As_{1-y}N_y$ alloys, offering novel design opportunities for a widespread number of applications ranging from photovoltaics [28] to optoelectronic communications [29] and terahertz sources [30], and including hydrogen-assisted defect engineering [31], have been recently suggested as new materials for near infrared optoelectronics [32].

Until recently, it has been expected that $GaAs_{1-y}N_y$ might generate a recent flurry of research activity and provided opportunities to engineer material properties suitable for very high efficiency hybrid solar cells [33] as well as synthesizing VCSELs (for use in fiber optic communications, based on a single step growth process on GaAs substrates [34]), but the poor transport properties limit its potential for use in solar cell and laser devices because of abnormalities of its conduction band [26].

Among the III-As-N quaternary systems which have not studied as extensively as the other narrower band gap such as $In_xGa_{1-x}As_{1-y}N_y$ [35] are the dilute $Al_xGa_{1-x}As_{1-y}N_y$ alloys, in which it is possible to tune the gap over a wide range (from Eg_{GaAs}= 1.424 eV to Eg_{AlN}= 6.2 eV) by varying the compositions *x* and *y*. This makes these systems attractive for application in opto-electronic devices operating over a spectral range from the deep infrared to the far ultraviolet.

This thesis is organized as follows: In chapter I, we have tried to answer this question: Did III-V nitrides have any technological significance? Chapter II is devoted to the theoretical tool "FP- LAPW method" used in this work, which is explained and formulated. In chapter III, the dilute III-As-N alloys in long wave-length vertical cavity surface emitting lasers in solar cells are studied. Results and discussion of electronic and optical properties have been given in Chapter IV. Finally, conclusion of the whole present work is outlined.

References of the introduction

[1] Physics of optoelectronics, Michael A. Parker, Published in 2005 by CRC Press Taylor & Francis Group 6000 Broken Sound Parkway NW, Suite 300 Boca Raton, USA.
[2] Rosencher Cambridge2004.
[3] Joachim Piprek (Editor), Optoelectronic Devices Advanced Simulation and Analysis, Department of Electrical and Computer Engineering University of California Santa Barbara, CA 93106 USA, 2005 Springer.
[4] sze790
[5] Talwar Assessment pti54
[6] Wolf, S.A., Awschalom, D.D., Buhrman, R.A., Daughton, J.M., von Molnár, S., Roukes, M.L., Chtchelkanova, A.Y., and Treger, D.M., Spintronics:
A Spin-Based Electronics Vision for the Future, Science (Washington, D.C., 1883–), 2001, vol. 294, pp. 1488–1495.
[7] Semiconductor Spintronics and Quantum Computation, Awschalom, D.D., Loss, D., and Samarth, N., Eds., Berlin: Springer-Verlag, 2002.
[8] Ball, P., Meet the Spin Doctors, Nature (London), 2000, vol. 404, p. 918.
[9] Awschalom, D.D. and Kikkawa, J. M., Electron Spin and Optical Coherence in Semiconductors, Phys. Today, 1999, vol. 52, no. 6, pp. 33–38.

[10] Molnar, S. and Read, D., Magneto-Transport in Magnetic Compound Semiconductors and Metals, J. Magn. Magn. Mater., 2002, vols. 242–245, p. 13.
[11] Pearton, S.J., Abernathy, C.R., and Norton, D.P.,
Hebard, A.F., Park, Y.D., Boatner, L.A., and Budai, J.D., Advances in Wide Band Gap Materials for Semiconductor Spintronics, Mater. Sci. Eng., 2003, vol. 40, p. 137.
[12] Pearton, S.J., Abernathy, C.R., Overberg, M.E., Thaler, G.T., Norton, D.P., Theodorpoulou, N., Hebard, A.F., Park, Y.D., Ren, F., Kim, J., and Boatner, L.A., Wide Band Gap Ferromagnetic Semiconductors and Oxides, J. Appl. Phys., 2003, vol. 93, p. 1.
[13] Spin-polarized surface-emitting lasers, P. Bhattacharya, M. Holub, and D. Saha, phys. stat. sol. (c) 3, No. 12, 4396 – 4400 (2006).
[14] Loucas Tsakalakos, Nanostructures for photovoltaics, Materials Science and Engineering R 62 (2008) 175–189
[15] Gang Li, Vishal Shrotriya, Yan Yao, and Yang Yang, Investigation of annealing effects and film thickness dependence of polymer solar cells based on poly(3-hexylthiophene), Journal of Applied Physics **98**, 043704 (2005)
[16] A. Mascarenhas, Yong Zhang, Dilute nitride based III–V alloys for laser and solar cell applications, Current Opinion in Solid State and Materials Science 5 (2001) 253–259
[17] S. N. Mohammad and H. Morko»c, Prog. Quantum Electronic 20, 361 (1996).
[18] A. Yamamoto, M. Tsujino, M. Ohkubo and A. Hashimoto, Sol. Energy Mater. Sol. Cells. 35, 53 (1994).
[19] S. Nakamura and G. Fasol, The blue laser diodes (Springer,Berlin 1997).
[20] A. Dagar, J. Christen, T. Riemann, S. Richler, J. Blassing, A. Diez, A. Krost, A. Alam and M. Heuken, Appl.Phys.lett. 78, 2211 (2001).
[21] I. Vurgaftman, J. R. Meyer, and L. Ram-Mohan, J. Appl. Phys. 89, 5815 (2001). and references sited therein.
[22] Wide band gap semiconductors, proceeding of the Seventh Trieste Semiconductors Symposium, 1992, edited by C. G. Van de Walle (North Holland, Amsterdam 1993).
[23] J. F. Kaeding, Y. Wu, T. Fujii, R. Sharma, P. T. Fini, J. S. Speck, and S. Nakamura, J. Crystal Growth. 272, 257 (2004).
[24] T. Kawashima, A. Miyazaki, H. Kasugai, S. Mishima, A. Honshio, Y. Miyake, M. Iwaya, S. Kamiyama, H. Amano, and I. Akasaki, J. Crystal Growth. 272, 270 (2004).
[25] O. Aktas, Z. F. Fan, S. N. Mohammad, A. E. Botchkarev, H. Morkoc, Appl. Phys. Lett. 69, 3872 (1996).

[26] K. Wang, R. R. Recber, Appl. Phys. Lett. 79, 1602 (2001).
[27] M. Kondow, K. Uomi, A. Niwa, T. Kitatani, S. Watahiki, Y. Yazawa, K. Hosomi, T. Mozume, Solid State Electron. 41 (1997) 209.
[28] For a review see: I. A. Buyanova and W. M. Chen, Physics and Applications of Dilute Nitrides (Taylor & Francis Books Inc., New York, 2004); M. Henini, Dilute Nitride Semiconductors (Elsevier, Oxford, 2005).
[29] J. S. Harris Jr., Semicond. Sci. Technol. 17, 880 (2002). H. Riechert, A. Ramakrishnan, and G. Steinle, Semicond. Sci. Technol. 17, 892 (2002).
[30] A. Patane', A. Ignatov, D. Fowler, O. Makarovsky, L. Eaves, L. Geelhaar, and H. Riechert, Phys. Rev. B 72, 33312 (2005).
[31] M. Felici, A. Polimeni, G. Salviati, L. Lazzarini, N. Armani, F. Masia, M. Capizzi, F. Martelli, M. Lazzarino, G. Bais,M. Piccin, S. Rubini, and A. Franciosi, Adv. Mater. 18, 1993 (2006).
[32] M. Kondow, T. Kitatani, S. Nakatsuka, M. C. Larson, K. Nakahara, Y. Yazawa, M. Okai, and K. Uomi, IEEE J. Sel. Top. Quantum Electron. 3, 719 (1997).
[33] T Whitaker, Solar Cells, Comp Semicond (1998) 4 (8) 32-40.
[34] M Kondow, M Sato, H Ando, Red shift of photoluminescence and absorption in GaAsN alloy layers, Jpn J Appl Phys (1996) 31 L853-5.
[35] K. Yamamoto, M. Uchida, A. Yamamoto, A. Masuda, A . Hashimoto, Optical Properties of RF-MBE Grown AlGaAsN, Phys. Stat. Sol (b) **234** (2002) 915-918.

I.1.Introduction

The MOVPE of III-Nitrides became important in the early 90s when I. Akasaki and S. Nakamura first demonstrated Nitride based light emitting diodes (LEDs). Group Ill-Nitrides semiconductor materials, including GaN, InN, A1N, InGaN, AlGaN and AlInGaN, i.e. (Al, In, Ga)N, are excellent semiconductors, covering the spectral range from UV to visible and to infrared, with unique properties very suitable for modern electronic and optoelectronic applications. [1].

The group III nitrides are distinguished by their unusual chemical stability, a characteristic that has thrown up unique challenges for device processing. Indeed, the group III nitrides have high bond energies compared to conventional III–V semiconductors. The large bond strengths and wide bandgaps make them essentially chemically inert and highly resistant to bases or acids at room temperature. most of the processing of III nitrides is currently conducted by dry plasma etching [2].

This group III nitrides represent an important class of materials with applications in high temperature electronics, optoelectronic devices operating in the visible and UV region of the spectrum, and cold cathodes. Owing to their combination of wide band gap, high thermal conductivity, high thermal stability and physical robustness they offer, in principle, an attractive route to such devices. There are however severe practical difficulties in their preparation which have prevented the realisation of their potential until relatively recently [1].

The impossible growth of high quality epitaxial nitrides and their uncontrollable conductivity had prevented the development of nitride-based devices for many years [3]. In 1986, a dramatic improvement in the crystal quality of GaN was achieved. In 1989, by achieving the production of p-type conduction and the control of conductivity of n-type in nitrides and due to the high quality GaN, the world's first GaN p–n junction blue/UV LED has been invented [4]. The second half of the 1990s witnessed an explosive expansion of research on nitrogen-containing semiconductor (SCs) [5].

The nitrides exhibit a direct gap then a good radiative efficiency, their absorption coefficient is around 4.104 cm^{-1} for radiations of wavelenghts less than 360 nm. The high majority of optoelectronic devices operating at short wavelenghts concern mainly the nitrides [6].

I.2. "Conventional" nitrides

GaN, InN, AlN, and their alloys can crystallize in both wurtzite and zinc-blende forms. GaN is a wide gap SC that usually crystallize in the wurtzite lattice (Hexagonal or α-GaN), but under certain conditions zinc-blende GaN (Cubic or β-GaN) can be grown on a zinc-blende substrate. Due to their metastable nature, the growth of single-phase cubic nitride films of sufficient homogeneity and crystal quality is still difficult and, in general the crystal quality of the cubic III N layers grown so far is inferior to that of the hexagonal nitrides [7]. Unlike all of the non-nitride wide gap III-V SCs, GaN has a direct energy gap that makes it suitable for blue lasers and LEDs [8]. Under high pressure, GaN and other nitrides experience a phase transition to the rocksalt lattice srtucture [9]. AlN is the endpoint of AlGaN alloys, which is technologiquely important because it is a key ingredient in most nitrides quantum well. Experimental studies of AlN have focused almost excusively on the wurzite phase, the only significant AlN-containing III-V phase with a direct energy gap and having the largest gap [5]. Although InN is rerely used in devices in its binary form, when alloyed with GaN it form a core constituant of the blue diode laser [10]. Its recommanded zero temperature gap is of 0.78 eV [11].

The lattice matching between the constituents of a multilayer structure is an important parameter that determines the absence of stress at the interfaces, which create non-radiative recombination centers. Since GaAs is a direct bandgap SC that can be doped *n* and *p* easily and AlGaAs can be manufactured on a wide range of composition with GaAs presenting a very low lattice mismatch (~ 0.1%) for all values of *x,* the GaAs-GaAlAs system has so far been the most studied and widely used to produce laser diodes, and the relative values of gaps and indices of GaAs and GaAlAs create a good confinement of electrons and photons [6].

Unfortunately, the lack of III–V materials with band gaps near 1 eV that are lattice matched to GaAs has hampered the development of VCSELs for use in long haul optical communications [12] as well as the development of high efficiency solar cells [13].

Nitrides form a specific sub-group of the III-V compounds characterized by high ionicity, very short length of bonds, low compressibility, and high thermal conductivity, which make them interesting and very useful: e.g., the extremely hard cubic BN competes with diamond as an abrasive powder, the high thermal conductivity of AlN makes it an ideal substrate material for microelectronics, and GaN is considered as a promising material for short-wavelength electroluminescent devices [14]. One can ask the follow question: in what way is the physical

behavior of III-nitrides different from that of the conventional III-Vs? InN, the narrowest gap member of the nitride family having a gap of about 0,7 eV, [15] expands the range of the direct band gaps covered by the group III-nitride alloys into a near infrared region. AlN is mainly used as buffer layer in heteroepitaxies where it provides good nucleation growth, and in alloys where it provides an adjustment of the gap [6]. The mysterious AlN, GaN, and InN materials belonging to the group-III nitrides, and their alloys have attracted enormous interest for use in high-power microwave transistors, applications in light emitting diodes (LED's) and laser diodes (LD's) ranging from the visible spectrum [16-19] to the deep ultra-violet (UV) [20,21], and future chemical [22] sensors applications in quantum cryptography [23] or in photocatalysis [24]. Despite the intensive study of $In_xGa_{1-x}N$ and $Al_xGa_{1-x}N$, found to be useful as well layers and cladding layers in QW-LD structures, respectively [25–27], little attention has been paid to $Al_xIn_{1-x}N$, due to difficulty in its growth mainly caused by thermal instability resulting from the spinodal phase separation phenomenon [28]. Although this phase separation makes the determination of AlInN structural properties difficult during its epitaxial growth, the possibility of lattice matching to GaN makes it an attractive alternative to InGaN and AlGaN for applications in GaN-based devices, such as cladding layers, Bragg mirrors, insulating layers, or channel layers in field effect transistors [29–31] and active layer for LED's in the spectral region from UV to infrared (IR). $Al_{0.83}In_{0.17}N$/GaN heterostructures are very useful and interesting when utilized as cladding layers with no strain leading to defects on LD's structures [32]. On the contrary, InGaN layers grown on GaN template substrates have the disadvantage of lattice mismatch, leading (for high In-content) to high misfit dislocation densities limiting the range of In composition [33]. To solve this problem, a Boron cause decreasing the lattice parameter of nitrides [34] is added to reduce the lattice mismatch between InGaN epitaxial layers and GaN substrates [33]. The BInGaN alloy offers the possibility to optimize the energy gap and lattice parameter independently of each other without inducing strain into layers, which is highly desirable for the band gap engineering of advanced optoelectronic heterostructures [35]. Another alloy belonging to the B-containing III-nitrides (B-III-N) group is BAlGaN that grows on AlN substrates experimentally [36], has an energy gap ranging from 3.6 to 6.2 eV and corresponding to the 344–200 nm wavelength range, respectively with respect to its application in light-emitting devices operating in the UV spectral region. The AlGaN ternary alloy is widely used, especially in heterostructures, since it is virtually lattice matching with GaN. The InGaN alloys are nonetheless of strong

content of GaN, whose gap is located in the range green-blue-violet of the visible spectrum, and very useful for optoelectronic devices [6].

I.2.1. Nitrogen-containing III-V semiconductors

The second half of the 1990s witnessed an explosive expansion of research on nitrogen-containing semiconductors, which has continued unabated to the present. Conventional nitrides such as GaN, InN, AlN, and their alloys are systems that can crystallize in both wurtzite and zinc-blende lattice forms, and the corresponding band structures are quite distinct due to differences in the underlying symmetries. However, ‘‘dilute’’ nitrides are alloys, in which a small N fraction on the order of a few percent is added to a conventional III–V semiconductor such as GaAs, GaInAs, or GaP.

I.2.2.$B_yAl_xIn_{1-x-y}N$ alloys for optoelectronic devices.

As mensioned above, being the most mysterious materials among the group-III nitrides, AlN, GaN, and InN and their alloys have attracted enormous interest for use in high-power microwave transistors, applications in light emitting diodes (LED’s) and laser diodes (LD’s) ranging from the visible spectrum [37–40] to the deep ultra-violet (UV) [41,42] and future chemical [43] sensors applications in quantum cryptography [44] or in photocatalysis [45]. Despite the intensive study of $In_xGa_{1-x}N$ and $Al_xGa_{1-x}N$, found to be useful as well layers and cladding layers in QW-LD structures, respectively [46–48], little attention has been paid to $Al_xIn_{1-x}N$, due to difficulty in its growth mainly caused by thermal instability resulting from the spinodal phase separation phenomenon [49]. Although this phase separation makes the determination of AlInN structural properties difficult during its epitaxial growth, the possibility of lattice matching to GaN makes it an attractive alternative to InGaN and AlGaN for applications in GaN-based devices, such as cladding layers, Bragg mirrors, insulating layers, or channel layers in field effect transistors [50–52] and active layer for LED’s in the spectral region from UV to infrared (IR). $Al_{0.83}In_{0.17}N$/GaN heterostructures are very useful and interesting when utilized as cladding layers with no strain leading to defects on LD’s structures [53].

On the contrary, InGaN layers grown on GaN template substrates have the disadvantage of lattice mismatch, leading (for high In-content) to high misfit dislocation densities limiting the

range of Incomposition [54]. To solve this problem, a Boron cause decreasing the lattice parameter of nitrides [34] is added to reduce the lattice mismatch between InGaN epitaxial layers and GaN substrates [54]. The BInGaN alloy offers the possibility to optimize the energy gap and lattice parameter independently of each other without inducing strain into layers, which is highly desirable for the band gap engineering of advanced optoelectronic heterostructures [55]. Another alloy belonging to the B-containing III-nitrides (B-III-N) group is BAlGaN that grows on AlN substrates experimentally [56], has an energy gap ranging from 3.6 to 6.2 eV and corresponding to the 344–200 nm wavelength range, respectively with respect to its application in light-emitting devices operating in the UV spectral region.

Since the imaginary part of the dielectric function $\varepsilon_2(\omega)$ can be strongly related to the joint band structure, we have seen that it is useful to calculate the two parts of e for $B_yAl_xIn_{1-x-y}N$. The shift ΔEg is to amend the energy band gap of $B_yAl_xIn_{1-x-y}N$ alloys, and used in calculations of the optical properties, are calculated from the experimental energy gap values for the binaries BN, AlN and InN that correspond to 6.0, 5.94 and 1.66 eV, respectively, and the available theoretical values of the same compounds are 5.74, 6.27 and 1.66 eV, respectively [57].

Acquaintance of electronic band structures of $B_yAl_xIn_{1-x-y}N$ is crucial to correct energy band gaps that underestimated by LDA and improving characteristics of $B_yAl_xIn_{1-x-y}N$ light emitters.

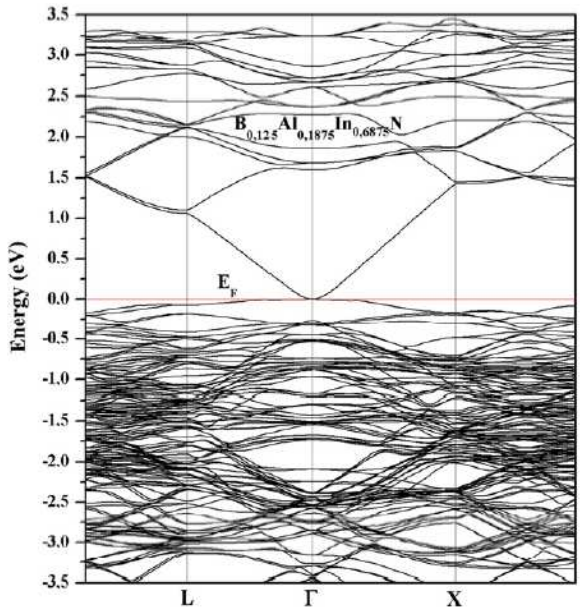

Fig. I.1 Band structure of $B_yAl_xIn_{1-x-y}N$ for $x = 0.187$ and $y = 0.125$.

One can easily remark the direct character of the gap of $B_{0.125}Al_{0.1875}In_{0.6875}N$, which is of great interest for optical transitions, as remarked previously for II–VI semiconductors alloys. Different methods are established as a flexible and valuable tool for studying the physical properties in a wide variety of materials, falls short of being a complete and general solution to many-electron problem. Imaginary part ε_2 indicates two inter-band transitions as shown in Fig. I.2; $B_yAl_xIn_{1-x-y}N$ is characterized by a strongest peak at 5.0 eV, might be strongly dependent on the ionic polarization of the $B_yAl_xIn_{1-x-y}N$ crystal due to the large electronegativity of N, and a weakest one for $B_yAl_xIn_{1-x-y}N$ at 5.71 eV.

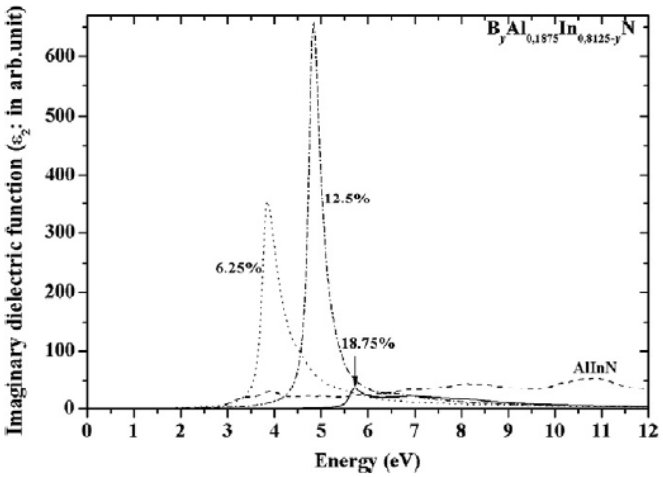

Fig.I.2 Imaginary part of the dielectric function of $B_yAl_xIn_{1-x-y}N$ alloys.

Fig. I.3(a) shows the reflectivity spectra along for $B_yAl_xIn_{1-x-y}N$ crystal due to the large electronegativity of N, and a weakest one for $B_yAl_xIn_{1-x-y}N$ at 5.71 eV. systems. It is interesting that there is an abrupt reduction in the reflectivity spectrum after 20 eV for the researched system confirming the occurrence of a collective plasmon resonance. The depth of the plasmon minimum is determined by the imaginary part of the dielectric function at the plasma resonance and is a representative of the overlap degree between the inter-band absorption regions.

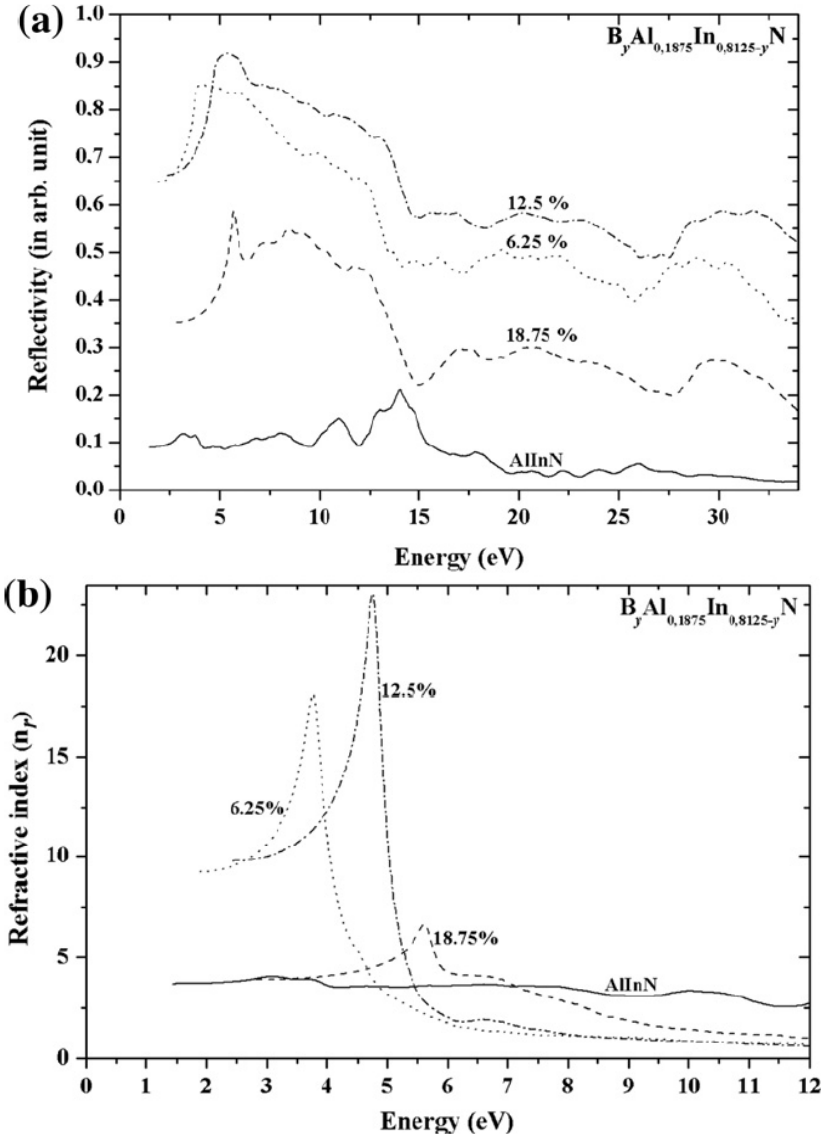

Fig.I.3 (a) Reflectivity and (b) refractive index of $B_yAl_xIn_{1-x-y}N$ alloys.

The calculated refractive index is shown in Fig. I.3(b). We note that at low energy these systems show high refractive indices, which decrease at higher energies.

The potential advantage of optoelectronic devices includes low sensitivity to temperature variations, low threshold current and high quantum efficiency (η). One of the key factors that determine η is the absorption coefficient α(ω), which is a strong function of the wavelength.

The calculated absorption coefficient α(ω) is shown in Fig. I.4(a). At low energies between 3.0 and 5.0 eV and at higher energies (at around 11.0 eV), this crystal shows a fast increasing absorption.

A strong increase in optical conductivity with increasing the photon energy has been observed for $B_yAl_xIn_{1-x-y}N$ alloys. Beyond the photon energy of 5.07 eV, the conductivity of

$B_{0.125}Al_{0.1875}In_{0.6875}N$ alloy dominates than of $B_{0.065}Al_{0.1875}In_{0.75}N$ alloy. The calculated optical conductivity dispersion σ(ω) for the investigated systems is shown in Fig. I.4(b). The peaks in the optical conductivity spectra are determined by the electric-dipole transitions between the occupied states to the unoccupied states.

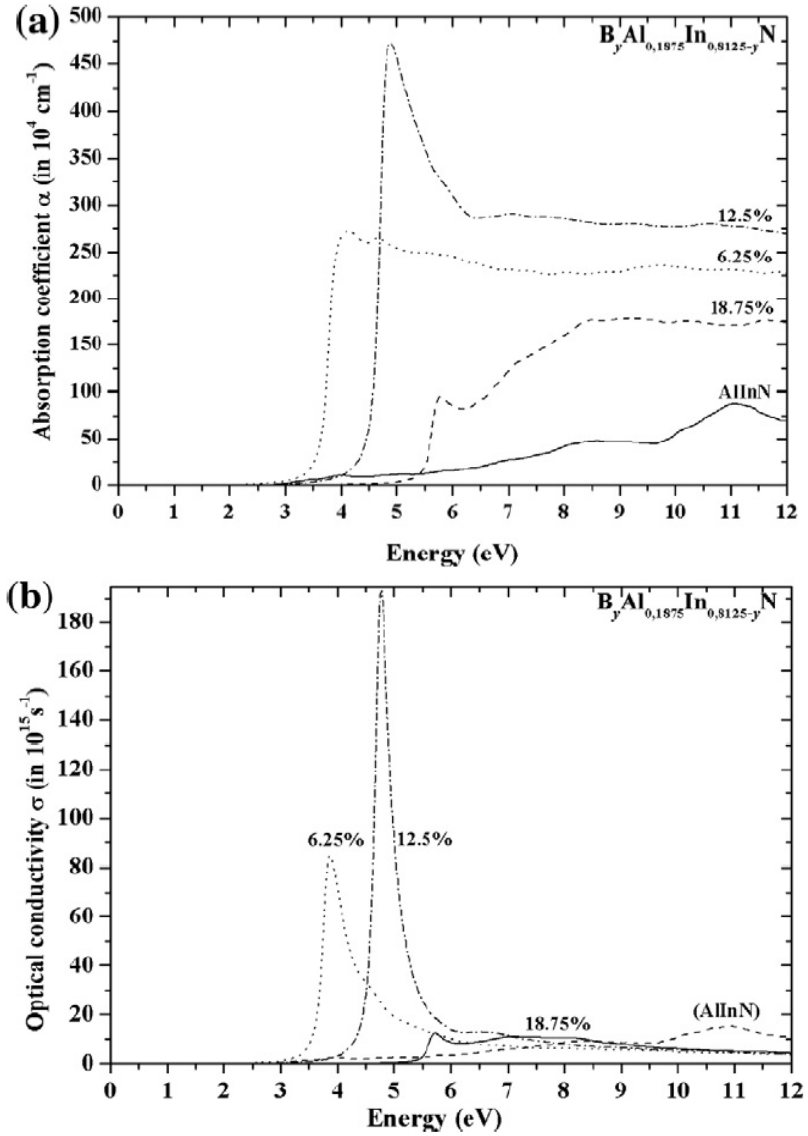

Fig.I.4 (a) Absorption and (b) conductivity of $B_yAl_xIn_{1-x-y}N$ alloys.

I.2.3. $B_yAl_xGa_{1-x-y}N$ matched to AlN substrate.

As mensioned above, the III-nitrides like GaN, AlN and related materials have attracted special attention with respect to their application in light emitting devices operating in the visible and deep ultraviolet spectral regions [58–63]. However, BN has features as high thermal conductivity, high hardness, high melting point and large bulk moduli suitable for

applications in electronics and optoelectronics devices [64,65]. In the group-III nitride heterostructures, which are important in the development of wide band gap devices [66], the problem of lattice mismatch between some epitaxial layers of III-N alloys and substrates can be solved by inducing Boron (B), as a constituent element, into the III-N systems and thus decreasing the lattice parameter of these alloys [34]. The BAlGaN quaternary system, derived from GaN, AlN and BN, is a promising material for a semiconductor laser that operates in the deep-ultraviolet spectral region [67]. Compact lasers and high sensitivity avalanche photodiode detectors in the ultraviolet range are needed for different applications such as biomedical, purification, covert communication and real-time detection of airborne pathogens[68]. BAlGaN, which can be lattice matched to AlN substrates[69], has band-gap energies in the range of 3.6 to 6.2 eV and corresponding wavelength emission ranging from 344 to 200 nm, when utilized as active layers in lasers [70]. Takano et al [71]. reported that B compositions in a $B_yAl_xGa_{1-x-y}N$/AlN quantum well vary in a range 1.5% to 13%, where the $B_yAl_xGa_{1-x-y}N$ layers can also be lattice matched to AlN. Although the III-nitrides have a stronger tendency to crystallize in the wurtzite (WZ) structure [72], research efforts toward a more complete understanding of the zinc-blende (ZB) nitride derived heterostructures have increased recently [73].

In order to estimate the effect of B incorporation into AlGaN, we have plotted in Figs. 5 the electronic band structure for $Al_xGa_{1-x}N$ and $B_yAl_xGa_{1-x-y}N$ with the compositional parameters x and (x, y) taken to be 0.0625 and (0.0625, 0.1875), respectively as representative examples. Both figures show that the ternary as well as the quaternary alloys have a direct gap and the substitution with Boron leads to an increase of the gap over a large range, which is of interest for optoelectronic devices [74].

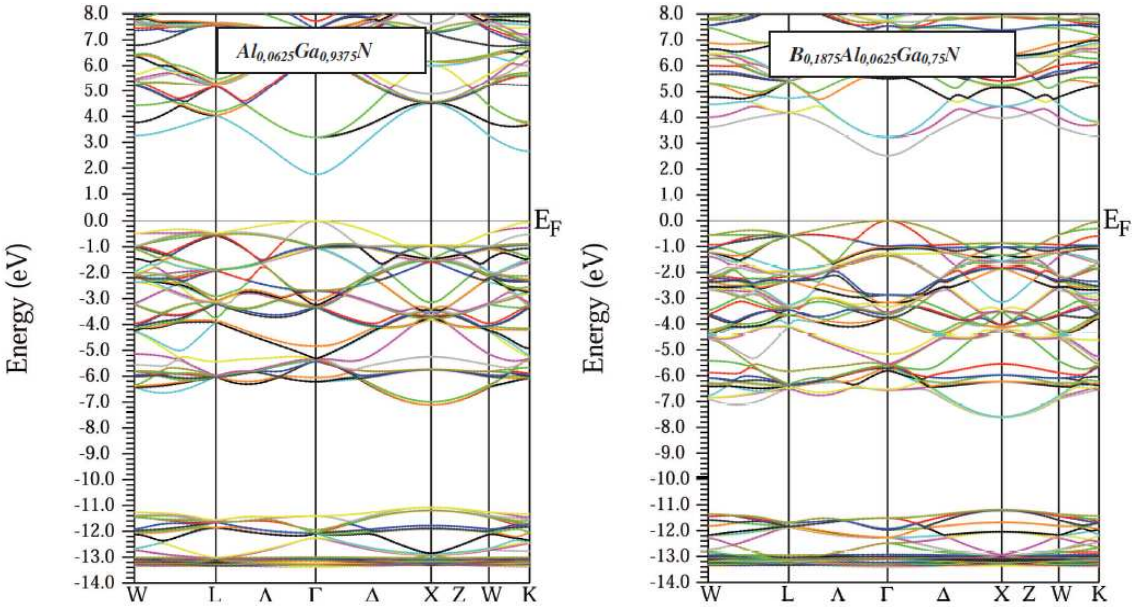

Fig.I.5 Band structures for $Al_{0.0625}Ga_{0.9375}N$ (Left), and $B_{0.1875}Al_{0.0625}Ga_{0.75}N$ (Right).

Moreover, while the III–V nitrides have a stronger tendency to crystallize in the hexagonal structure [75] h-GaN (α-III-N) and this can be obtained in habitual conditions of growth, the cubic structure c-GaN (β-III-N) of GaN, which is the prototype of the III-N materials [6], has many advantages over the hexagonal material (h-GaN), such as higher carrier mobility and ease of doping [76], although the (c-GaN) structure can be obtained in specific conditions of homoepitaxy on substrate (001) GaN or heteroepitaxy on substrate (111) GaAs [6]. The ternary and quaternary alloys of c-GaN and III–V compound SCs (e.g., $GaAs_{1-x}N_x$ and $In_xGa_{1-x}As_{1-y}N_y$) have attracted special interest because of their unique properties [77,78] and wide range of applications in optoelectronics and high-efficiency hybrid solar cells [79,80].

The wide bandgap SC GaN and related alloys (GaAlN, InAlN, InGaN, InGaAlN) exhibit many attractive properties far beyond Si and GaAs for high power and high frequency electronics as well as for visible and UV optoelectronic devices. One way to increase the flexibility of nitride alloys in term of structural, electrical and optical properties can be achieved by using boron [81]. The boron nitride (BN) has features of high thermal conductivity, hardness, melting point and large bulk moduli suitable for applications in electronics and optoelectronics devices [82, 83], so that by inducing Boron into the III-N systems, the lattice parameter decreases, and the problem of lattice mismatch between some epitaxial layers of III-N alloys and substrates can be solved [84].

Thus, the band gaps of these alloys may be well described through the quadratic relationship between the band gaps E_{gA} and E_{gB} of the endpoint compounds A and B and is given by [85]

$$E_{gAB}(x) = xE_{gA} + (1 - x)E_{gB} - bx(1 - x). \quad \text{(I.1)}$$

where, x is the fraction of compound B mixed in compound A, and b is the bowing parameter, which represents the divergence of the band gap energy from the linear interpolation. Alloys of mixed cation species, such as $Al_xGa_{1-x}As$, typically fit this trend quite well, as do alloys containing anion species of similar character, including $GaAs_xP_{1-x}$ [86]. For these materials, the atomic potentials of the two elements occupying either the cation or anion sublattice are substantially similar, and the bowing parameter in (I.1) is much smaller than the band gaps of the endpoint compounds. With advances in thin film growth techniques, it is now possible to fabricate single-phase alloys from constituents that are highly "mismatched" with respect to electronegativity, size, and/or ionization energy. The VCA approach to modeling the band gaps of these alloys is not applicable due to the localized nature of the impurity, and a single bowing parameter can no longer adequately describe the trend in the band gap.

Considering the linear interpolation and the band gap bowing of GaNAs and AlGaAs, the energy band gap, for example, of $Al_{1-x}Ga_xAs_yN_{1-y}$ is expressed as [87]

$$Eg_{AlGaAsN}(x,y) = xyEg_{GaAs} + x(1 - y)Eg_{GaN} + y(1 - x)Eg_{AlAs} + (1 - x)(1 - y)Eg_{AlN} + xy(1-y)b_{GaAsN} + xy(1-x)b_{AlGaAs} \quad \text{(I.2)}$$

where x and y denote the compositions of Ga and As in the AlGaAsN alloy, respectively and b_{GaAsN} and b_{AlGaAs} are the bowing parameters of GaNAs and AlGaAs, which have values of −20 eV [88] and −0.25 eV [89], respectively.

I.3. Dilute nitrides

The simple quadratic form applied to calculate the bowing and discussed above is not recommended to describe the "dilute" nitride alloys, in which a small N fraction on the order of a few percent is added to a conventional non-nitride III-V SC such as GaAs or GaInAs. If the effect on the valence bands is completely neglected, the model below is more used [5].

Due to large differences in the lattice constant and ionicity between the host binary and N-related binary, the dilute nitrides exhibit many unusual and fascinating physical properties. Among them the most prominent feature is the giant bowing in the band-gap energy [7].

Dilute nitrides are considered as highly mismatched semiconductor alloys of great technological importance for their applications in telecommunication devices and photovoltaic solar cells [1].

Dilute ternary and quaternary III–As–N alloys have received a great deal of attention both from a fundamental point of view as well as for applications in technology (e.g., photodetectors, modulators, amplifiers, and long wavelength vertical cavity surface-emitting lasers (LW-VCSELs), etc.) [90]. Dilute nitrides can be derived from the conventional III–V semiconductors (viz., GaAs) by the insertion of N into the group V sublattice – causing profound effects on the electronic properties of the resulting alloys [91]. Contrary to the general trends in the conventional alloy semiconductors where a smaller lattice constant generally increases the band gap, the smaller covalent radius and larger electronegativity of N cause a very strong bowing parameter in III–V–N compounds. Consequently, the addition of N to GaAs or GaInAs decreases the band gap (Eg) dramatically. This strong dependence of Eg on the N content in III–As–N has provided opportunities to engineer material properties suitable for the fibre-optical communications at 1.3 and 1.55μm wavelengths as well as high efficiency hybrid solar cells [92]

I.4 .The Band Anticrossing Model

Alloying offers the ability to tailor the band gap as well as the conduction and valence band edge positions of a semiconductor through the manipulation of its composition, enabling the use of these materials in a wide variety of applications, including power transistors, lasers, light emitting diodes, photodetectors, and solar cells. It is well known that alloys composed of two compounds of similar character can be treated within the virtual crystal approximation (VCA), where the potential of the periodic crystal is taken as an average of the atomic potentials of the constituents [93]. The dilute III–N–V alloys fall into this category of moderately or highly mismatched alloys [94].

Instead, a more advanced theory is required to calculate the electronic structure of these alloys in order to explain the composition dependence of the band gap as well as other optical and transport properties that cannot be accounted for by a simple bowing parameter.

Let us first consider the GaAsN system: alloying GaAs with N leads to giant bowing of the band gap energy – unlike to the AlGaAs conventional alloys, where band gap energy changes almost linearly according to the virtual crystal approximation model. Contrary to the general trends in the conventional alloy semiconductors where a smaller lattice constant generally increases the band gap, the smaller covalent radius and larger electronegativity of N cause a

very strong bowing parameter in III–V–N compounds. Consequently, the addition of N to GaAs %decreases the band gap (Eg) dramatically [95].

The band gap of GaAsN decreases approximately by 150 meV per 1% nitrogen concentration increase [96], which is confirmed by photoluminescence and infra-red absorption measurements [97], leads to a strong band gap bowing attibuted to the repulsive interaction between the localized states of N and the delocalized states of the host semiconductor [98], caused by significant difference between As and N in ionic radii (0.75 Å for As and 1.2 Å for N), electronegativity (Pauling's: χ_N= 3.0 and χ_{As}= 2.0), seize (atomic radii: 0.92Å for N and 1.39 Å for As) and bonds (the Ga-N bond is more than twice as stiff as the Ga-As bond) [99].

In this section, we intend to detail the band anticrossing theory, which was developed to explain the anomalous characteristics observed in dilute nitrides and similar alloys, and highlight some of the major experimental findings achieved to date. A number of theoretical approaches have been applied to explain the optical bowing in dilute nitride alloys. First-principles local density approximation (LDA) calculations, carried out by Wei and Zunger, utilized a composition dependent bowing parameter to explain the large band gap reduction in $GaAs_{1-x}N_x$ [100]. Due to band gap errors introduced in the LDA method, this model was replaced by empirical pseudopotential calculations that increasingly focus on the interactions of N-clusters [101]. Alternatively, a band anticrossing (BAC) model has been proposed to explain the properties of III–V dilute nitrides as well as other mismatched alloys. The BAC model describes the electronic structure of highly mismatched alloys by considering the interaction between the delocalized states of the host semiconductor and the localized states of the impurity. The large changes in the electronic structure in dilute III–V nitrides and other semiconductor alloys containing isoelectronic impurities of high electronegativity or low ionization energy can be explained by the band anticrossing model [95].

The physical property peculiar to the $GaAs_{1-x}N_x$ and $In_yGa_{1-y}As_{1-x}N_x$ alloys, which have been recently suggested as new materials for near infrared optoelectronics [100], is the giant bowing of the band-gap energy as a function of nitrogen concentration. Incorporation of small amount (typically less than a few %) of nitrogen into GaAs, which produces a dilute $GaAs_{1-x}N_x$ alloy, strongly reduces the band-gap energy covering from ~1.0 eV to ~1.4 eV [101-103]. This behaviour is markedly different from conventional semiconductor alloys. The unusual property of $GaAs_{1-x}N_x$ has been solved by a band-anticrossing (BAC) model [104, 105]; namely, the extended conduction band state and localized nitrogen resonant state interact with

each other, which results in the formation of E_- and E_+ states owing to the anticrossing between the two states. Note that the BAC model predicts the splitting of the conduction band into the E_- and E_+ subbands and a nonparabolic electron dispersion relation for the E_- band, which corresponds to the fundamental band edge. The BAC theory has been successfully applied to explain the optical and electronic properties of a wide variety of III–V and II–VI highly mismatched alloys, including dilute III–V nitrides, with highly electronegative impurities. An anticrossing interaction with a nearby localized level introduced by the highly electronegative impurity species restructures the conduction band of a host semiconductor, resulting in a split conduction band and a reduced fundamental band gap.

According to the BAC model, the interaction of highly localized N states with the extended states of the SC matrix leading to the formation of the two subbands E_- and E_+ (Fig.I.6) is given by the dispersion relations [106]

$$E_{\pm}(k) = \frac{1}{2}\left\{ \left[E_M(k) + E_N \right] \pm \sqrt{\left[E_M(k) - E_N \right]^2 + 4V^2{}_{NM}} \right\} \tag{I.3}$$

where E_N is the energy of the N state , $E_M(k)$ is the dispersion relation for the conduction band of the N-free SC matrix (AlGaAs), and V_{MN} is the matrix element coupling those two types of states.

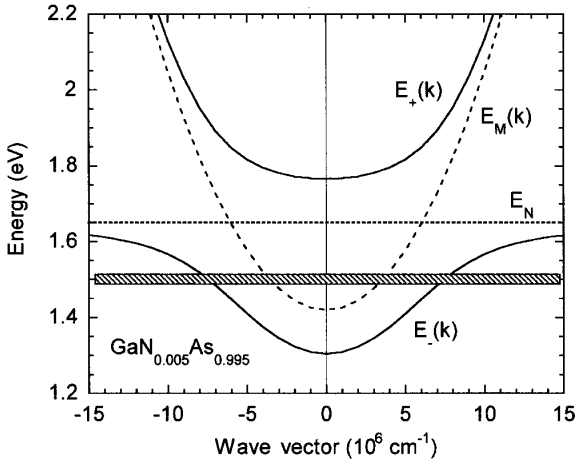

Fig.I.6 The band structure of a $GaN_{0.005}As_{0.995}$ alloy calculated using the band anticrossing model showing the splitting of the conduction band into two nonparabolic subbands $E_1(k)$ and $E_2(k)$. The dashed and dotted lines represent the unperturbed conduction band of the host semiconductor matrix $E_M(k)$ and the dispersionless, highly localized E_N level. The shaded area represents the approximate maximum energy location of the Fermi energy, $E_{F\max}$. Ref.[K. M. Yu, W. Walukiewicz, W. Shan, J. W. Ager III, J. Wu, and E. E. Haller, J. F. Geisz, D. J. Friedman, and J. M. Olson, Nitrogen-induced increase of the maximum electron concentration in group III-N-V alloys, Physical Review B Volume 61, Number 20 15 May 2000-II].

A large increase of the effective mass in both subbands compared to GaAs is mentioned and the inverse density of states effective mass is defined as [107]

$$\frac{1}{m_{\pm}^{*}(k)}=\frac{1}{2m_{M}(k)}\left\{1\pm\frac{\left[E_{M}(k)-E_{N}\right]}{\sqrt{\left[E_{M}(k)-E_{N}\right]^{2}+4V^{2}{}_{NM}}}\right\} \quad \text{(I.4)}$$

From a certain percentage of nitrogen, the band gap is splitted into two sub-bands, such that the higher the concentration of nitrogen increases the more important the break-up becomes. Based on this BAC model, the shifting down energy gap is given by [108]

$$\Delta E_{g}=\frac{\left[\sqrt{\left[E_{N}-E_{M}\right]^{2}+4V_{NM}^{2}}-\left[E_{N}-E_{M}\right]\right]}{2} \quad \text{(I.5)}$$

Here, the gap E_{-} , which is responsible for the reduction in the fundamental band gap [109], for $Al_xGa_{1-x}As_{1-y}N_y$ alloys can be given by [110]

$$E_{-\left(Al_{x}GaAsN_{y}\right)}=\frac{1}{2}\left[E_{gAl_{x}Ga_{1-x}As}+E_{N}-\sqrt{\left[E_{gAl_{x}Ga_{1-x}As}-E_{N}\right]^{2}+4V_{MN}(y)}\right] \quad \text{(I.6)}$$

where $V_{MN}=C^{2}{}_{MN}.y$ and C_{MN} depending on the electronegativity difference between N and the group V of the host matrix does not depend on the Al fraction in AlGaAsN and equals to 2.7eV [107].

References of Chap. I

[1] III-Nitride Semiconductor Materials, Zhe Chuan Feng *National Taiwan University, Taiwan, Published by* Imperial College Press, 2006.

[2] Hadis Morkoc¸ Handbook of Nitride Semiconductors and Devices "Vol. 2: Electronic and Optical Processes in Nitrides", 2008 WILEY-VCH Verlag GmbH & Co. KGaA, Weinheim

[3] I. Akasaki, H. Amano, Jpn. J. Appl. Phys. 36 (1997) 5393.

[4] Isamu Akasaki, Key inventions in the history of nitride-based blue LED and LD, Journal of Crystal Growth 300 (2007) 2–10

[5] I. Vurgaftman and J. R. Meyer, Band parameters for nitrogen-containing semiconductors, Journal of Applied Physics, **94**, Number 6 15 September 2003.

[6] Henry Mathieu, Hervé Fanet, Physique des semiconducteurs et des composants électroniques Cours et exercices corrigés, 6e édition (2009), Dunod Paris.

[7] S. Adachi, Properties of Semiconductor Alloys: Group-IV, III-V and II-VI Semiconductors, Edition first published 2009, John Wiley & Sons Ltd, New York, 2009.

[8] I. Vurgaftman J. R. Meyer, and L. R. Ram-Mohan, Band parameters for III–V compound semiconductors and their alloys, Journal of Applied Physics Volume 89, Number 11 1 June 2001
[9] P. E. Van Camp, V. E. Van Doren, and J. T. Devreese, Phys. Rev. B **44**, 9056 (1991)
[10] The Blue Laser Diode, edited by S. Nakamura and G. Fasol (Springer, Berlin, 1997).
[11] J. Wu, W. W. Walukiewicz, K. M. Yu, J. W. Ager, III, E. E. Haller, H. Lu, W. J. Schaff, Y. Saito, and Y. Nanishi, Appl. Phys. Lett. **80**, 3967 (2002).
[12] Giboney KS, Aronson LB, Lemoff BE. The ideal light source for datanets. IEEE Spectrum 1998;35(2):43–53.
[13] Whitaker T. Solar cells. Comp Semicond 1998;4(8):32–40.
[14] I. Gorczyca and N.E. Christensen, Band structure and high-pressure phase transition in GaN, AlN, InN and BN, Physica B 185 (1993) 410-414.
[15] V. Yu. Davydov, A.A. Klochikhin, R.P. Seisyan, V.V. Emtsev, S.V. Ivanov, F. Bechstedt, J. Furthmuller, H. Harima, A.V. Mudryi, J. Aderhold, O. Semchinova, J. Graul, Phys. Stat. Solidi (b) 229 (2002) R1. ; J. Wu, W. Walukiewicz, K.M. Yu, J.W. Ager III, E.E. Haller, H. Lu, W.J. Scha, Y. Saito, Y. Nanishi, Appl. Phys. Lett. 80 (2002) 3967.
[16] S. Nakamura, T. Mukai, M. Senoh, Jpn. J. Appl. Phys. 30 (1991) L1998.
[17] S. Nakamura, Science 281 (1998) 956.
[18] S. Nakamura, M. Senoh, S. Nagahama, N. Iwasa, T. Yamada, T. Matsushita, Y. Sugimoto, H. Kiyoku, Appl. Phys. Lett. 69 (1996) 4056.
[19] S. Nakamura, M. Senoh, S. Nagahama, N. Iwasa, T. Yamada, T. Matsushita, H. Kiyoku, Y. Sugimoto, Jpn. J. Appl. Phys. 35(1996) L74.]
[20] Y. Taniyasu, M. Kasu, T. Makimoto, Nature 441 (2006) 325.
[21] V. Adivarahan, W.H. Sun, A. Chitnis, M. Shatalov, S. Wu, H.P. Maruska, M.A. Khan, Appl. Phys. Lett. 85 (2004) 2175.
[22] B.S. Kang, F. Ren, B.P. Gila, C.R. Abernathy, S.J. Pearton, Appl. Phys. Lett. 84 (2004) 1123.
[23] S. Kako, C. Santori, K. Hoshino, S. Götzinger, Y. Yamamoto, Y. Arakawa, Nat. Mater. 5 (2006) 887.
[24] H.S. Jung, Y.J. Hong, Y. Li, J. Cho, Y. Kim, G. Yi, ACS Nano 2 (2008) 637.
[25] I. Akasaki, S. Sota, H. Sakai, T. Tanaka, M. Koike, H. Amano, Electron. Lett. 32 (1996) 1105.
[26] S. Nakamura, M. Senoh, S.I. Nagahama, N. Iwasa, T. Yamada, T. Matsushita, Y. Sugimoto, H. Kiyoku, Jpn. J. Appl. Phys. 36 (1997) L1059.
[27] N. Yamada, Y. Kaneko, S. Watanabe, Y. Yamaoka, T. Hidaka, S. Nakagawa, E. Marenger, T. Takeuchi, S. Yamaguchi, H. Amano, I. Akasaki, Proceedings of the 10th IEEE Lasers and Electro-Optics Society Annual Meeting, San Francisco, CA, Nov. 10–13 (1997) PD1.2.
[28] T. Matsuoka, Appl. Phys. Lett. 71 (1997) 105.

[29] J.F. Carlin, C. Zellweger, J. Dorsaz, S. Nicolay, G. Christmann, E. Feltin, R. Butte, N. Grandjean, Phys. Stat. Sol. (b) 242 (2005) 2326.
[30] A. Dadgar, F. Schulze, J. Blasing, A. Diez, A. Krost, M. Neuburger, E. Kohn, I. Daumiller, M. Kunze, Appl. Phys. Lett. 85 (2004) 5400.
[31] I.M. Watson, C. Liu, E. Gu, M.D. Dawson, P.R. Edwards, R.W. Martin, Appl. Phys. Lett. 87 (2005) 151901.
[32] S. Yamaguchi, M. Kariya, S. Nitta, H. Kato, T. Takeuchi, C. Wetzel, H. Amano, I. Akasaki, J. Cryst. Growth 195 (1998) 309.
410 Y. Al-Douri et al. / Superlattices and Microstructures 51 (2012) 404–411
[33] S. Gautier, G. Orsal, T. Moudakir, N. Maloufi, F. Jomard, M. Alnot, Z. Djebbour, A.A. Sirenko, M. Abid, K. Pantzas, I.T. Ferguson, P.L. Voss, A. Ougazzadenm, J. Cryst. Growth 312 (2010) 641.
[34] V.A. Elyukhin, Phys. Stat. Sol. (c) 2 (2005) 3556.
[35] T. Kimura, T. Matsuoka, Jpn. J. Appl. Phys. 46 (2007) L574.
[36] T. Takano, M. Kurimoto, J. Yamamoto, H. Kawanishi, J. Crys. Growth 237–239 (2002) 972.
[37] S. Nakamura, T. Mukai, M. Senoh, Jpn. J. Appl. Phys. 30 (1991) L1998.
[38] S. Nakamura, Science 281 (1998) 956.
[39] S. Nakamura, M. Senoh, S. Nagahama, N. Iwasa, T. Yamada, T. Matsushita, Y. Sugimoto, H. Kiyoku, Appl. Phys. Lett. 69 (1996)
4056.
[40] S. Nakamura, M. Senoh, S. Nagahama, N. Iwasa, T. Yamada, T. Matsushita, H. Kiyoku, Y. Sugimoto, Jpn. J. Appl. Phys. 35
(1996) L74.
[41] Y. Taniyasu, M. Kasu, T. Makimoto, Nature 441 (2006) 325.
[42] V. Adivarahan, W.H. Sun, A. Chitnis, M. Shatalov, S. Wu, H.P. Maruska, M.A. Khan, Appl. Phys. Lett. 85 (2004) 2175.
[43] B.S. Kang, F. Ren, B.P. Gila, C.R. Abernathy, S.J. Pearton, Appl. Phys. Lett. 84 (2004) 1123.
[44] S. Kako, C. Santori, K. Hoshino, S. Götzinger, Y. Yamamoto, Y. Arakawa, Nat. Mater. 5 (2006) 887.
[45] H.S. Jung, Y.J. Hong, Y. Li, J. Cho, Y. Kim, G. Yi, ACS Nano 2 (2008) 637.
[46] I. Akasaki, S. Sota, H. Sakai, T. Tanaka, M. Koike, H. Amano, Electron. Lett. 32 (1996) 1105.
[47] S. Nakamura, M. Senoh, S.I. Nagahama, N. Iwasa, T. Yamada, T. Matsushita, Y. Sugimoto, H. Kiyoku, Jpn. J. Appl. Phys. 36
(1997) L1059.

[48] N. Yamada, Y. Kaneko, S. Watanabe, Y. Yamaoka, T. Hidaka, S. Nakagawa, E. Marenger, T. Takeuchi, S. Yamaguchi, H. Amano, I. Akasaki, Proceedings of the 10th IEEE Lasers and Electro-Optics Society Annual Meeting, San Francisco, CA, Nov. 10–13 (1997)
PD1.2.

[49] T. Matsuoka, Appl. Phys. Lett. 71 (1997) 105.

[50] J.F. Carlin, C. Zellweger, J. Dorsaz, S. Nicolay, G. Christmann, E. Feltin, R. Butte, N. Grandjean, Phys. Stat. Sol. (b) 242 (2005) 2326.

[51] A. Dadgar, F. Schulze, J. Blasing, A. Diez, A. Krost, M. Neuburger, E. Kohn, I. Daumiller, M. Kunze, Appl. Phys. Lett. 85 (2004) 5400.

[52] I.M. Watson, C. Liu, E. Gu, M.D. Dawson, P.R. Edwards, R.W. Martin, Appl. Phys. Lett. 87 (2005) 151901.

[53] S. Yamaguchi, M. Kariya, S. Nitta, H. Kato, T. Takeuchi, C. Wetzel, H. Amano, I. Akasaki, J. Cryst. Growth 195 (1998) 309.

[54] S. Gautier, G. Orsal, T. Moudakir, N. Maloufi, F. Jomard, M. Alnot, Z. Djebbour, A.A. Sirenko, M. Abid, K. Pantzas, I.T. Ferguson, P.L. Voss, A. Ougazzadenm, J. Cryst. Growth 312 (2010) 641.

[55] T. Kimura, T. Matsuoka, Jpn. J. Appl. Phys. 46 (2007) L574.

[56] T. Takano, M. Kurimoto, J. Yamamoto, H. Kawanishi, J. Crys. Growth 237–239 (2002) 972.

[57] Al-Douri, B. **Merabet**, H. Abid, R. Khenata, First-principles calculations to investigate optical properties of $B_yAl_xIn_{1-x-y}N$ alloys for optoelectronic devices, Superlattices and Microstructures 51 (2012) 404–411.

[58] S. Strite and H. Morkoc¸, *J. Vac. Sci. Technol. B* 10 (1992) 1237.

[59] C. G. Van de Walle, *Physica B* 185 (1993) ix–x.

[60] H. Morkoc¸, S. Strite, G. B. Gao, M. E. Lin, B. Sverdlov and M. Burns, *J. Appl. Phys.* 76 (1994) 1363.

[61] F. A. Ponce and D. P. Bour, *Nature* 386 (1997) 351.

[62] S. Nakamura, *Solid State Commun.* 102 (1997) 237.

[63] J. Chen, Z. H. Levine and J. W. Wilkins, *Appl. Phys. Lett.* 66 (1995) 1129.

[64] T. Takayama, M. Yuri, K. Itoh, T. Baba and J. S. Harris Jr., *J. Cryst. Growth* 222 (1–2) (2001) 29.

[65] H. Wang, H. Xu, X. Wang and C. Jiang, *Phys. Lett. A* 373 (2009) 2082.

[66] S. Nakamura, *The Blue Laser Diode-GaN Based Light Emitters and Lasers* (Springer, Berlin, 1977).

[67] T. Takano, M. Kurimoto, J. Yamamoto and H. Kawanishi, *J. Cryst. Growth* 237/239 (2002) 972.

[68] A. Ougazzaden, S. Gautier, C. Sartel, N. Maloufı, J. Martin and F. Jomard, *J. Cryst. Growth* 298 (2007) 316.

[69] M. Haruyama, T. Shirai, H. Kawanishi and Y. Suematsu, *Proc. Int. Symposium on Blue Laser and Light Emitting Diodes*, 1996, pp. 106.

[70] M. Tsubamoto, T. Honda, J. Yamamoto, M. Kurimoto, M. Shibata, M. Haruyama and H. Kawanishi, *Proc. 2nd Int. Conf. Nitride Semiconductors*, 1997, pp. 250.

[71] K. Yamamoto, M. Uchida, A. Yamamoto, A. Masuda and A. Hashimoto, *Phys. Status Solidi B* 234 (2002) 915; A. Hashimoto, T. Kitano, K. Takahashi, H. Kawanishi, A. Patane, C. T. Foxon and A. Yamamoto, *Phys. Status Solidi B* 228 (2001) 283.

[72] A. Zunger, *Phys. Status Solidi B* 216 (1999) 117.

[73] S. C. P. Rodrigues, G. M. Sipahi and E. F. da Silva Jr., *Microelectron. J.* 36 (2005) 434.

[74] Lakhdar Djoudi, Abdelhadi Lachebi, Boualem **Merabet**, Hamza Abid, First-principle calculation of structural and electronic properties of zinc-blende $B_yAl_xGa_{1-x-y}N$ matched to AlN substrate, Modern Physics Letters B, **26**, (2012) 1250159-1 to 13.

[75] A. Zunger, Physica Status Solidi B 216 (1999) 117.

[76] Yang H, Brandt O, Wessermeier M, Behrend J, Schonherr HP, Ploog KH. Appl Phys Lett 1996;68:244.

[77] Bi WG, Tu CW. Appl Phys Lett 1997;70:1068.

[78] Uesugi K, Suemune I. Jpn J Appl Phys 1997;36:L1572.

[79] Friedman DJ, Geisz FJ, Kurtz SR, Myers D, Olston JM. J Cryst Growth 1998;195:409.

[80] Kurtz SR, Allerman AA, Jones ED, Gee JM, Banas JJ, Hammons BE. Appl Phys Lett 1999;74:729.

[81] A. Ougazzaden, S. Gautier, T. Aggerstam, J. Martin, M. Bouchaour, T.Baghdadli,S.Ould Saad, S. Lourdudoss, N. Maloufi, Z. Djebbour, F. Jomard, Progress on new wide bandgap materials BGaN, BGaAlN and their potential applications, Quantum Sensing and Nanophotonic Devices IV, edited by Manijeh Razeghi, Gail J. Brown, Proc. of SPIE Vol. 6479, 64791G, (2007)

[82] T. Takayama, M. Yuri, K. Itoh, T. Baba, J.S. Harris Jr, J. Cryst. Growth. 222/(1-2) (2001) 29.

[83] H. Wang, H. Xu, X. Wang c, C. Jiang, Physics Letters A 373 (2009) 2082.

[84] V. A. Elyukhin, phys. Stat. sol. (c) 2/10 (2005) 3556.

[85] M. Cardona, Phys. Rev. 129, 67 (1963)

[86] H.C. Casey, M.B. Panish, J. Appl. Phys. 40, 4910 (1969); W. Shan, W. Walukiewicz, J. Wu, K.M. Yu, J.V. Ager III, S.X. Li, E.E. Haller,J.F. Geisz, D.J. Friedman, S.R. Kurtz, J. Appl. Phys. 93, 2696 (2003); A.G. Thompson, M. Cardona, K.L. Shaklee, J.C. Woolley, Phys. Rev. 146, 601 (1966)

[87] Sheng-Horng Yen, Mei Ling Chen, Yen-Kuang Kuo, Gain and threshold properties of InGaAsN/GaAsN material system for 1.3 μm semiconductor lasers, Optics and Laser Technology 39 (2007) 1432-1436; Chang YA, Kuo HC, Chang YH, Wang SC, simulation of 1300-nm

$Al_{0.4}Ga_{0.6}As_{0.986}N_{0.014}$ /$GaAs_{1-x}N_x$ quantum well lasers with various $GaAs_{1-x}N_x$ strain compensated barriers.Opt Commun 2004;204:194-202

[88] Chtourou R, Bousbih F, Bouzid SB, Charfi FF, Harmand JC, Ungaro G, at al. Effect of Nitrogen and temperature on the electronic band structure of $GaAs_{1-x}N$ alloys. Appl Phys Lett 2002; 80 (12): 2075-7

[89] S. Adachi, GaAs and Related Materials: Bulk Semiconducting and Superlattice Properties,World Scientific, Singapore, 1994.

[90] D.N. Talwar, Assessing the Preferential Chemical Bonding of Nitrogen in Novel Dilute III–As–N Alloys, Dilute III-V Nitride Semiconductors and Material Systems Physics and Technology, Ayse Erol Editor, Springer-Verlag Berlin Heidelberg 2008

[91] W.G. Bi, C.W. Tu, Appl. Phys. Lett. 70, 1608 (1997); L. Bellaiche, S.H. Wei, A. Zunger, Appl. Phys. Lett. 70, 3558 (1997); W. Shan, W. Walukiewicz, J.W. Ager, E.E. Haller, J.F. Geisz, D.J. Friedman, J.M. Olson, S.R. Kurtz, Phys. Rev. Lett. 82, 1221 (1999); I. Vurgaftman, J.R. Meyer, L.R. Ram-Mohan, J. Appl. Phys. 89, 5815 (2001); P.J. Klar, H. Gr¨uning, J. Koch, S. Sch¨afer, K. Volz, W. Stolz, W. Heimbrodt, A.M. Kamal Saadi, A. Lindsay, E.P. O'Reilly, Phys. Rev. B: Condens. Matter 64, 121203 (2001)

[92] J.F. Geisz, D.J. Friedman, J.M. Olson, S.R. Kurtz, B.M. Keyes, J. Cryst. Growth 195, 401 (1998)

[93] W. Walukiewicz, K. Alberi, J. Wu, W. Shan, K.M. Yu, and J.W. Ager III, Dilute III-V Nitride Semiconductors and Material Systems Physics and Technology, Ayse Erol Editor, Springer-Verlag Berlin Heidelberg 2008

[94] M. Weyers, M. Sato, H. Ando, Jpn. J. Appl. Phys. 31, L853 (1992); N. Baillargeon, K.Y. Cheng, G.F. Hofler, P.J. Pearah, K.C. Hsieh, Appl. Phys. ett. 60, 2540 (1992); W.G. Bi, C.W. Tu, J. Appl. Phys. 80, 1934 (1996); J.C. Harmand, J. Ramos, E.V.K. Rao, G. Saint-Girons, R. Teissier, G. Le Roux, L. Largeau, G.J. Patriarche, J. Cryst. Growth 227–228, 553 (2000); B.N. Murdin, M. Karmal-Saadi, A. Lindsay, E.P. O'Reilly, A.R. Adams, G.J. Nott, J.G. Crowder, C.R. Pidgeon, I.V. Bradley, J.P.R. Wells, T. Burke, A.D. Johnson, T. Ashley, Appl. Phys. Lett. 78, 1568 (2001).

[95] C. Skierbiszewski, Experimental Studies of GaInNAs Conduction Band Structure, Dilute III-V Nitride Semiconductors and Material Systems Physics and Technology, Ayse Erol Editor, Springer-Verlag Berlin Heidelberg 2008.

[96] K .Uesugi, I. Suemune, Jpn. J. Appl. Phys. 36 (1997) L1572

[97] M. Weyers, M. Sato, H. Ando, Jpn. J. Appl. Phys. 31 (1992) L835

[98] W. Shan, W. Walukiewicz, J.W. Ager III, E.E. Haller, J.F. Geisz, D.J. Friedman, J.M. Olson, Sarah R. Kurtz, Applied Physics Letters, 82 (1999) 1221

[99] J.C Phillipsin, A.M. Alper, L. Margrave, A.S. Nowick, In bonds and bands in semiconductors, Academic Press, New York (1993); L. Bellaiche, S.-H. Wei, A. Zunger, Phys. Rev. B 54 (1996) 17568.

[100] S.H. Wei, A. Zunger, Phys. Rev. Lett. 76, 664 (1996)

[101] T. Mattila, A. Zunger, Phys. Rev. B 60, R11245 (1999); Y. Zhang, A. Mascarenhas, H.P. Xin, C.W. Tu, Phys. Rev. B 63, 161303 (2001); P.R.C. Kent, L. Bellaiche, A. Zunger, Semicond. Sci. Technol. 17, 851 (2002)

[102] M. Kondow, T. Kitatani, S. Nakatsuka, M. C. Larson, K. Nakahara, Y. Yazawa, M. Okai, and K. Uomi, IEEE J. Sel. Top. Quantum Electron. 3, 719 (1997).

[103] M. Weyers, M. Sato, and H. Ando, Jpn. J. Appl. Phys. 31, L853 (1992).

[104] W. G. Bi and C. W. Tu, Appl. Phys. Lett. 70, 1608 (1997).

[105] W. K. Hung, M. Y. Chern, Y. F. Chen, Z. L. Yang, and Y. S. Huang, Phys. Rev. B 62, 13028 (2000).

[106] W. Shan, W. Walukiewicz, J. W. Ager III, E. E. Haller, J. F. Geisz, D. J. Friedman, J. M. Olson, and S. R. Kurz, Phys. Rev. Lett. 82, 1221 (1999).

[107] J. Wu, W. Shan, W. Walukiewicz, K. M. Yu, J. W. Ager III, E. E. Haller, H. P. Xin, and C. W. Tu, Phys. Rev. B 64, 085320 (2001); C.Skierbiszewski, P.Perlin, P.Wisniewski, W.Knap, and T.Suski, Appl. Phys. Lett., vol.76, Number 17 (2000); W Zawadski, Adv. Phys. 23, 435 (1974)

[108] K.M.Yu, W.Walukiewicz, J.Wu, J.W.Beeman, J.W.Ager, Appl. Phys. Lett., vol.90, N_0 5 (2001) , 2227

[109] K.M. Yu, W. Walukiewicz, J. Wu, J.W. Beeman, J.W. Ager III, E.E. Haller, W. Shan, H.P. Xin, C.W. Tu, Applied Physics Letters 90 (2001) 2227.

[110] W. Shan, W. Walukiewicz, J. W. Ager III, E. E. Haller, J. F. Geisz, D. J. Friedman, J. M. Olson, Sarah R. Kurtz, *J. Appl. Phys.*, **86**, (1999), 2349.

II.1 Solar cells

II.1.1 Breaf history of solar cells

Mankind needs energy for living. Besides the energy in our food necessary to sustain our body and its fuctions (100W), 30 times more energy is used on average to make our life more comfortable. Electrical energy is one of the most useful forms of energy, since it can be used for almost everything. All life on earth is based on solar energy following the invention of photosynthetis by the algae. Producing electrical energy through photovoltaic energy conversion by solar cells is the human counterpart. for the first time in history, mankind is able to produce a high quality energy form from solar energy directly, without the need of the plants. Since any sustainable, i.e., long term energy supply must be based on solar energy, photovoltaic energy conversion will become indispensable in the future. Photons, particules of light, to which the human eye reacts (that is which we see) have energies $\hbar\omega=h\upsilon$ between 1.5 eV and 3 eV. They always move with the velocity of the light, $c_0=3\ 10^8$ m/s in the vacuum and $c= c_0/n$ in a medium with refractive index n. To convert the wavelength to photon energy, one can used the relationship [1]

$$\lambda=\frac{c}{h\nu(eV)}\ (\mu m) \qquad \text{(II.1)}$$

We can describe this light as an electromagnetic wave whose location is discribed by the square of the field strength. photons obey the laws of quantum mechanics and not those of the more common Newtonian mechanics. the difference become apparent only for particles of very low energy (including the mass) [2].

The concept of converting light to electricity was first introduced with the discovery of the photovoltaic (PV) effect by Edmond Becquerel in 1839 [3], who [4] found that two different brass plates immersed in a liquid produced a continuous current when illuminated with sunlight, with the invention of the crystalline Si-based cell first revealed to the world by researchers at Bell Labs in 1954, when [4] Chapin et al. [5] had discovered, invented, and demonstrated the silicon single-crystal solar cell with 6% efficiency; and over the few following years, researchers brought the silicon solar cell efficiency up to 15%. Indeed, in 1 h the sun radiates upon the earth as much energy as is used in 1 year by humanity [4]. Unfortunately, the bulk Si solar cells have been demonstrated with an efficiency of nearly 25% [6] are prohibitively expensive for mass production [3].

The solar cell industry remained small until the first Arab oil embargo in 1973. After 1973, the flat-plate silicon module was brought down to earth and modified for weather resistance.

This transition also included major improvements in cell and module fabrication that brought down costs dramatically [4]. In the late 1970s, it was discovered that good cells could be made with multicrystalline wafers as long as the crystal size is at least 20 times larger than the optical absorption length [7]. Most important, annual production quantities have grown dramatically. Worldwide production exceeded 1 GW/year in 2002 and rose to over 3.8 GW/year by 2006.

By 2007, modules with multicrystalline cells accounted for about 45% of sales and modules with single - crystal cells accounted for about 40% of sales.


(a)

(b)

Fig. II.1 a) Two - kilowatt PV array from JX Crystals Inc on a commercial building flat rooftop.
b) Solar cell electricity generating field in Shanghai, China. System designed by JX Crystals Inc, Ref. [4].

II.I.2 Priciples and concepts of solar cells

Solar cells, converting optical radiation into electrical energy with high conversion efficiency, are among the major candidates providing long duration power at low operating cost and free of pollution for space and terrestrial applications [1].

Photovoltaic energy conversion in solar cells consists of two essentials steps. First, absorption of light (solar radiation producing chemical energy) generetes an electron-hole pair. The electron and hole are then separated by the structure of the device -electrons to the negative terminal and holes to the positive terminal thus generating electrical power (by generating current and voltage) [8]. The structure of a solar cell is much better represented by a SC absorber in which the conversion of solar heat into chemical energy takes place and by two semi-permeable membranes which at one terminal transmit electrons and block holes and the second terminal transmit holes and block electrons [2].

The solar cell is simply a photodiode which operates without external bias and delivers his photocurrent into a load. Under the illumination, the characteristic I (V) of the diode does not passe by the origin of coordinates, there is a region in which the product VI is negative, the diode provides power. If we limit ourselves to this region counting the reverse current positively, the characteristic I (V) reduces to Figure (2) [9].

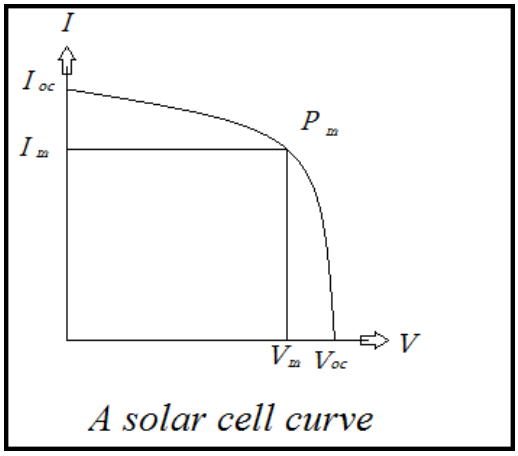

Fig. II.2 Solar cell curve.

The solar cell is assumed to have ideal I-V characteristics [1]. A constant current source

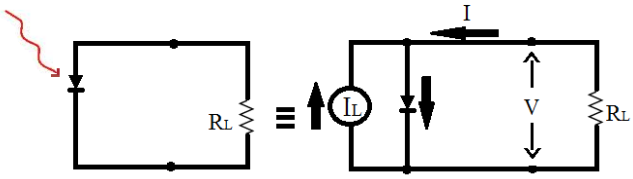

Fig.II. 3 Idealized equivalent circuit of a solar cell.

(I_L) resulting from the exitation of excess carriers by solar radiation is in parallel with the junction and the diode saturation current (I_s) are connected by the I-V characteristics of such a device given by [1,9]

$$I = I_L - I_s(e^{qV/kT} - 1) \qquad \text{(II. 2)}$$

I is the current through load resistance R_L.

The first term is the photocurrent, the second is a direct current resulting from the polarization of the diode in the forward direction by the voltage V that appears across the load resistor R_L. I_L is the short circuit current $I_L = I_{sc}$. the open circuit voltage is then

$$V_{oc} = \frac{kT}{e}\ln(I_L / I_s + 1) \qquad \text{(II. 3)}$$

The power supplied by the battery is given by the product *VI*

$$I = V\left[I_L - I_s(e^{qV/kT} - 1)\right] \qquad \text{(II. 4)}$$

This power is maximum at the point P_m (Fig.II. 2), defined by $dP/dV=0$

$$I_L - I_s(e^{qV/kT} - 1) - \frac{eV}{kT}e^{qV/kT} = 0 \qquad \text{(II. 5)}$$

The voltage V_m and the current I_m at the point P_m are given by

$$[1 + q\frac{V_m}{kT}]e^{qV_m/kT} = 1 + \frac{I_L}{I_s} \qquad \text{(II. 6)}$$

$$I_m = I_s \frac{qV_m}{kT} e^{\frac{qV_m}{kT}} \qquad \text{(II. 7)}$$

The output power is thus given by $V_m I_m$ which can be written as

$$P_m = V_m I_m = F_s V_{oc} I_{sc} \quad \text{(II. 8)}$$

where F_s is the fill factor or *shape factor*. it measures the rectangular character of the curve I (V). It varies from 0.25 for a low efficiency cell to 0.9 for an ideal cell [9].

II.1.3. Thin film solar cells

The obtained data for crystal geometries and band structures can be used to preselect compounds as candidate materials for specific optoelectronic applications. The procedure is used for finding new buffer layer materials for thin film solar cells based on chalcopyrite absorber layers such as $CuInSe_2$ (CISe) or $Cu(In,Ga)Se_2$ (CIGSe). In most high efficiency thin-film solar cells, the chalcopyrite absorber layer is separated from the ZnO-based window layer by a thin buffer layer. CdS is frequently used as buffer layer material. However, the heavy metal cadmium is harmful for the environment. As more and more large-size solar cells are manufactured, the necessity to find a replacement for cadmium increases. A suitable alternative buffer material must fulfill various criteria: its crystal structure must match well with that of the absorber layer to ensure a good contact. The band gap must be suitably large to avoid absorption losses of the incoming light. At the absorber-buffer interface, the conduction band of the absorber should be close to the Fermi level (inverted interface), and a barrier reduction should be avoided in order to minimize recombination.We use the calculated lattice constants and band gaps of half-Heusler materials to select potential substitutes of CdS [10].

For low-cost thin-film solar-cells, ternary Cu-based chalcopyrite semiconductors such as p-type $CuInSe_2$ or $Cu(In,Ga)Se_2$ are excellent light absorber materials, In these chalcopyrite solar-cells, a CdS-buffer layer of around 50 nm thickness between the light absorber and the n-type ZnO window layer is used to increase the performance of the device [11]. Record efficiencies of 19.9% have been reported for the ZnO/CdS/Cu(In,Ga)Se2 heterojunctions [12]. However, the heavy metal Cd is harmful to the environment and then much research activity is undertaken to replace CdS by a less toxic buffer layer material. To achieve good solar cells performances, an accurate design of the heterojunction between absorber and buffer layer is crucial. A suitable alternative buffer material must fulfill various criteria: its crystal structure must match well with that of the absorber layer to ensure good contacts. The band gap must be suitably large to avoid absorption losses of the incoming light [10]. It's desirable to have an inverted absorber/buffer interface (i.e., the conduction band of the absorber should be close to

the Fermi level) and a barrier reduction should be avoided in order to minimize recombination [13]. For a reasonably small absorption loss, the band gap of the buffer material should not be smaller than 2 eV and the lattice parameter should be around 5.9 Å for a good lattice matching with the absorber material [10].

II. 1. 4. Multijunction solar cells

The current state of art for high efficiency solar cells is the 32% efficient triple junction solar cell comprising of $GaInP_2$, GaAs and Ge absorbers [14]. Multijunction solar cells consisting of InGaP, InGaAs, and Ge are known as super-high-efficiency cells and are now used for space applications. Multijunction cells lattice-matched to Ge substrates have been improved, and their conversion efficiency has reached 31% [15,16]. Light concentration is one of the important issues for the development of an advanced photovoltaic (PV) system using high-efficiency solar cells. High-efficiency multijunction cells under high concentration have been investigated for terrestrial application [17,18]

It is considered that the temperature of solar cells considerably increases under light concentrating operations. The conversion efficiency of solar cells decreases with increasing temperature.[1,19]

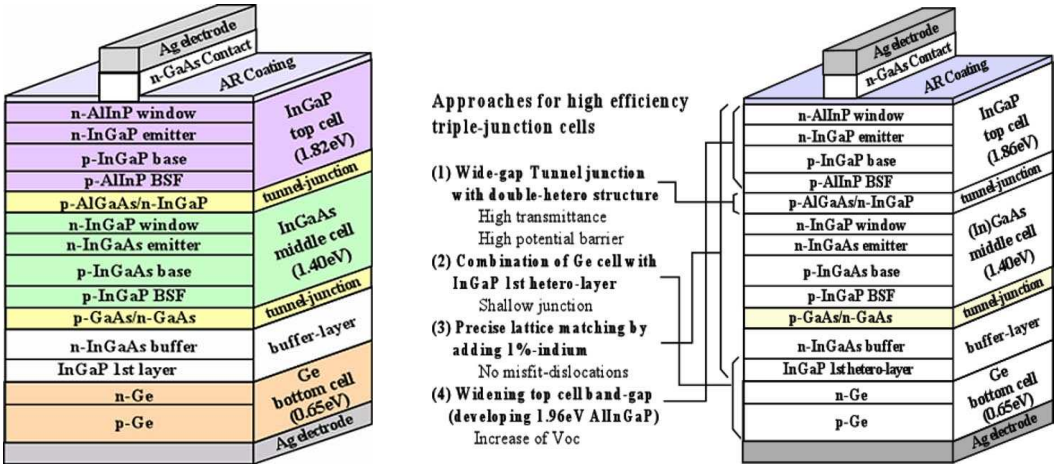

Fig. II.4. Schematic illustration of the InGaP/InGaAs/Ge triple-junction solar cell, Ref. [33].

II. 1. 5. Quantum well (QW) solar cells

The inclusion of QWs in a p-i-n diode structure extends the solar cell absorption spectrum, which results in a higher short circuit current density (J_{sc}). There is also evidence of an advantageous QW recombinaison rate, leading to a higher open circuit voltage (V_{oc}). The net result is an increase in photovoltaic conversion efficiency (η) [20].

The use of quantum wells to enhance solar cell efficiencies has been the subject of a number of studies in recent years. While multijunction cascade cells utilizing stacks of superlattice

regions were proposed as early as 1984. [21]. most work on quantum well cells has been carried out since 1990 when Barnham and co-workers at Imperial College began investigating less complicated structures [22]. Shortly after their initial proposal [23], Barnham's group demonstrated experimentally that the conversion efficiency of p-i-n photodiodes illuminated by broadband radiation could be enhanced simply by inserting quantum wells in the intrinsic region of the device [24]. This clearly established that the additional carrier generation and photocurrent resulting from extension of the absorption spectrum to lower energies can outweigh the accompanying drop in terminal voltage resulting from recombination of carriers trapped in the quantum wells, and stimulated further research [25].

The indirect bandgap of Si makes optical absorption inefficient due to the requirement of phonon emission/ scattering with photons in order to conserve crystal momentum. Then Si is not the ideal semiconducting material for solar energy conversion [4].

$In_xGa_{1-x}N$ alloys feature a band gap ranging from the near infrared (0.7eV) to the ultraviolet (3.4eV) [26, 27]. This range corresponds very closely to the solar spectrum making $In_xGa_{1-x}N$ alloys apromising candidate for radiation-resistant multi-junction solar cells [28]. Furthermore, it has been shown that $In_xGa_{1-x}N$ can be grown directly on Si substrates by a low temperature process, providing the potential for cheap multi-junction solar cells [29].Dilute nitride materials with a 1eV band-gap that are lattice matched to GaAs substrates are attractive for high efficiency multi-junction solar cells [30].

The development of a low-cost thin film solar cell device has attracted worldwide research interest during the past 2–3 decades in order to convert sunlight into electrical power. Most successful two systems are based on inorganic semiconducting compounds, CdTe and CIGS absorbers. At present, the highest reported conversion efficiencies for lab-scale devices stand at 16.5% and 19.7% [31] for CdTe and CIGS solar cells, respectively [32]. Photovoltaic power generation is becoming increasingly widespread as a clean energy source that is gentle to the earth. Environmental factors such as solar irradiation and module temperature strongly affect the generating performance of the photovoltaic systems [33-36]. It is well known that conversion efficiency decreases when the temperature of the solar cell increases [1,37].

II.2. Vertical cavity surface emitting lasers: VECSLs

II. 2.1. History of Lasers

After the invention of the microwave amplification by stimulated emission of radiation (MASER), in 1954 by Townes et al. and the subsequent operation of optical masers and lasers

(l remplacing m in maser and standing for light) in ruby, SC were suggested for use as laser materials. The theoretical calculations of Bernard and Durrafourg in 1961 set fouth the necessary conditions for lasing using quasi-Fermi levels. In 1962, Dumke showed that laser action was indeed possible indirect gap SCs and set forth important creteria for such action. In late 1962, three groups headed by Hall, Nattan and Quist announced almost simmultneously that they had achieved lasing in SCs [1]. The pulsed radiation of 0.84 μm was obtained from a liquid-nitrogen-cooled, forward-biased GaAs p-n junction. Shortly thereafter, Holonyak and Bevacqua announced laser action in the ternay compound $GaAs_{1-x}P_x$ jonction at 0.71 μm. I n 1971, Hayashi et al. achieved thecontineous operation of junction lasers at room temperature by the use of double heterojunction. This structure was first propsed by Kroemer, Alferov and Kazanirov. Since this discovery, many new laser materials have been found. The wavelength of coherent radiation has been extended from the UV to the visible and e out of the far-IR spectrum (~0.3 to ~30 μm) [1].

The invention of the laser and the subsequent development of low-loss optical fibers started a revolution in the communications industry about more than fourty years ago, and fibers are not used only for long-distance communication, but for connecting swintching stations in the local telephone company, delivering cable television signals to the neighborhoods in the cities, and connecting local area networks in medium -to large- seize offices [38]. They are considered the most important light sources for optcal-fiber communication systems, and also have significant potential for applications in many areas of basic research and technology, such as high resolution gas spectroscopy and atmospheric pollution monitoring. Altough laser diodes are increasingly used as a light source in optical particle measurement technology, offering the advantages of very small size, very low weight, and have recently become commercially available with a sufficient optical output power at an acceptable price, they have the disadvantages of needing a matched current source and of having a generally higher noise level than gas lasers [39]

II.2.2. Laser threshold

Light emission in a SC usually proceeds from electron-hole recombination in regions where they are in excess in comparison with levels allowed by thermodynamic equilibrium. A SC *p-n* junction pumped electrically beyond its transparency threshold, will be able to amplify those electromagnetic modes (i.e. photons) that satisfy the Bernard-Durrafourg criterion.

As long as the transparency threshold has not been reached, the diode behaves exactly as a LED, releasing spontaneous emission in all possible directions. Between the transparency

threshold and the onset of laser oscillation, (J_{trans}□J□ $J_{threshold}$), stimulated emission dominates over spontaneous emission, the diode is referred to as being superluminescent.

Once this threshold has been surpassed, the carrier densities in the junction are *clamped* to their threshold values $n_{threshold}$ and the condition requiring equality between the gain and the cavity losses is satisfied [40].

II.2.3. Quantum well laser diodes

To increase the confinement factor Γ, we realize a Separate Confinement Heterojonction (SCH). The carriers are confined in a quantum well of thickness d_p, and the photons are confined in a waveguide of width d_{ph}

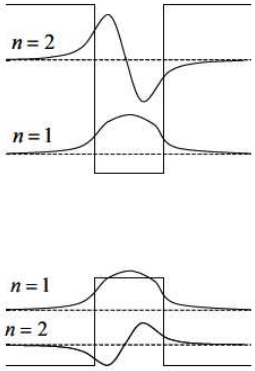

Fig.II. 5. Well of finite depth. Energy levels and wave functions, Ref. [9]

This confinement factor can be improved by replacing the single well by a multiple quantum well structure. If the SC_1 layers are thin ($L_1 \approx 100$ Å) electronic states in each well are quantified and have a structure of subband energy. If in addition the SC_2 layers are relatively thick ($L_2 > 200$ Å) the probability that an electron moves from one well to the other by tunneling through the barrier is low, the wells are independent of each other [9].

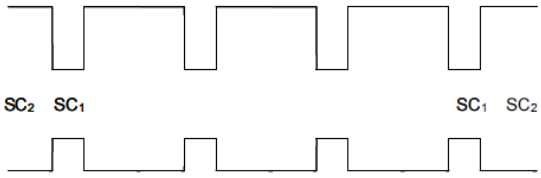

Fig. II.6. Multiple quantum well structure of type I, Ref. [9].

Compared to the single well, the multiple quantum certainly increase the confinement factor Γ, but in parallel reduce the gain g, especially at low injection. Indeed, the carriers are then distributed in N_p wells instead of one. The result is that for comparable injections, the carrier density in the active zone is N_p times lower in the multiple quantum well structure than that in the single quantum well structure. It is therefore desirable to keep the single well and improve the confinement factor. This is achieved by replacing the step index optical guide by a graded index guide. The composition, and consequently the index and gap of the alloy constituting

the optical waveguide, vary gradually. These structures are called the GRaded INdex-SCH (GRIN-SCH) structures [9]. To decrease the threshold current further, one is naturally drawn to decrease the size of the active region down to quantum length scales (i.e. to make use of potential wells that are so narrow as to confine and quantize the motions of carriers in directions perpendicular to the heterointerfaces) [40].

II.2.4. Concepts of QW lasers

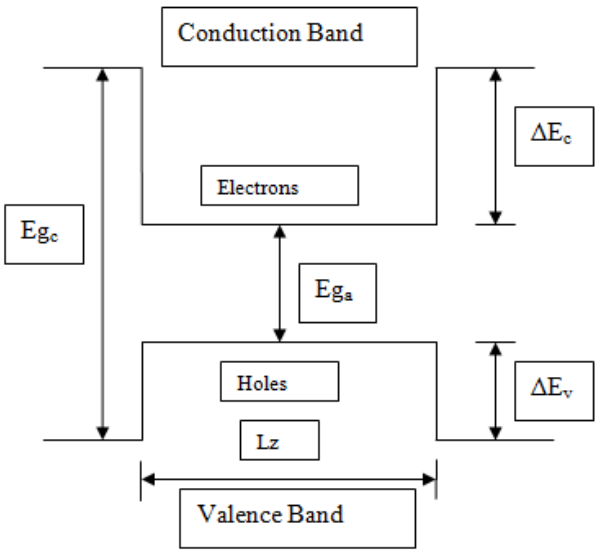

Fig.II. 7. Band model for a quantum well structure.

To increase the performance of heterostructure lasers, it is advantageous to reduce the thickness of the active region using the techniques of epitaxy, MBE and MOCVD, we obtain a single quantum well laser (whose active layer is of dimension <20 nm), or multiple quantum well (separated by barriers of a material of SC which a higher gap than that of the well), hence the significant change observed in some parameters of the laser (such as gain, the density of states, etc..) and reducing the threshold by a factor of 10 or more [41]. The double advantage of the quantum well is of a few nm to reduce the spatial extension of electrons and holes, and to confine their energy distributions by the two-dimensional nature of the density of states [42], but when the carriers are confined and since the thickness d of the active zone is well below the optical wavelength, the photons then occupy a volume extending beyond active area, hence the risk to lose in recovery carriers- photons the acquired carrier confinement [9]. The effectiveness of this recovery is characterized by the optical confinement factor of photons Γ measuring the proportion of the radiation density effectively interacting with the active medium [42]. Note that the small recovery between the guided wave and the quantum well reduces gain. In a single quantum well structure, the width d of the active zone is well

below the wavelength λ of the radiation, and the expression of the confinement factor [40] can be approximated

$$\Gamma_{sw} = (2\pi^2/\lambda^2)\,(n^2_{int} - n^2_{ext})\,d^2 \qquad \text{(II. 9)}$$

To increase Γ, we realize a Separate Confinement Heterojuction (SCH), where the carriers are confined in a quantum well of thickness L_z, and photons are confined in a waveguide of width d_{ph} . Γ is further improved by replacing the single quantum well by a multiple quantum well structure [43]. Γ of a multi quantum well structure (s) MQWis approximated to

$$\Gamma_{MQW} = (2\pi^2/\lambda^2)\,(d_w/d)\,(Nd)^2(\acute{n}^2_a - n^2_c) \qquad \text{(II. 10)}$$

The confinement factor of a MQW structure, compared to that of a single well, increases certainly but at the expense of reducing gain; it is therefore desirable to rconserve the single wells and improve Γ, this is achieved by replacing the waveguide index step guide by a graded-index, where the composition (hence the index) of the alloy constituting the guide varies gradually, these structures are called *GR*aded *I*ndex *I*ndex-*SCH* (*GRIN-SCH*) [9].

II.2.5. Principles of VCSELs

The edge emitting semiconductor lasers present a certain number of inconveniences. First, they tend to be multimodal principally due to spatial hole burning. This behaviour generates noise, most notably as a result of mode hopping due to small thermal fluctuations. Second, the laser emission is divergent making efficient coupling to optical fibres a significant technological challenge [40].

The conventional laser is often referred to as an edge emitter because laser output is from the edge of a semiconductor chip. With edge emission, the transverse and lateral modes of the laser depend on the cross section of the heterostructure gain region, which is transversely very thin for carrier confinement and laterally wide for output power. The result is highly elongated near and far fields that do not match well to the circular cross section of an optical fiber. Also, the output beam is highly astigmatic, with full angle beam divergence of as much as 50° in the transverse dimension. This makes the design and fabrication of coupling optics challenging. From a manufacturing aspect, facet mirrors are fabricated either by cleaving or etching, so that optical testing of the laser chip cannot be performed until many of the fabrication and packaging processes are completed. Lastly, due to the long (10^2 to $10^3\lambda$) optical cavity, an edge emitter typically lases on multiple longitudinal modes, or is prone to mode hop. While each of the above problems can be addressed at least in part by special

structures, these structures add to the complexity and cost of the laser diodes [44]. Some of the edge-emitting laser diodes inconveniences can be partially avoided by using vertical cavity surface emitting lasers (VCSELs), which circumvents the problems arising from edge emission by having its resonator axis in the vertical (epitaxial growth) direction [44]. In a structure of vertical cavity laser VCSEL, the reflective faces of the cavity are no longer cleaved faces perpendicular to the plane of the junction, as in edge-emitting laser diode, but are carried out by Bragg mirrors, DBR (Distributed Bragg Reflector), located above and below the active region. The radiation is emitted perpendicular to epitaxial layers, in a slightly divergent beam (~ 8 °), of circular section [43]. VCSELs now rival conventional edge-emitting laser diodes in efficiency, and surpass them by a wide margin in threshold current [45].

Historically, the very first surface emitting laser was fabricated during the first years of the semiconductor laser's history but the structure of this device was far from the vertical-cavity lasers that we know today [46]. VCSELs that we know appeared much later. first proposed and Suggested in 1977 by Kenichi Iga *et al.* at the Tokyo Institute of Technology, Tokyo, Japan [47] then demonstrated for the first time at the end of the 1970s [48], the first GaAs-based VCSELs operating in continuous wave mode at room temperature were demonstrated at the end of the 1980s [49] and InP-based devices at the beginning of the 1990s [50]. The room temperature pulsed operation has been achieved in 1984 [51], and continuous-wave room-temperature operation in 1988 [52].

These devices were then extensively developed on GaAs and InP substrates with emitting wavelengths varying between 0.8 and 1.6 μm primarily for data communications and high speed optical interconnects. Indeed, very interesting properties, such a high potential modulation rate combined with a low threshold and a low divergence circular output beam, made VCSELs ideal laser sources for these kind of applications such as optical interconnects or high speed data transfers [53]. Long-Wavelength VCSELs (LW-VCSELs) are key devices in optical fiber metropolitan-area networks [54] and interesting light sources for future massively parallel optical interconnects [55- 58].

Their potential advantages include ultralow-threshold operation, easy fabrication of two-dimensional arrays, and easy coupling to optical fibers. Compared with edge-emitting semiconductor lasers, VCSELs offer a variety of advantages. The main advantages of the VCSELs are an inherent single longitudinal mode, a small divergence angle, a low threshold current, the capability of ultrahigh bit rate modulation, ease of forming a two-dimensional

laser array, and good scalability and integrability with other optoelectronic components [59]. The underlying concept of VCSELs is quite simple, a laser cavity is fashioned along the epitaxial growth axis allowing controlled deposition of extremely thin layers (with thicknesses less than amicrometre) and perfectly parallel cavity mirrors (precise to within a monolayer). The mirrors are Bragg reflectors formed by epitaxially depositing alternating semiconductor layers of appropriate thickness and composition. Metallic mirrors are not employed for several reasons:sufficiently high quality epitaxial deposition of metals onto III-V semiconductors is not possible, metals absorb infrared light and would adversely affect the threshold currents in such devices [40]. The VCSEL's active medium is embedded in a short λ cavity and a single longitudinal mode operation is automatically realized. To keep the loss low, both mirrors should be highly reflective. They are usually realized as stacks of λ/4 distributed Bragg reflectors. The vertical cavity represents a one-dimensional microcavity [59, 60].

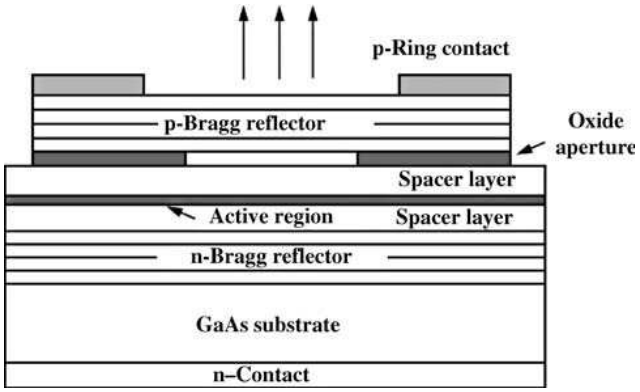

Fig.II.8 Schematic structure of a high bandwidth single mode top emitting GaAs VCSEL, Ref. [59, 60]

In a typical VCSEL, an optical cavity is formed along the device's growth direction, with distributed Bragg reflectors (DBRs) typically forming the cavity mirrors [61].

The VCSEL has the optical cavity axis along the direction of current flow rather than perpendicular to the current flow as in conventional laser diodes. The active region length is very short compared with the lateral dimensions so that the radiation emerges from the "surface" of the cavity rather than from its edge. The reflectors at the ends of the cavity are dielectric mirrors made from alternating high and low refractive index quarter-wave thick multilayers. Such dielectric mirrors provide a high degree of wavelength selective reflectance at the required free surface wavelength λ if the thicknesses of alternating layers d_1 and d_2 with refractive indices n_1 and n_2 are such that $n_1d_1 + n_2d_2 = 1/2.\lambda$, which then leads to the constructive interference of all partially reflected waves at the interfaces. Since the wave is

reflected because of a periodic variation in the refractive index as in a grating, the dielectric mirror is essentially a distributed Bragg reflector (DBR). High reflectance end mirrors are needed because the short cavity length L reduces the optical gain of the active layer inasmuch as the optical gain is proportional to $\exp(g_L)$ where g is the optical gain coefficient. There may be 20 - 30 or so layers in the dielectric mirrors to obtain the required reflectance (~99%). The whole optical cavity looks "vertical" if we keep the current flow the same as in a conventional laser diode cavity. The active layer is generally very thin (< 0.1 μm) and is likely to be a multiple quantum well (MQW) for improved threshold current. The required SC layers are grown by epitaxial growth on a suitable substrate which is transparent in the emission wavelength. For example, a 980 nm emitting VCSEL device has InGaAs as the active layer to provide the 980 nm emission, and a GaAs crystal is used as substrate which is transparent at 980 nm. The dielectric mirrors are then alternating layers of AlGaAs with different compositions and hence different bandgaps and refractive indices. The top dielectric mirror is etched after all the layers have been epitaxially grown on the GaAs substrate. In practice, the current flowing through the dielectric mirrors give rise to an undesirable voltage drop and methods are used to feed the current into the active region more directly, for example, by depositing "peripheral" contacts close to the active region. There are presently various sophisticated VCSEL structures. The vertical cavity is generally circular in its cross section so that the emitted beam has a circular cross section, which is an advantage. The height of the vertical cavity may be as small as several microns. Therefore the longitudinal mode separation is sufficiently large to allow only one longitudinal mode to operate. However, there may be one or more lateral (transverse) modes depending on the lateral size of the cavity. In practice there is only one single lateral mode (and hence one mode) in the output spectrum for cavity diameters less than ~8 μm. Various VCSELs in the market have several lateral modes but the spectral width is still only ~0.5 nm, substantially less than a conventional longitudinal multimode laser diode. With cavity dimensions in the microns range, such a laser is referred to as a microlaser. One of the most significant advantages of microlasers is that they can be arrayed to construct a matrix emitter that is a broad area surface emitting laser source. Such laser arrays have important potential applications in optical interconnect and optical computing technologies. Further, such laser arrays can provide a higher optical power than that available from a single conventional laser diode. Powers reaching a few watts have been demonstrated using such matrix lasers [61].
For fabricating 1.3 or 1.55 μm communications range VCSELs this has necessitated the use of InP substrates, AlAs/GaAs Bragg reflectors and complex fusion bonding steps or the use of

Bragg reflectors synthesized from alternate ternary or quaternary alloys which exhibit poorer reflectivity and thermal conductivity [62].

Despite the commercial production of GaInAsN/GaAs-based laser diodes, the optical quality of the ternary GaAs(In)N and quaternary GaIn(Al)AsN layers is still poor [63-65]. The III–As–N alloys have shown the evidence of inhomogeneities with broad photoluminescence (PL) line widths, variable PL decay times, and short minority carrier diffusion lengths. Fortunately, with high-temperature anneals of 600–900°C, the non-radiative recombination sites can be removed [65].

II.2.Spin-VECSELs

Semiconductor spintronics – a new field of research exploring the interplay between magnetism and electronics – has received considerable attention at both experimental and theoretical levels with the ultimate goal of utilizing electron spin to make smaller, faster, and more versatile devices than those based solely on electron charge.

II.2.6.a How one can inject spin polarized carriers?

Let us take the example of Spin LED:

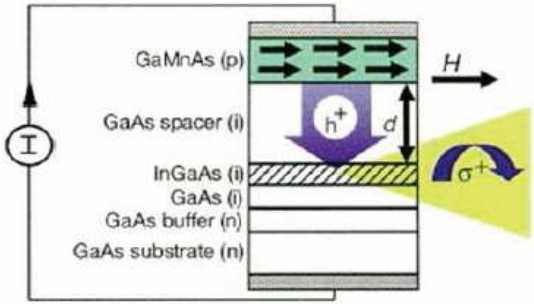

Fig.II.9. Diode electroluminescente SpinLED (Spin Light Emitting Diode), Ref. [66].

one example of injection of spin is the spin LED, which injects spin polarized carriers constitued of an injector (made of ferromagnetic material) in a quantum well. Radiative recombinaison of these carriers induces the emission of a circularly polarized light.The spin injector can be realized of a diluted magnetic semiconductor (DMS). Fig. II.9 shows the diagram of sush a device [66]. Spin-polarized holes are injected via the magnetic semiconductor GaMnAs. A Spin-polarized current is carried in the non-magnetic layer GaAs to the InGaAs quantum well, where the polarized-holes recombine with electrons of the same spin causing the emission of circularly polarized photons.

II.2.6.b AlGaAs(Mn) for integrated optical isolators and spintronics.

Since the discovery of high temperature ferromagnetism in dilute magnetic semiconductors (DMSs) such as Mn-doped III-Vs, whose magnetic state has controlled by an external electric field [67], it has been intensively studied in order to fabricate new functional semiconductors (SCs) taking advantage of the spin degree freedom in DMSs [68]. The interest in III-Mn-Vs, formed by doping nonmagnetic host SCs with magnetic acceptors such as GaAs and the transition metal (Tm) Mn, is due to possible applications in spintronics as the source of a spin polarized current or as the base material for a chip that can simultaneously store and process data [69], and high correlation of their electronic, optical and magnetic properties [70-72], which are sensitive to external stimuli such as illumination with light [73]. Although the induced magnetic properties of doped materials are often difficult to discriminate from those of other magnetic impurities due to the intrinsic magnetic behavior of Tms [74], III-Mn-Vs in which Mn acts both as a source of local moments [75], show also a great deal of promise due to their potential applications in magneto optics and optical fiber networks [76-78]. III-V-based-DMSs, such as (Ga,Mn)As, pseudomorphically grown on GaAs, adding a new dimension to GaAs/AlGaAs heterostructures [79] and having a large Verdet's constant [78], is promising for use in integrated optical isolators and can be integrated together with GaAs-based lasers [80].

Moreover, it should be emphasized that optical isolators ensure stable emission of SC lasers in which the nonreciprocity of the magneto-optical (MO) effects plays a key role in the process of isolation [81-83]. MO effects, indeed, can be enhanced by incorporating one-dimensional SC photonic crystals integrating lasers and isolators, so high-performance low-cost devices may be realized [84]. Hence the necessity to increase MO activity in GaAs-based materials, by introducing fine particles of the ferromagnetic (FM) MnAs into thin films of GaAs [85]. In GaAs/AlGaAs/GaMnAs quantum wells (QWs), however, Schulz et al. [86] reported a Mn diffusion from a FM GaMnAs layer into the nonmagnetic GaAs QW through the AlGaAs barriers. Although the spin polarizated carriers injected into the QW showed a strong spin lifetime increase [86,87], Mn ions act as non-radiative recombination centers in the QW [88]. In this way, Amemiya et al. [89] have fabricated a waveguide isolator, where the MnAs layer grown on the SC optical amplifier waveguide was of poor crystalline structure, showing a soft hysteresis curve with small remanence. Trying to overcome this problem, we have proposed another system as an alternative to MnAs resulting from AlGaAs, to our knowledge not studied and best-understood as extensively as the other DMSs like GaMnAs: AlGaMnAs, that

we have predicted its behavior when used as an optical isolator. Fig.II.10 shows a cross section of a waveguide isolator that consists of a ferromagnetic AlGaMnAs layer and a GaAs-based SC optical amplifier (a multiple quantum well) sandwiched between two AlGaAs guiding layers (barriers), whose the upper guiding layer is covered with the ferromagnetic AlGaMnAs layer over an upper cladding layer. The Light passes through the SC optical amplifier perpendicular to the figure (*z* direction) [90].

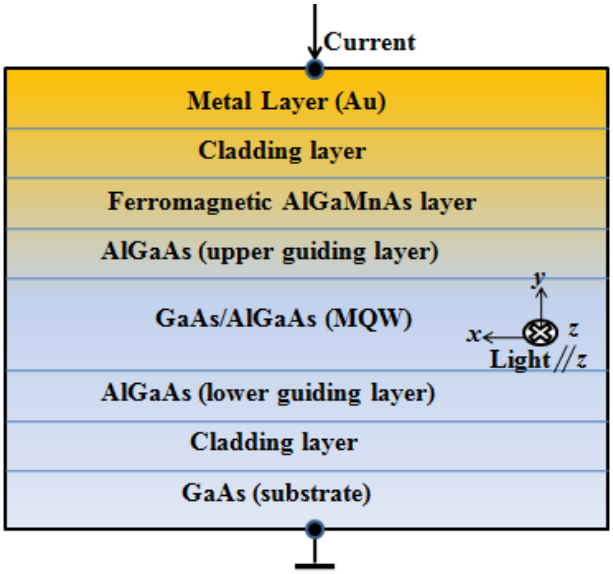

Fig.II.10 A cross section of the waveguide isolator.

In order to know how the Mn incorporation may affect AlGaAs and deeply understand the correlated electronic, optical and magnetic properties of III-Mn-Vs, we have performed total energy calculations on zinc blende (ZB) $(Al_xGa_{1-x})_{1-y}Mn_yAs$, grown by molecular beam epitaxy by Morishita et al. [91], and used in field effect transistors as channel layers by Chiba et al. [92], with (*x*, *y*) respectively, (≤0.5, 0.06) and (0.056, 0.046). The LDA + U scheme, giving spin down and up gap energies of, respectively, 0.988 and 0.625 eVforAlGaMnAs, has been successfully used to describe better the strong correlations in the Mn d-shell, although the weak hybridization betweenMn3d and As 4p states found for both majority-band and minority-band states. The lowest optical properties of AlGaMnAs compared to those of AlGaAs are mainly due to the non radiative recombination centers in the GaAs QW, while the Mn ions' diffusion into the nonmagnetic GaAs QW from the FM layer. From the intrinsic spin polarization found to be 100 % and the large magnetic moment of 4.014 lB per Mn-dopant, we can say that a system such as AlGaMnAs may be not only

an attractive alternative to MnAs for the realization of integrated optical isolators but also, as a DMS, a good candidate for spintronics [90].

II.2.6.c. Principles of Spin-VECSELs

The spin-polarized vertical-cavity surface-emitting laser (spin-VCSEL) promises a number of advantages over a conventional VCSEL. As a consequence of optical selection rules, spin-polarized electrons couple selectively to either the left- or right-circularly polarized lasing mode in a VCSEL such that pumping with a 100% spin-polarized current would result in a laser featuring circularly-polarized stimulated emission with half the threshold current. Additional advantages may include enhanced intensity and polarization stability, greater modulation bandwidth, polarization control, and reduced wavelenth chirp. The ability to controllably modulate the optical polarization of semiconductor lasers between orthogonal states in addition to its intensity would enable telecommunications networks with enhanced bandwidth. Other applications benefitting from polarization control in a VCSEL include optical computing and reconfigurable optical interconnects [93].

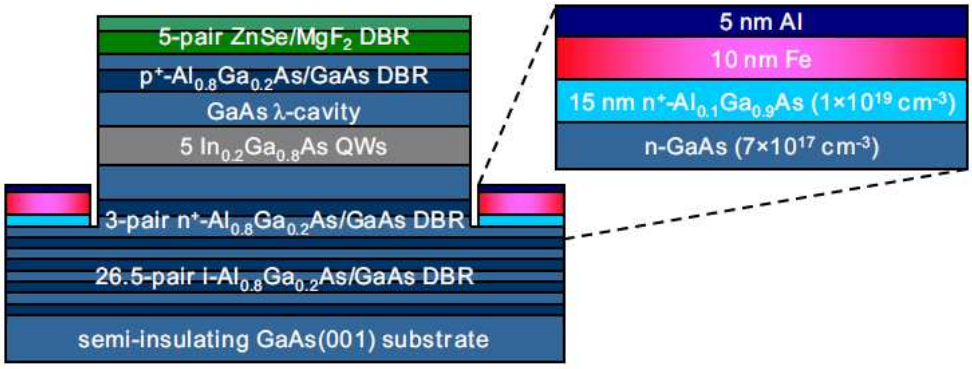

Fig.II.11 Schematic cross section of the spin-laser heterostructure with a zoomed view of the regrown Al/Fe/$Al_{0.1}Ga_{0.9}As$ Schottky tunnel barrier spin injector, Ref. 93.

References of chap.2

[1] S. M. Sze: Physics of Semiconductor Devices (A Wiley-Inter science Publication, 1981) 2nd ed., p. 833.

[2] Peter Wurfel, Physics of solar cells from principles to new concepts, Wiley-VCH Verlag GmbH & Co. KGaA, Weinheim, Berlin 2005.

[3] [E. Becquerel, La lumière: ses causes et ses effets, tome second, Paris (1867), p. 122.]

[4] Solar cells and their applications, Edited by Lewis Fraas and Larry Partain, Second Edition, A John Wiley & Sons, Inc., Publication, Hoboken, New Jersey, 2010

[5] D.M. Chapin, C.S., Fuller, G.S. Pearson, A new silicon p–n junction photocell for converting solar radiation into electrical power, J. Appl. Phys. 25 (1954) 676.

[6] J. Zhao, A. Wang, M.A. Green, F. Ferrazza, Appl. Phys. Lett. 73 (1998) 1991.

[7] H. C. Card , and E. S. Yang . *IEEE - TED* **24** , 397 (1977).

[8] Solar cells materials, manifacture and operation, edited by tom Markvart and luis Castaner, Elsevier, 2005.

[9] Henry Mathieu, Hervé Fanet, Physique des semiconducteurs et des composants électroniques Cours et exercices corrigés, 6^{e} édition (2009), Dunod Paris.

[10] Thomas Gruhn, Comparative *ab initio* study of half-Heusler compounds for optoelectronic applications**,** Physical Review B **82**, 125210 (2010).

[11] D. Kieven and R. Klenk, physical review B81 075208 (2010).

[12] I. Repins, M. A. Contreras, B. Egaas, C. DeHart, J. Scharf, C.L. Perkins, B; To and R. Noufi, Prog. Photovoltaics 16, 235 (2008).

[13] R. Klenk, Thin solid films 387, 135 (2001).

[14] Whitaker T. Solar cells. Comp Semicond 1998;4(8):32–40.

[15] J.M. Olson, S.R. Kurtz, and A.E. Kibbler, Appl. Phys. Lett. 56, 623 (1990).

[16] T. Takamoto, T. Agui, E. Ikeda, and H. Kurita, Proceedings of the 28th IEEE Photovoltaic Specialists Conference (Anchorage, 2000), p. 976]

[17] H.L. Cotal, D.R. Lillington, J.H. Ermer, R.R. King, and N.H. Karam, Proceedings of the 28th IEEE Photovoltaic Specialists Conference (Anchorage, 2000), p. 955.

[18] A.W. Bett, F. Dimroth, G. Lange, M. Meusel, R. Beckert, M. Hein, S.V. Riesen, and U. Schubert, Proceedings of the 28th IEEE Photovoltaic Specialists Conference (Anchorage, 2000), p. 961.]

[19] A.L. Fahrenbruch and R.H. Bube, Fundamentals of Solar,Cells (Academic Press, Inc., 1983), pp. 238–239.]

[20] Bor Wen Liou, high Photovoltaic of $In_xGa_{1-x}N$/GaN-based solar cells with a multiple-quantum well structure on SiCN/Si(111) substrates, Japanese Journal of allplied physics 48 (2009) 072201.

[21] R. J. Chaffin, G. C Osboum, L. R. Dawson, and R. M. Biefeld, Proceedings of the 17th IEEE Photovoltaic Specialists Conference, 1984, pp. 743-746.

[22] Neal G. Andersona, ideal theory of quantum well solar cells, J. Appl. Phys. **78**, 1850 (1995).

[23] K. W. J. Barnham and G. Duggan, J. Appl. Phys. 67, 3490 (1990).

[24] K. W. J. Barnham, B. Braun, J. Nelson, and M. Paxman, Appl. Phys. Lett. 59, 135 (1991).

[25] J.Wu,W.Walukiewicz, K.M.Yu, J.W.AgerIII, E.E.Haller, H.Lu, W.J.Schaff, Small band gap bowing in In1-xGaxN alloys, Appl. Phys. Lett. 80 (2002)4741–4743.

[26] J.Wu, When group III-nitrides go infrared: new properties and perspectives, J. Appl. Phys. 106 (2009) 011101-1–28.

[27] J. Wu, W. Walukiewicz, K.M. Yu, W.Shan, J.W.Ager III, E.E. Haller, H.Lu, W.J. Schaff, W.K.Metzger, S.Kurtz, Superior radiation resistance of In1-xGaxN alloys: Full-solar-spectrum photovoltaic material system,J.Appl.Phys.94 (2003) 6477–6482.

[28] L.A.Reichertz, K.M.Yu, Y.Cui, M.E.Hawkridge, J.W.Beeman, Z. Liliental-Weber, J.W.Ager III, W.Walukiewicz, W.J.Schaff, T.L.Williamson, M.A. Hoffbauer, InGaN thin films grown by ENABLE

and MBE techniques on silicon substrates, Mater. Res. Soc. Symp. Proc.1068(2008)C-06-02.
[29] Yongkun Sin, Stephen LaLumondiere, Toby Garrod, Tae Wan Kim, Jeremy Kirch, Luke Mawst, William T. Lotshaw, and Steven C. Moss, Carrier Dynamics in MOVPE-Grown Bulk Dilute Nitride Materials for Multi-Junction Solar Cells, Proc. of SPIE Vol. 7933 79330H-1 to 11, (2011).
[30] X. Wu, J.C. Keane, R.G. Dhere, C. Dehart, D.S. Albin, A. Duda, T.A. Gessert, S. Asher, D.H. Levi, P. Sheldon, in: 17th European Photovoltaic Solar Energy Conference, 22–26 October, 2001, Munich, Germany, p. 995.
[31] M.A. Contreras, K. Ramanathan, J. Abushama, F. Hasoon, D.L. Young, B. Egaas, R. Noufi, Prog. Photovolt: Res. Appl. 13 (2005) 209.
[32] I.M. Dharmadasa, Latest developments in CdTe, CuInGaSe2 and GaAs/AlGaAs thin film PV solar cells, Current Applied Physics 9 (2009) e2–e6.
[33] Kensuke Nishioka, Nobuhiro Sakitani, Kenichi Kurobe, Yukie YAmamoto, Yasuaki Ishikawa, Yukiharu Uraoka and Takashi Fuyuki, Analysis of the Temperature Characteristics in Polycrystalline Si Solar Cells Using Modified Equivalent Circuit Model, Jpn. J. Appl. Phys. Vol. 42 (2003) pp. 7175–7179; Kensuke Nishioka, Tsuyoshi Sueto, Masaki Uchida, and Yasuyuki Ota, Detailed Analysis of Temperature Characteristics of an InGaP/InGaAs/Ge Triple-Junction Solar Cell, Journal of Electronic Materials, Vol. 39, No. 6, 2010.
[34] Y. Hishikawa and S. Okamoto: Sol. Energy & Sol. Cells 33 (1994) terminal 157.
[35] M. Kameda, S. Sakai, M. Isomura, K. Sayama, Y. Hishikawa, S. Matsumi, H. Haku, K. Wakisaka, M. Tanaka, S. Kiyama, S. Tsuda and S. Nakano: Proc. 25th IEEE Photovoltaic Specialists Conf., Washington, 1996, p. 1049.
[36] S. Yoon and V. Garboushian: Proc. 1st WCPEC, Hawaii, 1994, p. 1500.1–3.
[37] A. L. Fahrenbruch and R. H. Bube: Fundamentals of Solar Cells (Academic Press, San Diego, CA, 1983) p. 238.
[38] Clifford R. Pollock, Fundamentals of optoelectronics, school of eletrical engineering, Cornell University, Richard D. Irwin, Inc., 1995.
[39] Dirk Semleit, Andreas Trampe, and Heinz Fissan, Aerosol Science and Technology **26:356-367** (1997).
[40] E.Rosencher, B.Vinter, Optoélectronique, 2^{e} édition, Dunod 2002.
[41] Romain Maciejko, Optoélectronique, Ecole Polytechnique de Montréal, 2002.
[42] Carl Asplund, Epitaxy of GaAs-based long wavelength Vertical Cavity Lasers, Doctoral thesis, Stockholm (Sweden) 2003.
[43] B.R.Nag, Physics of Quantum Well Devises, edition 2000, India.
[44] Weng W. Chow, Kent D. Choquette, Mary H. Crawford, Kevin L. Lear, *Member, IEEE*, and G. Ronald Hadley, *Senior Member, IEEE*, Design, Fabrication, and Performance of Infrared and Visible Vertical-Cavity Surface-Emitting Lasers, IEEE Journal of Quantum Electronics, VOL. 33, NO. 10, OCTOBER 1997.

[45] Weng w. chow and Stephan W koch, seminconductor laser fundamentals, Springer-verlag Berlin heidelberg, 1999.
[46] Melngailis I. Longitudinal injection-plasma laser of InSb. Appl. Phys. Lett. 1965; 6: 59-61.
[47] Iga K, Koyama F, Kinoshita S. Surface emitting semiconductor-lasers. IEEE J. Quantum Electron. 1988; 24: 1845-1855.
[48] Soda H, Iga K, Kitahara C, Suematsu Y. GaInAsP-InP surface emitting injection-lasers. Japon. J. of Appl. Phys. 1979; 18: 2329-2330.
[49] Lee YH, Tell B, Brown-Goebeler KF, Leibenguth RE, Mattera VD. Deep-red continuous wave top-surface-emitting vertical-cavity AlGaAs superlattice lasers. IEEE Photon. Technol. Lett. 1991; 3: 108-10911.
[50] Baba T, Yogo Y, Koyama F, Iga K. Near room temperature continuous-wave lasing characteristic of GaInAsP/InP surface emitting laser. Electron. Lett. 1993; 29: 913-914.
[51] K. Iga, S. Ishikawa, S. Ohkouchi, and T. Nishimura, "Room-temperature pulsed oscillation of GaAlAs/GaAs surface-emitting injection laser," *Appl. Phys. Lett.*, vol. 45, pp. 348–350, 1984.
[52] F. Koyama, S. Kinoshita, and K. Iga, "Room-temperature continuous wave lasing characteristics of GaAs vertical cavity surface-emitting lasers," *Appl. Phys. Lett.*, vol. 55, pp. 221–222, 1989.
[53] Mid-Infrared Semiconductor Optoelectronics, A. Krier Ed. Springer Series in OPTICAL SCIENCES, Springer-Verlag London Limited 2006.
[54] M. Tan, "Progress in long wavelength VCSELs," in *Proc. Lasers Electro-Optics Soc., 15th Annu. Meet. IEEE*, vol. 1, 2002, pp. 269–270.
[55] Sale, T. E. (1995) Vertical Cavity Surface Emitting Laser, John Wiley & Sons, Inc., New York.
[56] Hadley, G. R., Lear, K. L., Warren, M. E., et al. (1996) Comprehensive numerical modeling of vertical cavity surface emitting lasers [J]. IEEE Journal of Quantum Electronics, 32(4), 607 615.
[57] Margalit, N. M., Zhang, S. Z., and Bowers, J. E. (1997) Vertical cavity lasers for telecom applications [J]. IEEE Communications Magazine, 35(5), 164 170.
[58] Chow, W. W., Choquette, K. D., Crawford, M. H., et al. (1997) Design, fabrication, and performance of infrared and visible vertical cavity surface emitting lasers. IEEE Journal of Quantum Electronics, 33(10), 1810 1824.
[59] Jianjun Gao, East China Normal University, Shanghai, China, Optoelectronic Integrated Circuit Design and Device Modeling, John Wiley & Sons (Asia) Pte Ltd, first edition published 2011.
[60] Semiconductor Nanostructures for Optoelectronic Applications, Todd Steiner *Editor,* Artech House, Inc. Boston , London, 2004.
[61] Safa Kasap, Harry Ruda, Yann Boucher, An Illustrated Dictionary of Optoelectronics and Photonics: Important Terms and Effects, Version 1.3 (October 2000).
[62] Giboney KS, Aronson LB, Lemoff BE. The ideal light source for datanets. IEEE Spectrum 1998;35(2):43–53.
[63] For recent reviews, see: "Special issue: III–V–N Semiconductor Alloys", J.W. Ager,

W.Walukiewicz (eds.), Semicond. Sci. Technol. 17 (2002).
[64] "Special issue: The Physics and Technology of Dilute Nitrides", N. Balkan (ed.), J. Phys. Condens. Matter 16 (2004) ;M. Kondow, K. Uomi, A. Niwa, T. Kitatani, S. Watahiki, Y. Yazawa, Jpn. J. Appl. Phys. 1, Regul. Pap. Short Notes 35, 1273 (1996); *ibid*., Electron. Lett. 32, 2244 (1996); *ibid*., IEEE J. Sel. Top. Quantum Electron. 3, 719 (1997); *ibid*., J. Phys. Condens. Matter 16, S3229 (2004)
[65] J.S. Harris Jr., Semicond. Sci. Technol. 17, 1 (2002); *ibid*., GaInNAs and GaInNAsSb: Long wavelength lasers, in CRC LLC, Boca Raton, FL (Taylor & Francis London, UK), Chap. 14, p. 395 (2004)]; Dilute III-V Nitride Semiconductors and Material Systems: Physics and Technolog, published bay Ayse Erol, Springer-verlag Berlin, Heidelberg, series in material science, 2008.
[66] Y. Ohno, D. K. Young, B. Beschoten, F. Matsukura, H. Ohno, D. D. Awschalom, Nature 402, 790 (1999).
[67] H. Ohno, Science **281** (1998) 951-956.
[68] H. Ohno, D. Chiba, F. Matsukura, T. Omiya, E. Abe, T. Dietl, Y. Ohno & K. Ohtani, Nature **408** (2000) 944-946.
[69] Y. Unjong, A.M. Nili, K. Mikelsons, B. Moritz, J. Moreno, and M. Jarrell, Nonlocal Effects on Magnetism in the Diluted Magnetic Semiconductor $Ga_{1-x}Mn_xAs$, Physical Review Letters, PRL **104**, (2010) 037201.
[70] Semiconductor Spintronics and Quantum Computation edited by D. D. Awschalom, N. Samarth, and D. Loss (Springer-Verlag, Berlin, 2002).
[71] N. Samarth, Solid State Phys. **58**, (2004) 1.
[72] A. H. MacDonald et al., Nature Mater. **4**, (2005) 195.
[73] K.S. Burch, D.D. Awschalom, D.N. Basov, Journal of Magnetism and Magnetic Materials **320** (2008) 3207–3228
[74] Matteo Pesci, Federico Gallino, Cristiana Di Valentin, and Gianfranco Pacchioni, J. Phys. Chem. C 2010, **114**, 1350–1356, Nature of Defect States in Nitrogen-Doped MgO.
[75]T. Jungwirth, Jairo Sinova, J. Masek, J. Kucera, A.H. Mac Donald, Theory of ferromagnetic (III,Mn)V semiconductors, J. Mod. Phys. **78** (2006) 809.
[76] R. Q. Wu, G. W. Peng, L. Liu, Y. P. Feng, Z. G. Huang, Q. Y. Wu, Cu-doped GaN: A dilute magnetic semiconductor from first-principles study, Appl. Phys. Lett. **89** (2006) 062505
[77] T. Hayashi, Y.Hashimoto, S. Katsumoto, Y. Iye, Effect of low-temperature annealing on transport and magnetism of diluted magnetic semiconductor (Ga,Mn)As, Appl. Phys. Lett. **78** (2001) 1691.
[78] T. Kuroiwa, T. Yasuda, F. Matsukura, A. Shen, Y. Ohno, Y. Segawa, H. Ohno, Faraday rotation of ferromagnetic (Ga, Mn)As, Electron. Lett. **34**, (1998) 190.
[79] H. Ohno, F. Matsukura, T. Omiya, and N. Akiba, Spin-dependent tunneling and properties of ferromagnetic Ga,Mn.As, J. Appl. Phys. **85** (1999) 4277.
[80] H. Ohno, F. Matsukura, Y. Ohno, General Report Semiconductor Spin Electronics, JSAP

International **5** (2002) 4.

[81] M. Levy, R. Scarmozzino, R.M. Osgood Jr., R. Wolfe, F.J. Cadieu, H. Hedge, C.J. Gutierrez, G.A. Prinz, J. Appl. Phys. **75** (1994) 6286.

[82] H. Shimizu, M. Tanaka, Appl. Phys. Lett. **81** (2002) 5246.

[83] W. Zaets, K. Ando, IEEE Photonics Technol. Lett. **11** (1999) 1012.

[84] H. Shimizu, M. Miyamura and M. Tanaka: J. Vac. Sci. & Technol. B **18**, 2063 (2000).

[85] H. Akinaga, S. Miyanishi, K. Tanaka, W. Van Roy and K. Onodera: Appl. Phys. Lett. **76**, 97 (2000).

[86] R. Schulz, T. Korn, U. Wurstbauer, D. Schuh, W. Wegscheider, and C. Schüller, Ultrafast optical studies on GaAs/AlGaAs/GaMnAs quantum, 29th International Conference of the Physics of Semiconductors, AIP Conf. Proc. **1199**, 155 (2010).

[87] P. Van Dorpe, Z. Liu, W. Van Roy, V. F. Motsnyi, M. Sawicki, G. Borghs, and J. De Boeck, *Appl. Phys. Lett.*, **84**, 3495 (2004)

[88] R.C. Myers, M. Poggio, N. P. Stern, A. C. Gossard, and D. D. Awschalom, *Phys. Rev. Lett.* **95**, 017204 (2005).

[89] T. Amemiya, H. Shimizu, P.N. Hai, M. Tanaka, Y. Nakano, Nonreciprocal propagation of light without external magnetic fields in a semiconductor waveguide isolator with a MnAs layer, Journal of Magnetism and Magnetic Materials 310 (2007) 2161–2163.

[90] B. **Merabet**, Y. Al-Douri, H. Abid, Ali H. Reshak, Electronic and optical properties of $(Al_xGa_{1-x})_{1-y}Mn_yAs$ single crystal: a new candidate for integrated optical isolators and spintronics, Journal of Materials Science, J Mater Sci, DOI 10.1007/s10853-012-6792-5.

[91] Y. Morishita, A. Tsuboi, H. Suzuki, K. Sato, Molecular-Beam Epitaxy of AlGaMnAs, J. Magn. Soc. Jpn. **23** (1999) 93.

[92] D. Chiba, M. Yamanouchi, F. Matsukura, E. Abe, Y. Ohno, K. Ohtani, H. Ohno, Electric Field Effect on the Magnetic Properties of III–V Ferromagnetic Semiconductor (In,Mn).As and ((Al),Ga,Mn)As, Journal of superconductivity, J. superconductivity **16** (2003) 179.

[93] P. Bhattacharya, M. Holub, and D. Saha, Spin-polarized surface-emitting lasers, phys. stat. sol. (c) 3, No. 12, 4396–4400 (2006).

III. 1. Introduction

In the early twentieth century, the physicists discovered that the laws of classic mechanics cannot describe the behavior of small particles such as electrons [1], but these are governed by the laws of quantum mechanics that will allow to calculate and predict chemical and physical properties of the atomic and molecular systems. the knowledge of the electronic properties allows to obtain information on structural, mechanical, electrical, vibrational, thermal and optical properties. However, the electrons and the nuclei that compose the materials constitute a multiple bodies system in strong interactions, which means that the direct solution of Schrödinger equation is impossible. Thus, the expression used by Dirac in 1929 **[**2] "Progress in knowledge depends primarily on the development of approximation techniques as accurate as possible".

III.2. The basic approximations

A crystal consists of a very large number of interacting particles, the electrons and atomic nuclei, so that the calculation of the energy states system necessarily involves a number of simplifying assumptions. The total Hamiltonian of the system is written [3]

$$H_{tot} = T_n + V_{nn} + V_{ne} + V_{ee} + T_e \qquad \text{(III.1)}$$

where T_e and T_n represent the kinetic energies of electrons and nuclei and V_{ee}, V_{en} and V_{nn} are the energies of electron-electron interaction, electron-nucleus and nucleus nucleus, respectively. The first approximation is to limit the interactions between particles at the more important term that consists the Coulomb interaction. The Hamiltonian system is then written

$$H= -\frac{\hbar^2}{2}\sum_i \frac{\nabla^2_{\vec{R}_i}}{M_i} - \frac{\hbar^2}{2}\sum_i \frac{\nabla^2_{\vec{r}_i}}{m_e} - \frac{1}{4\pi\varepsilon_0}\sum_{i,j}\frac{e^2 Z_i}{\left|\vec{R}_i - \vec{r}_i\right|} + \frac{1}{8\pi\varepsilon_0}\sum_{i\neq j}\frac{e^2}{\left|\vec{r}_i - \vec{r}_j\right|} \qquad \text{(III.2)}$$

where the indices *i*, *j* and I, J refer respectively to the electrons and nuclei, Z is the nuclear charge. The stationary states of energy and the wave functions of the system are given by the solutions of the Schrödinger equation

$$H\,\psi(r, R) = E\,\psi(r, R) \qquad \text{(III.3)}$$

where *R* represents the coordinates of nuclei and *r* those of the electrons. Electrons and atomic nuclei have very different masses so that one can use the Born-Oppenheimer approximation to separate, as in the study of the hydrogen atom, the eigenvalue equation cores from that of the

electrons. The eigenstates of the system are then characterized by the wave functions products of the electron wave function by a wave nuclear function

$$\psi(r, R) = \psi_n(R)\, \psi_e(r, R) \qquad \text{(III.4)}$$

The Schrödinger equation is written

$$[T_e + T_n + V_{ee}+V_{en}+V_{nn}]\, \psi_n(R)\, \psi_e(r, R)=E\, \psi_n(R)\, \psi_e(r, R) \qquad \text{(III.5)}$$

and reduces to two interdependent equations

$$[T_e + V_{ee}+V_{en}]\, \psi_e(r, R)= E_e\,(R)\, \psi_e(r, R) \qquad \text{(III.6.a)}$$

$$[T_n + V_{nn}+ E_e\,(R)]\, \psi_n(R) =E\, \psi_n(R) \qquad \text{(III.6.b)}$$

These equations are the basic equations of the so-called "adiabatic approximation". The first gives the electronic energy for a determined value *R* of the nuclear coordinates. This electronic energy then appears as a potential contribution in the eigenvalue equation of motion of the nuclei. To study the electronic energy states of the crystal we use only the equation (III.6.a), the cores being assumed to be fixed to their equilibrium position. But this equation expresses the evolution of a many-body system and remains a very difficult problem not yet solved. To simplify this problem, we place ourselves in the approximation to an electron. This approximation is to globalize the electron-electron interactions and write that each electron evolves in a medium potential resulting from the presence of other electrons. The Schrödinger equation of an electron is then written

$$H_{HF}\, \psi_e(r) =E_e\, \psi_e(r) \qquad \text{(III.7)}$$

where H_{HF} is the Hartree-Fock Hamiltonian given by

$$H_{HF} = -\frac{\hbar^2}{2m}\nabla^2 - \sum_i \frac{e^2 Z_i}{\left|\vec{r} - \vec{R}_i\right|} + V_{coul} + V_{exch} \qquad \text{(III.8)}$$

The first term represents the interaction potential energy of electrons-nuclei, the V_{coul} and V_{exch} terms globalize the electron-electron interactions. The Hartree-Fock approximation, which reduces the *n* body problem to the one-electron one, is (in some cases) a poor approximation. Nevertheless, it is the only way to solve the problem and gives good results in calculating the structure of energy bands in semiconductors. Solving the Hartree-Fock equation is still a problem mathematically very difficult in that it requires a self-consistent

(autocoherent) approach. Indeed, the eigenfunctions depend on the Hamiltonian that is itself function of the eigenfunctions by its components V_{coul} and V_{exch}. This is the reason simplifies the problem by representing the potential see by the electrons with a term $V_c(r)$ so-called the "crystalline potential", which is constructed from atomic potentials associated with each atom constituting the crystal lattice, taking into account the symmetry properties of the crystal. The equation is then written

$$\left[-\frac{\hbar^2}{2m}\nabla^2 + V_C(r) \right] \Psi_n(k,r) = E_n(k)\Psi_n(k,r) \qquad \text{(III.9)}$$

Different methods exist for solving this equation and obtain the electronic states of the crystal: the LCAO (Linear Combinations of Atomic Orbitals), the OPW(Orthogonalized Plane Waves), the Pseudopotential method, the APW (Augmented Plane Waves),...

To summerize, in a multiple particles system, where strong interactions between electrons exist, the solution of the Schrödinger equation is available only with certain approximations. In terms of first principles methods, two main schools exist:

- The Hartree-Fock (HF) and post-Hartree-Fock approximations, common to chemists;
- The methods of the Density Functional Theory (DFT), most used by physicists.

Their common objective is to solve the Schrödinger equation without introducing a parameter adjusted to the experience, i.e., to determine the energy (E) and the wavefunction (Ψ) of a quantum system described by the equation $E\Psi = H\Psi$, where H is the Hamiltonian operator.

III.3. History of Density Functional Theory (DFT)

Thanks to the Born-Oppenheimer approximation, the problem of solving the Schrodinger equation is reduced to that of the behavior of electrons, but it remains still very complex. The Schrodinger equation does not admit analytical solutions except in very simple cases such is the case of the hydrogen atom **[4]**. The difficulty in describing the electron interaction requires making approximations to solve this problem. We have to be placed generally in a mean-field assumption, where each electron moves in an effective potential generated by the other nuclei and electrons. We can therefore look for the total wave function as a product of one particle wave functions. In 1928, Hartree [5] proposed an N electrons wave function $\psi(\mathbf{r}_1, \mathbf{r}_2, \ldots, \mathbf{r}_N)$ represented as the product of the one particle wave functions,

$$\phi\ (r_1, r_2, \ldots, r_N) = \phi_1(r_1)\ \phi_2(r_2) \ldots . \ \phi_N(r_N) \qquad \text{(III.10)}$$

A solution to $H\phi = E\phi$ is given by any state that meets the condition of stationarity

$$\delta \frac{\langle \phi | H | \phi \rangle}{\langle \phi | \phi \rangle} = 0 \qquad \text{(III.11)}$$

Each wave function to a particle is then the solution Schrödinger equation to an electron

$$\left[-\frac{1}{2}\nabla^2 + V_{ext} + \Phi_i \right] \phi_i(r) = \varepsilon_i \phi_i(r) \qquad \text{(III.12)}$$

where V_{ext} is the potential due to nuclei and Φ is the mean field representing the Coulomb interaction with the other electrons given by the Poisson equation

$$\nabla^2 \Phi_i = 4\pi \sum_{j=1, i \neq j}^{N} \left| \phi_j \right|^2 \qquad \text{(III.13)}$$

In the mean field theory, the electron motion is assumed uncorrelated. In 1930 Fock [6] showed that the wave function of Hartree (III.10) violates the exclusion principle of Pauli because it is not antisymmetric with respect to the exchange of any two particles. He proposed to correct this defect by adding an additional term of the non-local exchange, which complicates considerably the calculations. The wave function ϕ (r_1, r_2, . . ., r_N) is then replaced by a Slater determinant of one-electron wave functions, which is antisymmetric with respect to the exchange. We obtain then the Hartree-Fock equations

$$\left[-\frac{1}{2}\nabla^2 + V_{ext} + \Phi_i \right] \phi_i(r) + V_{exch} \phi_i(r) = \varepsilon_i \phi_i(r) \qquad \text{(III.14)}$$

where $V_{exch}\phi_i(r)$ is the added non-local exchange term

$$V_{exch}(r) = -\sum_{i \neq j} \int dr \frac{\phi_j^*(r')\phi_i^*(r')}{\left| r - r' \right|} \phi_j(r) \qquad \text{(III.15)}$$

The system of equations (III .14) can be resolved with a self-consistent manner to the extent that the potential depends on the wave functions. The Hartree-Fock approximation leads to good results, especially in molecular physics, but it still provides an upper bound to energy. It does not include the effects of electron correlations. It can be improved by including the correlation effects beyond the approximation: This is called the configuration interaction. This method leads, in principle, to the exact wave function but it is extremely expensive because the number of configurations increases very rapidly with the number of electrons. Therefore, it can only treat the systems with few electrons as small molecules. The Hartree-Fock is still an essential reference point. Shortly after the original paper by Schrodinger, Thomas [7] and Fermi [8] proposed an alternative method of solving the equation of Schrodinger based solely on the electron density ρ (r). The Thomas-Fermi method assumes that the movements of electrons are uncorrelated and that the kinetic energy can be described by a local

approximation based on the results for free electrons (proportional to $[\rho(r)]^{5/3}$). A little later, Dirac [9] proposed that the exchange effects are taken into account by incorporating a term from the energy density in exchange a gas electron homogeneous. The Thomas-Fermi approximation is fairly rudimentary. For example, it does not allow the formation of molecules. It was nevertheless successfully applied in the field of plasma physics. All these works were essential to developing the density functional theory (DFT) which we will present now. In 1964, Hohenberg and Kohn [10] have shown the following theorems relied on the DFT :

1. The energy of the ground state of a system with many electrons in an external potential $V_{exch}(r)$ can be written:

$$E\left[\rho(r)\right] = \int V_{exch}(r)\rho(r)dr + F\left[\rho(r)\right] \qquad \text{(III.16)}$$

where ρ (r) is the electron density and F[ρ(r)] is a universal functional of ρ that contains the kinetic and Coulomb contributions to energy. And there is one relationship to an additive constant between $V_{exch}(r)$ and ρ. The functional F[ρ(r)] is universal in the sense that it does not depend on external potential which acts on the system. this functional is not accurately known. The $\int V_{exch}(r)\rho(r)dr$ term represents the nuclei-electrons interaction.

2. Variational principle: the functional F[ρ(r)] reaches its minimum according to the variations of ρ(r) when the density reaches its ground state:

$$E_0 = \min E\left[\rho(r)\right] \qquad \text{(III.17)}$$

The minimum value of E[ρ(r)] is the energy of the ground state. The density that leads to this energy is the exact density of the ground state. It remains to determine F[ρ(r)]; formally:

$$\mathrm{F}[\rho(\mathrm{r})] = T\left[\rho(r)\right] + V_{ee}\left[\rho(r)\right] \qquad \text{(III.18)}$$

where T [ρ (r)] is the kinetic energy of the electronic system and V_{ee} [ρ (r)] is the term of the electron-electron interactions. As we do not know the expression of T neither that of V_{ee}, Kohn and Sham have proposed the following separations:

first:

$$T\left[\rho(r)\right] = T_s[\rho(\mathrm{r})] + (T[\rho(\mathrm{r})] - T_s[\rho(\mathrm{r})]) \qquad \text{(III.19)}$$

where $T_s[\rho(r)]$ is the kinetic energy of an electron gas without interaction and with the same electron density. This term comes from an artificial construct. There is no known expression of T_s in terms of ρ (r), however, we know how to calculate it by reintroducing an orbital description $(\rho(r) = \sum_i f_i |\phi_i(r)|^2)$, where f_i are the occupation numbers of orbitals.

second:

$$V_{ee}[\rho(r)] = E_H[\rho(r)] + (V_{ee}[\rho(r)] - E_H[\rho(r)]) \quad \text{(III.20)}$$

where $E_H[\rho(r)]$ is the Coulomb interaction energy of a classical charge distribution (that is to say that does not take into account the discrete aspect of the electrons). It is written by

$$E_H[\rho(r)] = \frac{1}{2}\int \frac{\rho(r)\rho(r')}{|r-r'|}dr \quad \text{(III.21)}$$

Finally, F [ρ (r)] splits into three parts

$$F[\rho(r)] = T_S[\rho(r)] + E_H[\rho(r)] + E_{ex}[\rho(r)] \quad \text{(III.22)}$$

where we define the terms of exchange and correlation

$$E_{ex}[\rho(r)] = [V_{ee}[\rho(r)] - E_H[\rho(r)]] + [T[\rho(r)] - T_s[\rho(r)]] \quad \text{(III.23)}$$

In $E_{ex}[\rho(r)]$, the exchange energy comes from the fact that the wave function of a system with many electrons, which are fermions, must be antisymmetric with respect to the exchange of any pair of electrons. This antisymmetry products a spatial separation between the electrons of the same spin, which reduces the Coulomb energy of the electronic system. It is this contribution which is called the exchange energy. The exchange energy of a uniform electron gas is known. The Coulomb energy can be reduced even if the electrons with opposite spins are spatially separated. This difference is called the correlation energy. It is very difficult to calculate the correlation energy of a complex system. In summary, $E_{ex}[\rho(r)]$ is a term containing the exchange and correlation contributions to the energy and the contribution from electronic interactions not taken into account in T_S and E_H.

Finally the only unknown of our problem becomes the term of exchange and correlation $E_{ex}[\rho(r)]$ which is not easy to calculate but, as it will be checked, has the advantage to be much smaller. It is mostly much smaller than $\int V_{ext}(r)[\rho(r)]dr$, $E_{ex}[\rho(r)]$ and $E_H[\rho(r)]$, three terms that determine general properties of the system. We deduce the equations of Kohn and Sham [11] that solve the problem:

$$V_{eff}(r) = V_H[\rho(r)] + V_{xc}[\rho(r)] + V_{ext}(r) \qquad \text{(III.24)}$$

$$\rho(r) = \sum_{i=1}^{N} f_i \left|\phi_i(r)\right|^2 \qquad \text{(III.25)}$$

$$\left[-\frac{1}{2}\nabla^2 + V_{eff}(r)\right]\phi_i(r) = \varepsilon_i \phi_i(r) \qquad \text{(III.26)}$$

where: ϕ_i are the states to a single particle

$V_H[\rho(r)] = \frac{1}{2}\int \frac{\rho(r')}{|r-r'|}dr'$ is the Hartree potential for electrons

$V_{xc}[\rho(r)] = \frac{\partial E_{xc}[\rho(r)]}{\partial \rho(r)}$ is the potential still unknown of exchange and correlation.

The Equation (III .26) can be seen as a Schrodinger equation for a single particle where the external potential has been replaced by the effective potential defined in (III .24). The wave functions so obtained have no physical meaning. The original problem is therefore for the resolution of N equations of this type. So far the DFT is an accurate method, but in order to that the DFT and the Kohn and Sham equations become usable in practice, we need to provide a form of $E_{xc}[\rho(r)]$ and for this you have to go through an approximation.

III.4. The Local Density Approximation (LDA)

To approximate the density functional $E_{xc}[\rho(r)]$, Kohn and Sham proposed in 1965 the local density approximation (LDA). In this approximation, we assume that the electron density varies sufficiently slowly within the system so that we can write:

$$E_{xc}^{LDA}[\rho(r)] = \int \rho(r)\varepsilon_{xc}^{\text{hom}}(\rho(r))d^3r \qquad \text{(III.27)}$$

where $\varepsilon_{xc}^{\hom}(n)$ is the energy density of a homogeneous electron gas of a density n. In other words, we assume that around each point r, we can replace the real system by a homogeneous electron gas of density ρ (r).

The term exchange of such a gas has been determined exactly by the techniques Monte Carlo by Ceperley et al. [12]. which have tabulated the exchange-correlation term $\varepsilon_{xc}^{\hom}$ depending on the radius of Wigner-Seitz $r_s = [\frac{3}{4\pi}\rho(r)]^{\frac{1}{3}}$ There are many works parameterization $\varepsilon_{xc}^{\hom}$ such as for example those of Vosko, Wilk and Nusair [13] or Perdew and Zunger [14]. All these functionals usually lead to very similar results.

III. 5. The Generalized gradient approximations (GGA)

The results from an LDA calculation are often satisfactory. But the generalized gradient approximation (GGA) is used in many cases (but it is not systematic) better describe the bonds and thus give better results on total energies and geometries for best weak bonds. It also tends to take better into account the inhomogeneity of the density than the LDA. The exchange-correlation energy in GGA is written as follows:

$$E_{xc}^{LDA}[\rho(r)] = \int f(\rho(r), |\nabla\rho(r)|) d^3r \qquad \text{(III.28)}$$

where *f* is a function of the local density and local density gradient. Like $\varepsilon_{xc}^{\hom}$ in LDA, in GGA f must be set in an analytical form in order to facilitate the calculations and as there are different forms of $\varepsilon_{xc}^{\hom}$ in LDA, there are different parametrizations of the function *f* in GGA., In Fig.III.1, the self-consistent cycle of the Density Functional Theory (DFT) is given:

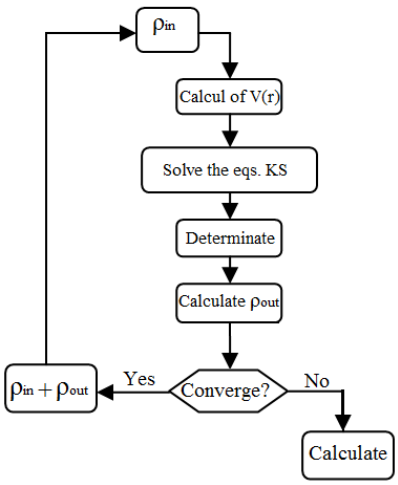

Fig.III.1 Self-consistent cycle of the density functional theory (DFT).

III . 6. What is a pseudo potential?

We seek to study the system {core+ electrons} and thus to calculate:

$$E_{ext}[\rho(r)] = \frac{1}{\Omega}\int_{\Omega} V_{ext}(r)\rho(r)dr \qquad \text{(III.29)}$$

where $V_{ext}(r)$ is the Coulomb potential created by the naked nuclei. We have seen that one can distinguish between two types of electrons: the core electrons and valence electrons. Core orbitals are the lowest in energy, are located near the nucleus, are largely insensitive to the environment and do not participate in chemical bonds. In addition, they are difficult to represent on a plane wave as they generally have large oscillations around the nuclei. In contrast, the valence orbitals are not localized and thus extend away from the nucleus. What they determine to first order the physicochemical properties. The idea introduced by Fermi is then the simplification of electronic structure calculations by eliminating heart conditions. The effect of core electrons is replaced by an effective pseudopotential. The system which is treated in this system is not {the naked nucleus + electrons} but {[naked nucleus +core electrons] + valence electrons} = {"ions"+ valence electrons}. one therefore seeks to replace a potential electron-nuclei by a lower potential, which reflects the screening of the nucleus by the core electrons. The pseudopotentials are potentials that lead to a reference electron configuration of the isolated atom to the exact eigenvalues and eigenfunctions as regular as possible, consistent with the atomic wave functions beyond a certain radius chosen called cutoff radius r_c. These eigenfunctions, called pseudofunctions, have the same properties diffusion (the same logarithmic derivatives) that the wave functions real. They are asked to have the greatest potential transferability that is to say that they are usable in as many

systems as possible, that is to say, in different thermodynamic environments. There are three main types of pseudopotentials, which each have their advantages and disadvantage:

* The pseudopotentials of maintained stnorm introduced by Hamman et al. [15].

* The ultra-soft pseudopotentials introduced by Vanderbilt [16].

* The "dual-space Gaussian" pseudopotentials introduced by Goedecker et al. [17].

III. 7. Methods for calculating the electronic structures

To better understand all properties (electronic, optical, thermal, mechanical or magnetic) of the materials, different methods for calculating electronic structures have been developed and made available to researchers:

*III.7.1 Empirical methods: using the experience to find the values of parameters, which can be applied to process of materials formation (flow, spraying, crystallization).

* III.7.2 Semi-empirical methods: requiring atomic parameters and experimental results to predict other properties that have not yet been determined experimentally, and also for studying complex systems.

* III.7.3 Ab-initio (or first-principles) methods: that use only the atomic constants as input parameters for solving the Schrödinger equation, and can accurately determine the spectroscopic, structural, and energetic properties.

The researchers have developed methods of first principles, based on theoretical concepts, for solving the Schrödinger equation based on the DFT, including three groups:

*III.7.4 Methods based on a linear combination of atomic orbitals (LCAO) [18, 19], used, for example, for the bands "d" of the transition metals.

*III.7.5 The methods derived from the orthogonalized plane waves (OPW) [19, 20], that suit better the conduction band of "sp" character for simple metals.

*III.7.6 The cellular methods of the type "augmented plane wave (APW)" **[**21] and the method of the function Green of Korringa, Kohn and Rostoker (KKR) [22,23], applicable to a wider variety of materials.

*III.7.7 The Linearized methods developed by Andersen **[**24**]** : Linearized augmented plane wave (LAPW) and linearized "Muffin-Tin" orbitals (LMTO), that can save several orders of magnitude in computation time.

III.8. The Linearized Augmented Plane Wave (LAPW) method

The LAPW method is an improved method of augmented plane waves (APW) developed by Slater [25- 27] In 1937, Slater describes the Augmented Plane Wave (APW) method in his article [21]. In the vicinity of an atomic nucleus, the potential and wave functions are of the form "Muffin-Tin" (MT) with a spherical symmetry inside the MT sphere of a radius R_α. Between Atoms, the potential and wave functions can be considered as being smooth. Consequently, the wave functions of the crystal are developed in different bases depending on the considered region: Radial Solutions of the Schrödinger equation inside the MT

spheres and plane waves in the interstitial region (Figure III-2).

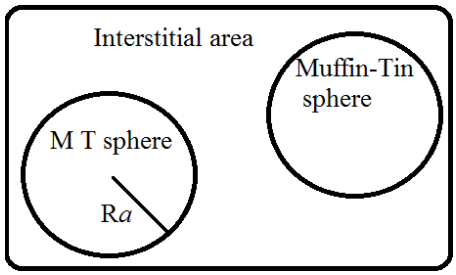

Fig.III. 2 Muffin-tin potential.

The unit cell is divided into (I) non-overlapping atomic spheres (centered at the atomic sites) and (II) an interstitial region (area). In the two types of regions different basis sets are used: inside atomic sphere, of radius R_α, a linear combination of radial functions times spherical harmonics $Y_{lm}(r)$, and in the interstitial region a plane wave expansion is used.

$$\phi(r) = \frac{1}{\Omega^{1/2}} \sum_G C_G e^{i(G+K)r} \qquad r>R_\alpha \qquad \text{(III.30)}$$

$$\phi(r) = \sum_{lm} A_{lm} U_l(r) Y_{lm}(r) \qquad r \square R_\alpha$$

(III.31)

Where Ω is the volume of the cell,. C_G and A_{lm} are the expansion coefficients in spherical harmonics Y_{lm}. The function U_l (r) is a regular solution of the Schrödinger equation for the radial part which can be written as:

$$\left\{-\frac{d^2}{dr^2}+\frac{l(l+1)}{r^2}+V(r)-E_l\right\}U_l(r)=0 \qquad \text{(III.32)}$$

where V (r) is the muffin-tin potential and E_l represents the energy of linearization. The radial functions defined by (III.32) are orthogonal to any eigenstate of the core but this orthogonality disappears at the sphere boundaries [24] as shown in the following Schrödinger equation:

$$(E_2-E_1)rU_1U_2=U_2\frac{d^2rU_1}{dr^2}-U_1\frac{d^2rU_2}{dr^2} \qquad \text{(III.33)}$$

where U_1 and U_2 are the radial solutions for the energies E_1 and E_2. The collection is constructed using the equation (III.32) and integrating by parts.

Slater justifies the choice of these particular functions noting that the plane waves are solutions of the Schrödinger equation when the potential is constant. As for the radial functions, they are solutions in the case of a spherical potential, when E_l is an eigenvalue. This approximation is very good for materials with cubic structure face-centered, and less satisfactorily with the decrease in symmetry of the material. To ensure continuity of the function ϕ(r) on the surface of the muffin-tin sphere, the A_{lm} coefficients must be developed according to the C_G coefficients of plane waves existing in the interstitial regions. These coefficients are thus expressed by the following expression:

$$A_{lm}=\frac{4\pi i^l}{\Omega^{1/2}U_l(R_\alpha)}\sum_G C_G\, j_l(|K+g|R_\alpha)Y_{lm}^*(K+G) \qquad \text{(III.34)}$$

The origin is taken at the center of the sphere, and A_{lm} coefficients are determined from those of plane waves C_G. The energy parameters E_l are called the variational coefficients of the APW method. The individual functions, labeled by G become thus compatible with the radial functions in the spheres, and we obtain the augmented plane wave (APWS). The APW functions are solutions of the Schrödinger equation in the spheres, but only for energy E_l. Consequently, the energy E_l must be equal to that of the band index G. This means that the energy bands (for a point k) cannot be obtained by a simple diagonalization, and it is necessary to treat the secular determinant as a function of energy. The APW method, and built, presents some difficulties related to the function U_l (R_α) that appears in the denominator of equation (III.34). Indeed, according to the value of the parameter E_l, the value of U_α (R_α)

can become zero at the surface of the muffin-tin sphere, resulting in separation of radial functions with respect to plane wave functions.

To overcome this problem several changes were made to the APW method, including those proposed by Koelling and Andersen [28]. The modification is to represent the wave function ϕ(r) inside the spheres by a linear combination of radial functions U_l (r) and their derivatives with respect to the energy U□(r), giving rise to the FP-LAPW method

III. 9. Principle of the LAPW method

In the LAPW method, the basic functions in the muffin-tin spheres are linear combinations of the radial functions U_l (r) Y_{lm} (r) and their derivatives U□$_l Y_{lm}$ (r) with respect to energy. The functions U_l are defined as in the APW method (III.32) and the Y_{lm} function U (r) must satisfy the following condition:

$$\left\{-\frac{d^2}{dr^2}+\frac{l(l+1)}{r^2}+V(r)-E_l\right\}rU_l(r)=rU_l(r) \qquad \text{(III.35)}$$

In the nonrelativistic case, these radial functions U_l (r) and U□$_l$ (r) ensure, to the surface of the muffin-tin sphere, the continuity with the plane waves outside. The wave functions thus augmented become basic functions (LAPW) of the FP-LAPW method:

$$\phi(r)=\frac{1}{\Omega^{1/2}}\sum_G C_G e^{i(G+K)r} \qquad r>R_\alpha \qquad \text{(III.36)}$$

$$\phi(r)=\sum_{lm}[A_{lm}U_l(r)+B_{lm}U_l(r)]Y_{lm}(r) \qquad r\square R_\alpha$$

(III.37)

Where the coefficients B_{lm} correspond to the function U□$_l$ (r) and are similar and that the coefficients A_{lm}. The LAPW functions are plane waves only in the interstitial areas as in the APW method. Inside the spheres, the LAPW functions are better suited than the APW functions. While E_l differs somewhat from the band energy E, a linear combination reproduce the radial function better than APW functions consisting of a single radial function. Therefore, the function U_l can be developed according to its derivative U□$_l$ and the energy E_l.

$$U_l(E,r)=U_l(E_l,r)+(E-E_l)U_l(E,r)+O[(E-E_l)^2] \qquad \text{(III.38)}$$

where $O[(E-E_l)^2]$ represents the squared energetic error.

The method LAPW ensures the continuity of the wave function at the surface of the muffin-tin sphere. But, with this procedure, the calculations become less accurate, compared to APW method, which reproduces the wave functions very well, while the FP-LAPW method causes an error on the wave functions of the order of $(E - E_l)^2$ and another on the energies of bands the order of $(E - E_l)^4$. Despite this order of error, the LAPW functions form a good basis which allows a single E_l, to obtain all the valence bands in a wide energy region. Where this is not possible, one can generally divide the energy window into two parts, which represents a great simplification compared to the APW method. In general, if U_l is equal to zero at the surface of the sphere, its derivative U'_l is not zero. Therefore, the problem of continuity on the surface of the sphere MT will not arise in the LAPW method. Takeda and Kubler [29] proposed a generalization of the LAPW method in which N radial functions and their (N - 1) derivatives are used. Each radial function owns its parameter E_{li} so that the error associated with the linearization is avoided. We find the standard LAPW method for N = 2 and E_{l1} close to E_{l2}, while for N> 2 errors can be reduced. Unfortunately, the use of derivatives of high order to ensure the convergence requires a much larger calculation time than in the standard FP-LAPW method. Singh [25] modified this approach by adding local orbitals at the base without increasing the cutoff energy of plane waves.

III. 10. Role of the energy of linearization (E_l)

The functions U_l and U'_l are orthogonal to any core state strictly restricted to the muffin-tin sphere. But this condition is satisfied only if there is no core states with the same *l*, and therefore, one risk confusing the semi-core states with the valence states. This problem is not treated by the APW method, while the non-orthogonality of some core states in the FP-LAPW method requires a delicate choice of E_l. In this case, we can not calculate without changing E_l. The ideal solution in such cases is to use a local orbital development. However, this option is not available in all programs, and in this case, one must choose a radius of the sphere as large as possible. Finally, it should be noted that various E_l should be defined independently of each other. The energy bands have different orbitals. For an accurate calculation of the electronic structure, E_l must be chosen to be as close as possible to the energy of the band, if the band has the same *l*.

III.11. Development in local Orbitals

The purpose of the LAPW method is to obtain accurate band energies near the energy of linearization E_l **[**24**]**. In most materials, it's sufficient to choose those energies near the center of the bands. This is not always possible and there are materials for which the choice of a single value E_l is not sufficient to calculate all energy bands, this is the case for materials with 4*f* orbitals [26,27] and transition metals [30,31]. This is the fundamental problem of the semi-core states that is intermediate between the valence state and the core. To remedy to this situation it's used either to use multiple energy windows, or using a local orbital development.

III.12. The LAPW+LO method

The development of the LAPW method in local orbitals is to change the orbitals from their base to avoid the use of multiple windows, using a third category of basis functions. The main idea is to treat all bands with a single energy window. Singh [25] proposed a linear combination of two radial functions corresponding to two different energies and the derivative with respect to the energy of one of these functions which gives rise to the LAPW + LO method:

$$\Phi_{lm} = [A_{lm}U_l(r,E_{1,l}) + B_{lm}U_l^{\cdot}(r,E_{1,l}) + C_{lm}U_l(r,E_{2,l})]Y_{lm}(r) \qquad \text{(III.39)}$$

Where the coefficients C_{lm} are of the same nature as the coefficients r□R_α A_{lm} and B_{lm} previously defined. Moreover, this change decreases the error in the calculation of the conduction and valence bands.

III. 13. The APW+*lo* method

Recently, the development of the Augmented Plane Wave (APW) methods from Slater's APW, to LAPW and the new APW+*lo* was described by Schwarz et al. 2001 [32].

The problem of the APW method was the energy dependence of all basic functions. This dependence has been eliminated in the LAPW + LO method, but with a larger set of basis functions. Recently, an alternative approach is proposed by Sjösted et al [33] named the APW + *lo* method. In this method, all the basic functions will be independent on energy and have always the same size as that of the APW method. In this sense, APW + *lo* combines the advantages of the APW method and those of the LAPW + LO method. All the basic functions of APW + *lo* contains two types of wave functions. The first are an augmented plane waves (APW), with a range of fixed energies E_l.

$$\Phi = \frac{1}{\Omega^{1/2}} \sum_{G} C_G e^{i(G+K)} \qquad r>R_\alpha \qquad \text{(III.40)}$$

$$\Phi = \sum_{lm} A_{lm} U_l(r) Y_{lm}(r) \qquad r \square R_\alpha$$

(III.41)

The second type of functions are local orbitals (*lo*) different from that of LAPW + LO method, defined by:

$$\Phi = 0 \qquad r>R_\alpha \qquad \text{(III.42)}$$

$$\Phi = [A_{lm} U_l(r, E_{1,l}) + B_{lm} U_l^{\cdot}(r, E_{1,l}) + C_{lm} U_l(r, E_{2,l})] Y_{lm}(r) \qquad r \square R_\alpha$$

(III.43)

In a calculation, a mixed basis APW + *lo* and LAPW can be used for different atoms and even for different values of the number *l*. In general, we describe the orbitals which converge more slowly with the number of plane waves (like the 3d states of transition metals), or atoms with a small sphere with the APW + lo basis and the rest with a base LAPW [34].

III. 14. The concept of the FP-LAPW method

The linearized augmented plane wave (LAPW) method is among the most accurate methods for performing electronic structure calculations for crystals. It is based on the density functional theory for the treatment of exchange and correlation and uses e.g. the local spin density approximation (LSDA) [32]. In the Full Potential linearized Augmented Plane Waves method (FP-LAPW) [34] no approximation is made on the shape of the potential nor on that of the charge density. These are rather developed in spherical harmonics of the lattice inside each atomic sphere, and Fourier series in the interstitial regions, hence the qualification of "Full-Potential". This method therefore ensures continuity of potential at the surface of the muffin-tin sphere and develops it as follows:

$$\Phi(r) = \sum_{K} V_K e^{iKr} \qquad r>R_\alpha \qquad \text{(III.44)}$$

$$\Phi(r) = \sum_{lm} V_{lm}(r) Y_{lm}(r) \qquad r \square R_\alpha$$

(III.45)

Similarly, the charge density is developed in the form:

$$\Phi(r) = \rho \sum_{K} V_K e^{iKr} \qquad r>R_\alpha \qquad \text{(III.46)}$$

$$\Phi(r) = \sum_{lm} \rho_{lm}(r) Y_{lm}(r) \qquad r \square R_\alpha$$

(III.47)

III.15. The Wien2k code

The Linearized Augmented PlaneWave (LAPW) method has proven to be one of the most accurate methods for the computation of the electronic structure of solids within density functional theory. A full-potential LAPW-code for crystalline solids has been developed over a period of more than twenty years. A first copyrighted version was called **WIEN** and it was published by Blaha et al. [35]. In the following years significantly improved and updated Unix versions of the original **Wien** code were developed, which were called Wien**93**, Wien**95** and Wien**97**. Now a new version, WIEN2k, is available, which is based on an alternative basis set. This allows a significant improvement, especially in terms of speed, universality, user-friendliness and new features. Wien2k is written in Fortran 90 and requires a Unix operating system since the programs are linked together via C-shell scripts. It has been implemented successfully on the Pentium systems running under Linux. It is expected to run on any modern Unix (Linux) system [32].

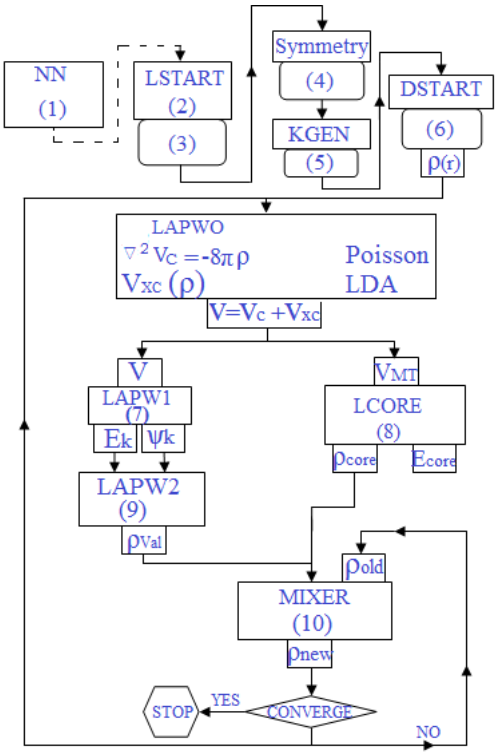

⊗

Fig. III.3 Algorithm of the FP-LAPW method (Wien2K code): (1) check the non-overloapping of spheres; (2) atomestic calcul $H\square_{nl}=E_{nl}\square_{nl}$; (3) atomic density (input file); (4) structure file (input file); (5) Generation of the *k*-mesh; (6) Superpossition of atomic densities; (7) $-\nabla^2+V\square_k= E_k\square_k$; (8) atomestic calcul $H\square_{nl}=E_{nl}\square_{nl}$; (9) $\rho_{val}=\square_k^*\square_k$; (10) $\rho_{new}=\rho_{old}$ $(\rho_{val}+ \rho_{core})$.

References of Chap. III

[1] L. De Broglie, Ann, Phys. **3**, 22 (1925).

[2] Dirac, Proc. Roy. Londres, **123**, 714 (1929).

[3] Henry Mathieu, Hervé Fanet, Physique des semiconducteurs et des composants électroniques Cours et exercices corrigés, 6e édition (2009), Dunod Paris.

[4] Nicolas Richard, Actinides et terres rares sous pression, Approche pseudopotentiel (Doctoral thesis) Département de physique théorique et appliquée, CEA/DAM - Direction Ile - De - France, 2002.

[5] D .R. Hartree. *Proc. Cambridge Philos . Soc.,* 24 :89, 1928.

[6] V . Fock . *Z. Phys.*, 61 :126, 1930.

[7] L.H . THOMAS . *Proc. Cambridge Philos . Soc.,* 23 :542, 1928.

[8] E. **Fer**m **I . *Z. Phy*s** ., 48: i 3, 1928.

[9] P.A .M . Dirac . *Proc . Cambridge Philos. Soc.*, 26:376, 1930.

[10P. Hohenberg and W . Kohn . *Phys. Rev. B,* 136:864, 1964.]

[11] W. Kohn and L.J . Sham . *Phys. Rev. A,* 140 :1133, 1965.

[12] D.M. Ceperley and B .J . Alder. *Phys. Rev . Le t t .* , 45:566, 1980.

[13] S .H. Vosko, L . Wilk, and M. Nusair. *Can . J. Phys* ., 58 :1200, 1980.

[14] J .P. Perdew and A . Zunger. *Phys. Rev. B,* 23:5048, 1981.

[15] D.R. Hamman, M. Schulter , and C . Chiang. *Phys. Rev. Lett .* , 43:1494, 1979.

[16] D. Vanderbilt . *Phys. Rev. B,* **41** :7892 , 1990.

[17] S. Goedecker, M. Teter , and J . Hutter . *Phys. Rev. B,* 54:1703, 1996 ; C . Hartwigsen, S . Goedecker , and J. Hutter . *Phys. Rev. B,* **58** :3641, 1998.

[18] F. Bloch, Z. Phys. **52**, 555(1928)., 19J. C. Slater, « Quantum Theory of Molecules and Solids », V2, Ch. 8 (1965).

[19] J. C. Slater, « Quantum Theory of Molecules and Solids », V2, Ch. 8 (1965).

[20] C. Herring, Phys. Rev. **57**, 1169 (1940).

[21J. C. Slater, Phys. Rev. **51**, 846 (1937).

[22] J. Korringa, Physica **13**, 392 (1947);

[23] F. S. Ham, B. Segall, Phys. Rev. **124**, 1786 (1961).

[24] O. K. Andersen, Phys. Rev. B **12**, 3060 (1975).

[25] D. Singh, Phys. Rev. B **43**, 6388 (1991).

[26] D. J. Singh, Phys. Rev. B **44**, 7451 (1991).

[27] S. Goedecker and K. Maschke, Phys. Rev. B **42**, 8858 (1990).

[28] S. Goedecker and K. Maschke, Phys. Rev. B **42**, 8858 (1990); O. K. Andersen, Phys. Rev. B **12**, 3060 (1975);

[29] T. Takeda and J. Kubler, J. Phys. F **5**, 661 (1979).

[30] D. J. Singh and H. Krakauer, Phys. Rev. B **43**, 1441 (1991).

[31] D. J. Singh, K Schwarz and P. Blaha, Phys. Rev. B **46**, 5849 (1992).

[32] User's Guide, WIEN2k 10.1 (Release 16.06.2010), Peter Blaha, Karlheinz Schwarz, Georg Madsen, Dieter Kvasnicka, Joachim Luitz, Vienna University of Technology, Inst. of Physical and Theoretical Chemistry Getreidemarkt 9/156, A-1060 Vienna/Austria.

[33] E. Sjösted, L. Nordström and D. J. Singh, Solid State Commun. **114**, 15 (2000).

[34] G. H. K. Madsen, P. Blaha, K. Schwarz, E. Sjösted and L. Nordström, Phys. Rev. B. **64**, 195134 (2001).

[35] P. Blaha, K. Schwarz, P. Sorantin, and S. B. Trickey, in Comput. Phys. Commun. 59, 399 (1990)

Part 1: Effect of nitrogen incorporation on the electronic and optical properties of AlGaAsN/GaAs quantum well lasers

IV. I. Introduction

Over the last few years, group III nitrides and their alloys have attracted a great deal of attention as being among the most important materials systems for optoelectronic and electronic applications. The band gap of the III-N-V systems depending strongly on the N-content as well as their lattice parameter and their electron effective mass has made of these alloys attractive materials for long wavelength vertical cavity surface emitting lasers (LW-VCSELs) and high efficiency hybrid solar cell applications. The InP-based systems have been the source for wide reach applications, but due to low electron confinement they have poor high-temperature characteristics and their cost remains too high to design a high volume modern data communication networks.

As such, the GaAs-based systems were proposed as an alternative to the InP-based ones to solve the above problems and a novel material for optoelectronics has been adopted, AlGaAsN, which has not been studied as extensively as the other narrower band gap III-N-V systems such as its homologous InGaAsN. The GaAs-based dilute group III-AsN materials systems with nitrogen content in the few percent range have attracted considerable current interest because of their use as active material in optoelectronic devices such as VCSELs on GaAs emitting at 1.3 μm.

QW lasers have been developed extensively since they exhibit many advantages, such as very low threshold current densities, high coupling efficiencies into optical fibre, single mode operation, narrow static and dynamic linewidth, high output power, large modulation bandwidth, and high lasing temperature. The design optimization of the QW lasers requires a large degree of numerical computation because there are several laser parameters involved such as the quantum well/barrier composition, the number of QWs, the cavity length and the facet reflectivity. The basic properties of AlGaNAs/GaAs materials are of great technological interest and the choice of varying N fraction has provided the flexibility of controlling both electronic and optical properties.

IV. 2. Approximate quantized energy levels

So as to calculate the optical transition wavelength between the quantized energy levels in the AlGaAsN/GaAs heterostructure, a schematic energy band diagram for a typical QW structure is shown in Fig. IV.1, where respectively, ΔE_c and ΔE_v are the discontinuities of the band edges of conduction and valance bands (CBs and VBs) at the heterojunction, E_{cn} and E_{vn} the

energy levels in CBs and VBs, E_g and $E_{tr} = E_g + E_{vn} + E_{cn}$ are the band gap energy and the transition energy between the two quantized energy levels, E_{fc} and E_{fv} are the quasi-Fermi levels for electrons and holes in the well. Assuming that the quantized levels for holes E_{vn} are measured from the top of the VB down into the VB and using the parabolic band model, we can obtain E_{vn} by solving the following eigenvalue equations [1]

$$\frac{m_{vb}}{m_{vw}} = \sqrt{\frac{\Delta E_v - E_{vn}}{E_{vn}}} = \{\tan, -\cot\} \frac{W\sqrt{2m_{vw}E_{vn}}}{(2\hbar)} \{n : even, odd\} \qquad \text{(IV.1)}$$

with $\hbar = h/2\pi$ the Planck's constant, W the well width, m_{vw} and m_{vb} the effectives masses of holes inside of the well and the barrier, respectively.

If $\Delta W_v = \frac{2\hbar}{\sqrt{m_{vw}}} / \sqrt{\Delta E_v \frac{m_{vb}}{m_{vw}}}$ and $\Delta Ev >> Evn$, this later is expressed by [1, 2]

$$E_{vn} = \frac{\left[\frac{(n+1)\pi}{2} \frac{(2\hbar/\sqrt{2m_{vw}})}{W + \Delta W_c}\right]}{\left[1 + \left\{\frac{(n+1)\pi}{2}\right\}^2 \frac{m_{vw}}{m_{vb}} \left(\frac{\Delta W_c}{W + \Delta W_c}\right)^3\right]} \qquad \text{(IV.2)}$$

It should be noted that (IV.2) is an accurate solution to (IV.1) when ΔEv becomes infinity:

$$E_{vn} = \left[\frac{(n+1)\pi}{2} . \frac{2\hbar/\sqrt{2m_{vw}}}{W}\right]^2 \qquad \text{(IV.3)}$$

If we neglect the $(\Delta W_v)^3$ term in (IV.2), we can interpret $(W + \Delta W_v)$ as an effective well width, where ΔWv is induced by a finite barrier height ΔEv. The energy levels E_{cn} for the CB are expressed by (IV.2) if we replace the subscript v by c. We have calculated the subband energies for the VB as a function of $Al_xGa_{1-x}N_yAs_{1-y}$ well widths, and plotted them in Fig.IV 2. For the limit when the well width reduces to zero, the first subband energy for the BV approaches the limit of the VB-edge discontinuity ΔE_v , whereas, the number of energy levels increases with the well width increasing. However, if the barrier width W_b is extremely large the Tunnel effect decreases and the QWs constituting the laser structure act independently. Note that the duplication of the levels (in Fig.IV. 2) is due to the Tunnel effect which decreases for an extremely large barrier width. In other hand, the variation of the effective masses shows the effects of the *strain* on the QW laser performances, which has important applications to optoelectronic and electronic devices.

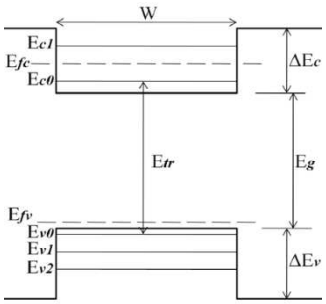

Fig.IV. 1 Band model for a quantum well structure.

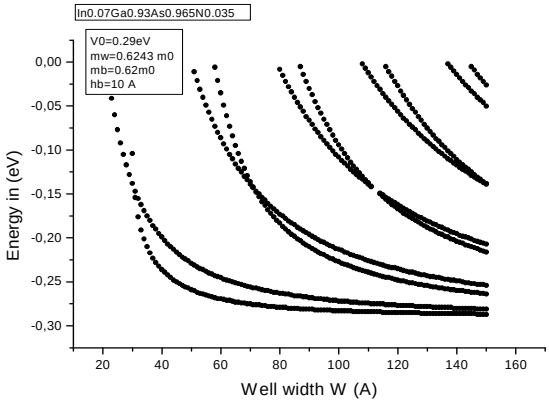

Fig.IV. 2 Quantized energy levels in the valence band(E_{vn}) of $Al_xGa_{1-x}As_{1-y}N_y$ QWs as a function of the well width (W).

The program calculating the variation of the energy as a function of the well width (unique well), given by Fig. IV.2, is as follows [3]

```
$debug
c-------------------------------------------------------------------------
c Author: N. SEKKAL
c Title: NewWidth.for
c Description: This programme calculates the eigenenergies of a quantum
c well versus the well width. It also calculates the charge
c density for a chosen confined level.
c-------------------------------------------------------------------------
implicit real*8(a-h,o-z)
parameter(nombre=10000,Cc=1.,Na=2,n1=1000,zero=0.)
dimension E(n1),E1(nombre+1),D1(nombre+1)
complex(8) A1(n1),A2(n1),B2(n1),B3(n1),M(4,4),Oran,Jj1
Real*8 Mb,Mp
integer Choix
Jj1=cmplx(0.,1.)
crc=.000130921055349
open(unit=1,status='unknown',file='width.dat')
write(*,*)'Choix=1 for energy ; Choix=2 for charge density'
read(*,*)Choix
if(choix.ne.1.and.choix.ne.2) then
print*,'stop, choix must be equal to 1 or to 2'
stop
endif
if(choix.eq.2)then
write(*,*)'Nv le niveau choisi'
read(*,*)nv
write(*,*)'n2 indice du point L abcisse'
read(*,*)n2
endif
write(*,*)'hauteur de barriere en meV'
read(*,*)Vb1
Vb=Vb1*crc
write(*,*)'Mb= barrier mass, example: 0.13 in AlAs'
read(*,*)Mb
write(*,*)'Mp= well mass, example: 0.067 in GaAs'
read(*,*)Mp
c-------------------------------------------------------------------------
```

```
In2=0
do A=2,200,1 ! A=largeur du puits
In2=In2+1
I=0
J=0
If(In2.eq.n2.and.choix.eq.2)then
print*,'fonction d''onde pour Largeur de puits=',A,' Angstroms'
endif
c-------------------------------------------------------------------------
do 10 E2=0,(Vb1-1.D-4),((Vb1-1.D-4)/Nombre)
I=I+1
E1(I)=E2*crc
Eee=E1(I)
call equ (Eee,Vb,Mp,Mb,Ro,xK)
call Trmat (Ro,xK,Mp,Mb,M,A,jj1)
call det(M,Oran)
D1(I)=CDABS(oran)
IF(I.lt.3) GOTO 10
IF (D1(I-2).gt.D1(I-1).AND.D1(I).gt.D1(I-1)) THEN
J=J+1
E(J)=E1(I-1)/crc
Eee=E1(I-1)
call equ (Eee,Vb,Mp,Mb,Ro,xK)
call Trmat (Ro,xK,Mp,Mb,M,A,jj1)
A1(J)=DCMPLX(1,0)
A2(J)=A1(J)*(-M(1,1)*M(2,3)+M(1,3)*M(2,1))/(M(1,2)*M(2,3)-
& M(2,2)*M(1,3))
B2(J)=A1(J)*(-M(1,2)*M(2,1)+M(1,1)*M(2,2))/(M(1,2)*M(2,3)-
& M(2,2)*M(1,3))
B3(J)=(-M(3,2)*A2(J)-M(3,3)*B2(J))/M(3,4)
IF (Choix.eq.1) THEN
write(1,*)A,E(j)
ENDIF
IF (Choix.eq.2.and.J.eq.Nv.and.In2.eq.N2)then
do Xx=-A*Na,-A/2.,A/2./100.
F1=ABS(A1(J))**2*DEXP(Ro*Xx)**2
write(1,*)Xx,F1
enddo
do Xx=-A/2.,A/2.,A/2./100.
F2=ABS(A2(J)*CDEXP(Jj1*xK*Xx)+B2(J)*CDEXP(-Jj1*xK*Xx))**2
write(1,*)Xx,F2
enddo
do Xx=A/2.,A*Na,A/2./100.
F3=ABS(B3(J)*DEXP(-Ro*Xx))**2
write(1,*)Xx,F3
enddo
write(1,*)A*Na,zero
write(1,*)-A/2.,zero
write(1,*)-A/2.,Cc
write(1,*)-A/2.,zero
write(1,*)A/2.,zero
write(1,*)A/2.,Cc
ENDIF
ENDIF
10 continue
!-------------------------------------------------------------------------
enddo
!-------------------------------------------------------------------------
END
c-------------------------------------------------------------------------
subroutine equ (Energie,hauteur,Mp,Mb,Ro,xK)
implicit real*8(a-h,o-z)
Real*8 Mb,Mp
Ro=DSQRT(2*Mb*(hauteur-Energie))
xK=DSQRT(2*Mp*Energie)
RETURN
END
c-------------------------------------------------------------------------
subroutine Trmat (Ro,xK,Mp,Mb,M,A,jj1)
implicit real*8(a-h,o-z)
Real*8 Mb,Mp
complex(8) M(4,4),jj1
M(1,1)=DEXP(-Ro*A/2)
M(1,2)=-CDEXP(-Jj1*xK*A/2)
M(1,3)=-CDEXP(Jj1*xK*A/2)
M(2,1)=M(1,1)*(Ro/Mb)
M(2,2)=(-Jj1*xK/Mp)*(-M(1,2))
```

```
M(2,3)=(Jj1*xK/Mp)*(-M(1,3))
M(3,2)=(-M(1,3))
M(3,3)=(-M(1,2))
M(3,4)=(-M(1,1))
M(4,2)=(Jj1*xK/Mp)*M(3,2)
M(4,3)=(-Jj1*xK/Mp)*M(3,3)
M(4,4)=(Ro/Mb)*(-M(3,4))
RETURN
END
c-------------------------------------------------------------------
subroutine det(M,MM)
complex(8) M(4,4),MM
MM = M(1,4)*M(2,3)*M(3,2)*M(4,1) -
&M(1,3)*M(2,4)*M(3,2)*M(4,1)-M(1,4)*M(2,2)*M(3,3)*M(4,1)+
&M(1,2)*M(2,4)*M(3,3)*M(4,1)+M(1,3)*M(2,2)*M(3,4)*M(4,1)-
&M(1,2)*M(2,3)*M(3,4)*M(4,1)-M(1,4)*M(2,3)*M(3,1)*M(4,2)+
&M(1,3)*M(2,4)*M(3,1)*M(4,2)+M(1,4)*M(2,1)*M(3,3)*M(4,2)-
&M(1,1)*M(2,4)*M(3,3)*M(4,2)-M(1,3)*M(2,1)*M(3,4)*M(4,2)+
&M(1,1)*M(2,3)*M(3,4)*M(4,2)+M(1,4)*M(2,2)*M(3,1)*M(4,3)-
&M(1,2)*M(2,4)*M(3,1)*M(4,3)-M(1,4)*M(2,1)*M(3,2)*M(4,3)+
&M(1,1)*M(2,4)*M(3,2)*M(4,3)+M(1,2)*M(2,1)*M(3,4)*M(4,3)-
&M(1,1)*M(2,2)*M(3,4)*M(4,3)-M(1,3)*M(2,2)*M(3,1)*M(4,4)+
&M(1,2)*M(2,3)*M(3,1)*M(4,4)+M(1,3)*M(2,1)*M(3,2)*M(4,4)-
&M(1,1)*M(2,3)*M(3,2)*M(4,4)-M(1,2)*M(2,1)*M(3,3)*M(4,4)+
&M(1,1)*M(2,2)*M(3,3)*M(4,4)
RETURN
END
c-------------------------------------------------------------------
```

IV. 3. The transition wavelength

The desired transition wavelength corresponding to the transition between quantized levels, based on equation IV.3, can be expressed as [2]

$$\lambda_n(\mu m) = \frac{1.24}{(E_0 + E_{cn} + E_{vn}) : (eV)} \qquad \text{(IV.4)}$$

In Figure 3, we have plotted the calculated transition wavelength λ_0 and λ_1, respectively for the first (1^{st}: n= 0) and second (2^{nd}: n= 1) transitions between electrons and heavy holes levels as a function of the well width for the $Al_{0.05}Ga_{0.95}N_{0.04}As_{0.96}$ (well)/GaAs (barrier) QW structure. The two curves correspond to the numerically calculated values of the wavelength by neglecting $(\Delta Wi)^3$ (i = c, v) in (IV.2) for both 1^{st} and 2^{nd} transitions and corresponding to the used parameter values in the calculation, listed in Table 1. The simulation results suggest that the AlGaAsN system has proved its high potential for applications in GaAs-based telecom lasers in the 1.3 μm range for an active layer width up to 20 nm. Knowing the GaAs, AlAs, GaN and AlN VB offsets of respectively –0.8, –1.33, –2.64 and –3.44 eV [4], a VB offset value for $Al_{0.05}Ga_{0.95}N_{0.04}As_{0.96}$ of –0.9 eV is adopted and a VB-edge discontinuity with GaAs of $\Delta E_v \approx 0.21\ \Delta E_g$ is assumed, i.e., $\Delta E_v/\Delta E_g$ = [– 0.8–(–0.9)]/[1.424–0,941].

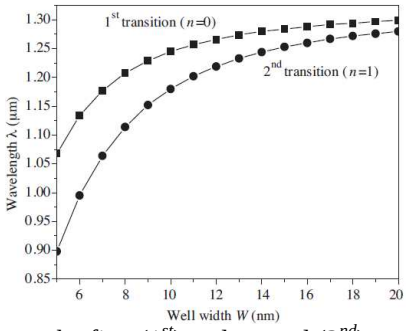

Fig.IV. 3. Wavelengths corresponding to the first (1^{st}) and second (2^{nd}) transitions between the quantized energy levels of conduction electrons and heavy holes as a function of the well width calculated for $Al_{0.05}Ga_{0.95}As_{0.96}N_{0.04}$ (well) and GaAs (barrier).

Table 1 *Parameter values used in the wavelength calculation*

	Band gap (eV)	Electronic effective mass (in m_0 units)	Heavy holes effective mass (in m_0 units)
GaAs	1.424[d]	0.0665[e]	0.62[f]
$Al_{0.05}GaAsN_{0.04}$	0.941[a]	0.0761[b]	0.6343[c]

[a, b ,c] This work with data of Ref. [7], [23], [24] and [4]. [d, e] Ref. [23, 4] . [f] Ref. [24]

Part 2: Optical properties of zinc-blende $Al_xGa_{1-x}As_{1-y}N_y$ materials

IV. 4. AlGaAsN an alternative to AlGaAs

As said above, the research on GaAs-based alloys has revealed important electronic and optical properties with many advantages over InP-based systems such as low cost devices. Although AlGaAs epitaxially grown on GaAs form heterojunctions with perfectly matched lattices and $Al_xGa_{1-x}As$ alloys should have a direct band gap in the Al mole fraction range up to ≈ 0.45, the conventional GaAs–AlGaAs material systems of semiconductor (SC) quantum well (QW) lasers have the disadvantage of relatively limited wavelength emission between 0.78 and 0.87 mm [5]. However, many applications require longer wavelengths belonging to the 1.3–1.55 mm range with minimal loss and dispersion. Nitrogen doped III–V SCs are widely studied due to their unique properties and device applications in high-efficiency hybrid solar cells such as long wavelength photo-detectors and diode lasers. The incorporation of small amounts of nitrogen (N) to form dilute IIIN- V alloys produces a profound effect, due to the chemical and size differences of the As and N atoms, on the fundamental band gap as well as the lattice parameter of the III-AsN materials. This strong non linear band gap reduction has been observed in N-ion-implanted AlGaAs and epitaxial AlGaAsN, where an anticrossing interaction of a narrow band of highly localized N states with the extended states of the III–V matrix splits the conduction band (CB) into two non-parabolic subbands. Note that the nitrogen induced has a negligible effect on the valance band (VB). This so-called band anticrossing (BAC) model has also predicted that the lower subband of the III–V-N

alloys should have a greatly increased electron effective mass compared to that of the III–V matrix. It is important to point out that the choice of varying N content in the III-AsN materials, such as AlGaAsN, hasprovided the flexibility of simultaneously controlling both electronic and optical properties. In order to investigate the properties of AlGaAsN as an alternative to AlGaAs, our calculations are based on a predicted separate confinement heterostructure (SCH) laser with a single QW, which consists of a n-$Al_{0.37}Ga_{0.63}As$ cladding layer grown on an n-GaAs substrate, an $Al_xGa_{1-x}As_{1-y}N_y$ QW, which is more suitable as an active layer (with x=9/32 and y=1/32) embedded in an undoped $Al_{0.28}Ga_{0.72}As$ waveguide (barrier layers), a p-$Al_{0.37}Ga_{0.63}As$ cladding layer and followed by a GaAs cup layer. A schematic of the studied QW system without the two end layers GaAs is presented in Fig. IV.4. The step in the band gap between $Al_{0.28}Ga_{0.72}As_{0.97}N_{0.03}$ and $Al_{0.28}Ga_{0.72}As$ is sufficient to confine the carriers in the active layer, and the step in refractive index between $Al_{0.37}Ga_{0.63}As$ and $Al_{0.28}Ga_{0.72}As$ confine the light.

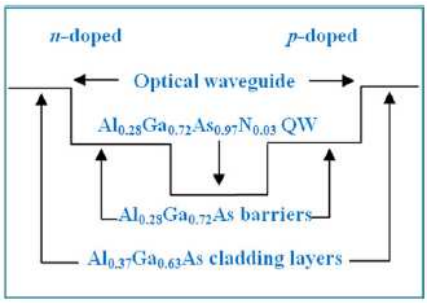

Fig. IV.4. Schematic diagram of studied quantum well (QW) system.

While the III–V nitrides have a stronger tendency to crystallize in the wurtzite (WZ) structure, the zinc-blende (ZB) structure of III–V-N systems owns several applications of greatest interest such as the realization of devices operating by inter-subband transition like quantum cascade lasers and some infrared detectors. Yeh et al. [6] predicted that while AlN has an indirect gap in the ZB structure, in the WZ structure the band gap will become direct. Can AlGaAsN be stabilized in the ZB structure? If so, will AlGaAsN have an indirect band gap? Munich and Pierret [7] predicted that the vast majority of AlGaAsN alloys crystallize in the ZB crystal. Yu et al. [8] reported that $Al_xGa_{1-x}As_{1-y}N_y$ alloys remain direct gap even for x>0.44 whereas the band gap of the $Al_xGa_{1-x}As$ is indirect. So, let us try to answer the follow question: In what way is the AlGaAsN material for interest for the QW laser and solar cell heterostructures?

IV. 5. Details of calculation

All calculations for binaries, ternaries and quaternary are based on the self consistent first principles Full Potential Linearized Augmented Plane Waves (FP–LAPW) method within the local density approximation (LDA), as embodied in the wien 2*k* code [9]. The unit cell is divided into non-overlapping muffin-tin (MT) spheres around the atomic sites and an interstitial region. The electronic configurations of Al, Ga, As and Nare Al:Ne 3s23p1, Ga:Ar $3d^{10}4s_24p^1$, As:Ar $3d^{10}4s^24p^3$ and N:He $s^22s^22p^3$. The MT radii (RMT) for Al, Ga, As and N atoms were adopted to be 2.13, 2.16, 2.17 and 2.11 Bohr, respectively. In the MF spheres, the l-expansion of the non-spherical potential and charge density was carried out up to l_{max}=10. In order to achieve energy eigenvalues convergence, the wave-functions in the interstitial region were expanded in plane waves with a cut-off of $k_{max}=8/R_{MT}$.We adopted a supercell approach for the $Al_xGa_{1-x}As$ and $Al_xGa_{1-x}As_{1-y}N_y$ band structure calculations on which are based the optical properties. Two *x* values (12/32≈0.37 and 9/32≈0.28) with a representative example of *y*=1/32≈0.03 were realized by substituting Al and As atoms by Ga and N, respectively. To model the $Al_{0.28}Ga_{0.72}As$, $Al_{0.37}Ga_{0.63}As$ and $Al_{0.28}Ga_{0.72}As_{0.97}N_{0.03}$ random alloys, we have used a small 64-atom $Al_nGa_{32-n}As_{32-m}N_m$ supercell with (n, m)=(9, 0), (12, 0) and (9, 1), respectively for the two ternaries and the quaternary, which corresponds to the 2√3x2√3x2√3 supercell. The atomic positions of the Al and N induced atoms are given for structures in their ideal and unrelaxed forms. The *k* integration over the Brillouin zone (BZ) is preformed using the Monkhorst and Pack mesh [10]. A mesh of 14 special *k*-points was taken in the irreducible wedge of the BZ for ternaries and quaternary. Since it is well known that the LDA to the density functional theory (DFT) underestimates the band gap of SCs, scissors operation with a rigid upward shift of the CB have been used to correct the LDA error in the energy gap of the ternaries and quaternary, which are calculated using the BAC model (Eq. (1)). For $Al_xGa_{1-x}As_{1-y}N_y$ and according to this model, the energy of the lower conduction subband E–, which is responsible for the reduction in the fundamental band gap [7], arising from the interaction of the Γ-CB states (represented by E_M the $Al_xGa_{1-x}As$ fundamental gap) with the localized N induced level E_N is derived from [11]

$$E_{-}(k)=\frac{1}{2}\left\{\left[E_M(k)+E_N\right]-\sqrt{\left[E_M(k)-E_N\right]^2+4C^2{}_{NM}\,y}\right\} \qquad \text{(IV.5)}$$

refer to Fig.IV. 5 for an illustration of the 2√3x2√3x2√3 supercell (displaying a N atom in an As site).

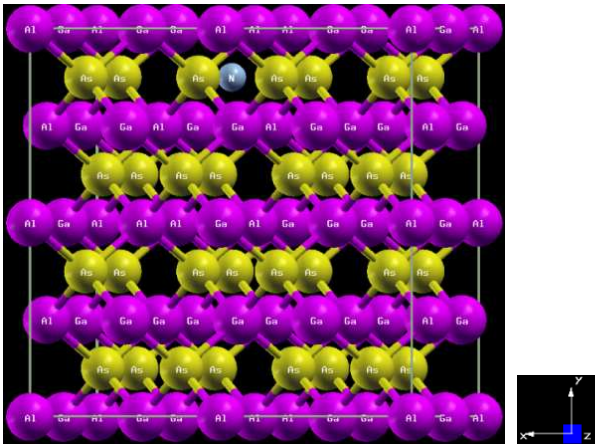

Fig.IV.5 Illustration of a $2\sqrt{3}x2\sqrt{3}x2\sqrt{3}$ $Al_xGa_{1-x}As_{1-y}N_y$ supercell.

Procz et al. [12] have analyzed the interband transitions in diluted $Al_xGa_{1-x}Ga_{1-y}N_y$, with $x \leq 0.37$ and $y \leq 0.04$ by photomodulated reflectance and have shown that the CB of these alloys can be described by the experimentally motived BAC model.

The AlxGa1-xAs fundamental band gap and the N level given relative to the GaAs VB edge energies are $E_M=E_0+1.402x$ and $E_N=1.625+0.069x$ (both in eV), respectively. E0 is the GaAs interband transition, C_{NM} is the matrix element for the coupling between the nitrogen-induced states and the extend lowest CB states, taken to be 2.32 eV [12] and (x, y) are the (Al, N) mole fractions.

IV. 6. Lattice match in $Al_xGa_{1-x}As$/GaAs heterostructure

To achieve AlGaAs/GaAs heterostructures with negligible interface traps, the lattices between the two SCs must be closely matched [13], since these traps become non-radiative recombination centers that cause the material quality to deteriorate [14]. We will investigate the lattice mismatch between the substrate GaAs and the cladding layer $Al_xGa_{1-x}As$ given by

$$\frac{\Delta a}{a_{GaAs}} = \frac{a_{AlGaAs} - a_{GaAs}}{a_{GaAs}}.100\% \qquad \text{(IV.6)}$$

where a_{AlGaAs} and a_{GaAs} are the lattice constants of GaAs and $Al_xGa_{1-x}As$, respectively, in the range of Al mole fraction $0 \leq x \leq 0.375$ and $\Delta a = a_{AlGaAs} - a_{GaAs}$. The simulated results listed in Table 2 indicate that the lattice constant increase with the increase in Al composition and that $Al_xGa_{1-x}As$ have a lattice mismatch with GaAs of 0.157%. If we best fit the results shown in Table 2 with the formula: $a_{AlGaAs}(x) = xa_{AlAs} + (1-x)a_{GaAs} - \delta x(1-x)$, the lattice parameter a_{AlGaAs} has a positive derivation from Vegard's law of $\delta = 0.0113 \pm 0.0024$ due to the relaxation of the Al–As and Ga–As bond lengths in AlGaAs.

Table 2 Structural parameters for binaries and ternaries. Calculated lattice constant (a_{cal}) and bulk modulus ($B_{cal.}$) for GaAs and AlAs are compared to experimental data aexp.and $B_{exp.}$. B_0 and $\Delta a/a$ are the pressure derivative of B and the lattice mismatch between GaAs and AlGaAs, respectively.

Material	a_{cal}(Å)	A_{exp}(Å)	B_{cal}(GPa)	B_{exp}(GPa)	*B'*	*Δa/a(%)*
GaAs	5.6103[a]	5.6103[b,c,d,e]	75.813[a]	76[g] 77[h]	4.3077[a]	-
AlAs	5.6396[a]	5.6605[f]	76.028[a]	77[h]	4.3608[a]	-
$Al_{0.125}Ga_{0.875}As$	5.6121[a]	-	80.173[a]	-	4.3643[a]	0.032[a]
$Al_{0.25}Ga_{0.75}As$	5.6158[a]	-	79.671[a]	-	4.3507[a]	0.098[a]
$Al_{0.375}Ga_{0.625}As$	5.6191[a]	-	79.471[a]	-	4.2890[a]	0.0157[a]

[a] This work. [b, f] Ref. [13]. [c] Ref. [18]. [d] Ref. [19].
[e] Ref. [25]. [g] Ref. [26]. [h] Ref. [27].

IV. 7. Band structure of $Al_{0.37}Ga_{0.63}As$ and $Al_{0.28}Ga_{0.72}As_{0.97}N_{0.03}$

As emphasized in Fig. IV.6, the maximum of the VB and the minimum of the CB in the band structure for $Al_{0.37}Ga_{0.63}As$ are both found at Γ, the symmetry point. As a consequence of using LDA approximation, the calculated band gap energies are underestimated compared with the experimental data for binaries and the BAC model values for ternaries and quaternary. The shifts ΔE_g to amend these gap energies, calculated from the experimental values of GaAs and AlAs on the one hand and the BAC values for $Al_xGa_{1-x}As$ and $Al_xGa_{1-x}As_{1-y}N_y$ on the other, used in calculations of the optical properties are presented in Table 3 as well as the atomic positions of the Al and N induced atoms, all in Cartesian coordinates. From the band structure of $Al_{0.28}Ga_{0.72}As_{0.97}N_{0.03}$ shown in Fig. IV.7 (right) and Fig. IV.8 (left), one can then remark the direct character of the gap and predict that the direct-to-indirect band gap transition may occur for $x<0.5$ [7].

Table 3 Fundamental band gap energies and their gap's nature as well as the atomic positions (in Cartesian coordinates) of the Al and N induced atoms. $E_{0(BAC)}$ and $E_{g(VCA)}$ are the BAC model and Vegard's law gap energies for $Al_xGa_{1-x}As_{1-y}N_y$ and $Al_xGa_{1-x}As$. ΔE_g is the corresponding energy shift calculated to correct the energy gap that the LDA underestimates. For binaries, experimental data were adopted to calculate ΔE_g.

Material	E_{0exp}(eV)	E_{0BAC}(eV)	E_{gVCA}(eV)	ΔE_g	*Gap's nature*
GaAs	3.018[c]	-	-	1. 089[a]	Indirect [a,e,f]
AlAs	1.424[c,e]	-	-	1.144[a]	Direct [a,c,d,e,f]
$Al_{0.\ 28}Ga_{0.72}As$	-	1.802[a]	1.872[b]	1.127[a]	Direct [a,g]
$Al_{0.28}GaAsN_{0.03}$	-	1.306[a]	1.944[b]	1.802[a]	Direct [a,h,i]
Al, N positions					
Al_1(0.00,0.00,0.00)					
Al_2(0.50,0.00,0.00)					
Al_3(0.00,0.50,0.00)					
Al_4(0.50,0.50,0.00)					
Al_5(0.00,0.00,0.50)					
Al_6(0.50,0.00,0.50)					
Al_7(0.00,0.50,0.50)					
Al_8(0.50,0.50,0.50)					
Al_9(0.25,0.25,0.00)					
Al_{10}(0.75,0.25,0.00)					
Al_{11}(0.25,0.75,0.00)					
Al_{12}(0.75,0.75,0.00)					
N(0.625,0.875,0.875)					

[a] This work with data of Ref. [12].
[b, f] This work with $E_{g\ GaN}$=3.299 eV and $E_{g\ AlN}$=5.4 eV from the Ref. [4].
[c] Ref. [13]. [d] Ref. [18]. [e] Ref. [19].
[g] Ref. [28]. [h] Ref. [7].

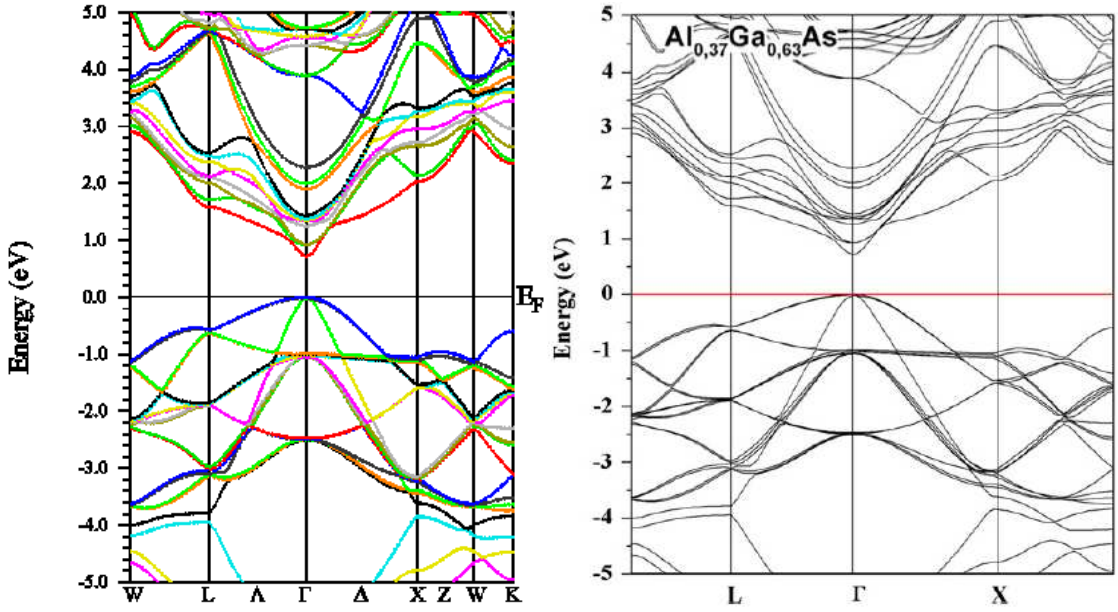

Fig. IV.6 Band structure of $Al_{0.37}Ga_{0.63}As$. The Fermi level (E_F) is taken as zero energy.

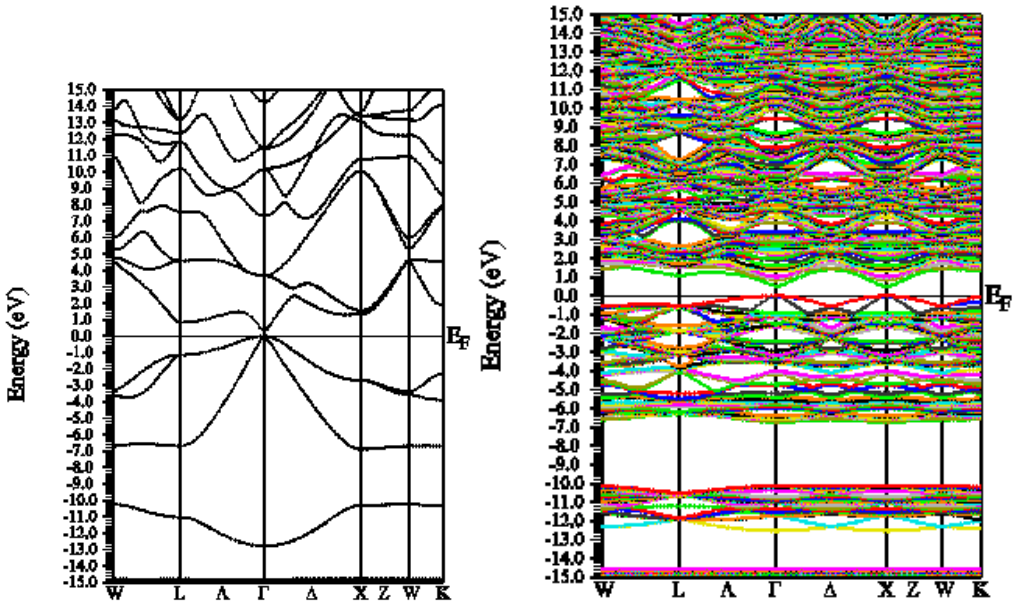

Fig.IV. 7 Band structure of GaAs (left) and $Al_{0.28}Ga_{0.72}As_{0.97}N_{0.03}$(right). The Fermi level (E_F) is taken as zero energy.

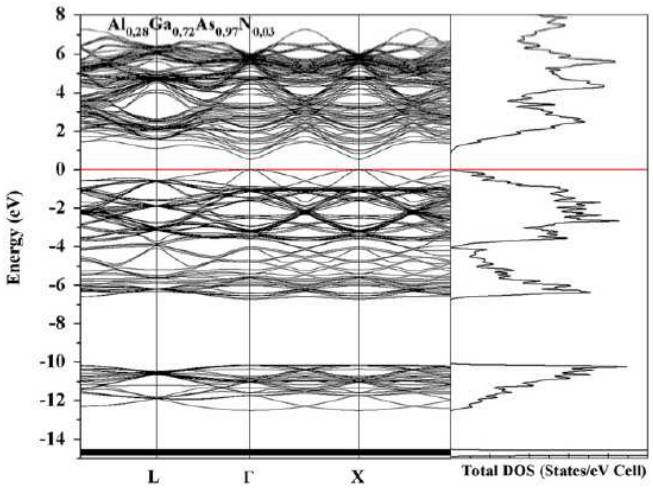

Fig. IV.8 Band structure and total DOS of$Al_{0.28}Ga_{0.72}As_{0.97}N_{0.03}$. Zero energy is taken at E_F.

IV. 8. Charge density of $Al_{0.28}Ga_{0.72}As_{0.97}N_{0.03}$

N doping of $Al_xGa_{1-x}As$ alloys leads to strong spatial correlation effects between the atoms whose origin is the transformation of the bonds after redistribution of the atoms on their lattice sites [15]. On increasing N content at a fixed Al composition in $Al_xGa_{1-x}As_{1-y}N_y$, eventually all Al atoms available are used up for formation of Al–N bonds instead of Ga–N bonds [16] since the enthalpy of formation of AlN is significantly larger than that for the other constituent binary compounds [17]. The ionic character of any alloy can be related to the charge transfer between the cationic and the anionic sites; for this reason, we have calculated the total charge density of $Al_{0.28}Ga_{0.72}As_{0.97}N_{0.03}$, which is illustrated along all the bonds and in the (1 1 0) plane containing Al, Ga, As and N atoms (Fig. IV.9). One can see clearly for the Al–N bond that the bonding charge is displaced strongly towards the N atom, due to the difference between the electronegativity values of the two atoms. The calculated electron charge distributions show that the ionic character of AlGaAsN tends to be more significant.

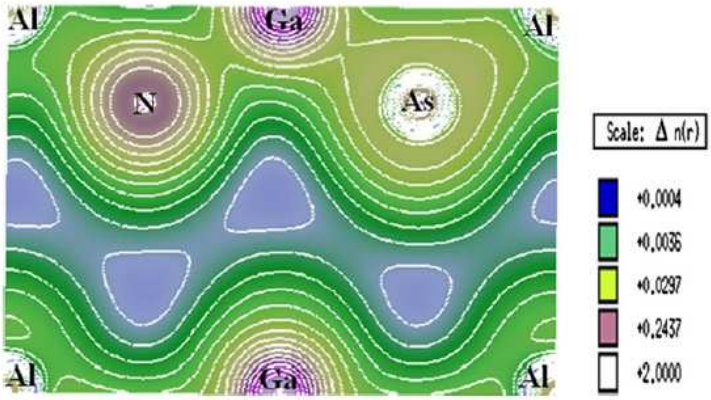

Fig. IV.9 Contour plot of total valence charge density in (1 1 0) plane for $Al_{0.28}Ga_{0.72}As_{0.97}N_{0.03}$.

IV. 9. Dielectric function

Acquaintance of optical properties is of great importance in the design and analysis of optoelectronic devices such as light sources and detectors. At all photon energies E=ħω these properties are described for a medium by the complex dielectric function [18]

$$\varepsilon(\omega) = \varepsilon_1(\omega) + i\varepsilon_2(\omega) \qquad \text{(IV.7)}$$

where the two parts of the dielectric function, real ε_1 and imaginary ε_2, are connected by the Kramers–Kronig relations. Fig. IV.9 displays spectral variations of ε_1 and ε_2 from numeric calculations for $Al_{0.28}Ga_{0.72}As_{0.97}N_{0.03}$. In Fig. IV.10, we show the fundamental peak energies of ε_2 for GaAs, $Al_{0.28}Ga_{0.72}As$, $Al_{0.28}Ga_{0.72}As_{0.97}N_{0.03}$, collected in Table 4 as well as the indirect band gap energy E_g^L, which also plays an important part in the spectra of both ε_1 and ε_2 [18].

Table 4: Calculated peaks of the dielectric function $\varepsilon_2(\omega)$ for $Al_{0.28}Ga_{0.72}As$ and $Al_{0.28}Ga_{0.72}As_{0.97}N_{0.03}$. Calculated E_1 and E_2 transitions, indirect band gap $E_g{}^L$, static optical parameter $\varepsilon_1(0)$ and real part of the refractive index at the corresponding fundamental band gap energies $n_r(E_g)$ for GaAs (compared with experimental data), $Al_{0.28}Ga_{0.72}As$ and $Al_{0.28}Ga_{0.72}As_{0.97}N_{0.03}$ are given.

Material	$E_g{}^L$(eV)	E_1(eV)	E_2(eV)	$\varepsilon_1(0)$	$n_r(E_g)$
GaAs $_{(cal.)}$	0.907[a]	4.427[a]	6.218[a]	9.364[a]	3.177[a]
GaAs $_{(exp.)}$	1.73[b]	3.0[c]	5.1[c]	13.20[d]	3.642[d]
$Al_{0.28}Ga_{0.72}As$	1.557[a]	4.782[a]	6.618[a]	17.556[a]	4.364[a]
$Al_{0.28}GaAsN_{0.03}$	1.105[a]	4.059[a]	8.329[a]	52.346[a]	7.544[a]

[a] This work. [b] Ref. [17]. [c, d] Ref. [24].

Since $\varepsilon_2(\omega)$ can be strongly related to the joint density of states (DOS) function, we have also calculated the total DOS of $Al_{0.28}Ga_{0.72}As_{0.97}N_{0.03}$ as illustrated in Fig. IV.8 above,where the energy zero is taken at the Fermi energy level (E_F). From the calculated partial DOS of the quaternary alloy grouped in the total DOS (Fig. IV.8), three prominent series of bands are to be taken into account: VB2 localized in the energy range (-12.479, -10.088) eV, which arises primarily fromthe As 4s states with a slight contribution of N 1s and Al 3s states; VB3 contained in the range (-6.713, E_F) eV, which consists of amixture of Al 3s, N 1s and Ga 4s states and CB1 situated in the range (0.528, 7.243) eV, which arises primarily fromthe Ga 4p states with a slight contribution of N 2s, As 4p and Al 3p states. One can mostly remark the presence of N states in all bands and the absence of the Ga 3d and As 3d states contribution.

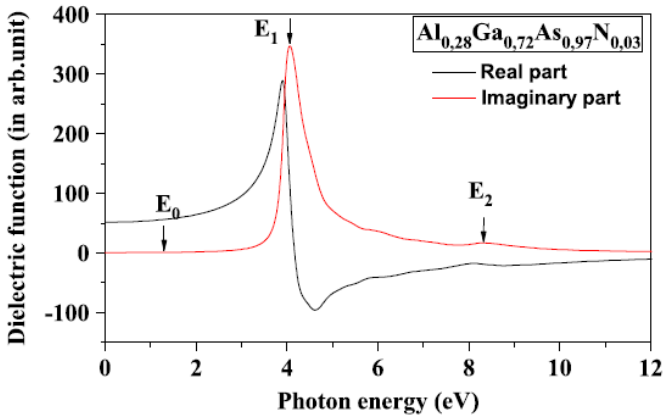

Fig. IV.9. Spectral variations of the two parts of dielectric function, real (e1) and imaginary (e2), for Al0.28Ga0.72As0.97N0.03.

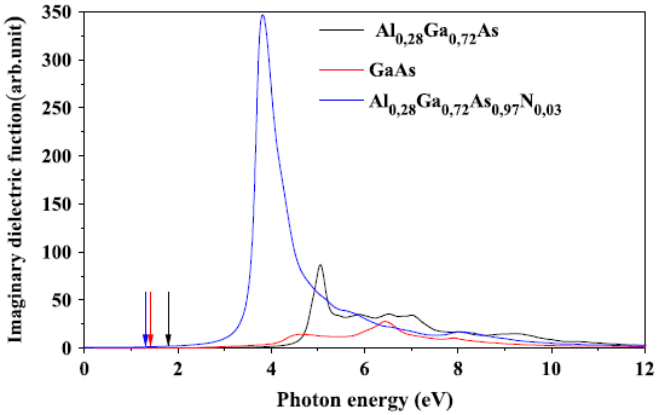

Fig. IV.10. Main peak energies of dielectric function o(e2) for GaAs, Al0.28Ga0.72As and Al0.28Ga0.72As0.97N0.03. Band gaps are displayed by arrows.

IV. 10. Refractive index

Knowledge of the optical index of SCs turns out to be of fundamental importance in opto-electronics [19]. The complex refractive index $n(\omega) = n_r(\omega) + ik(\omega)$ is given by [18]

$$n(\omega) = [\varepsilon_1(\omega) + i\varepsilon_2(\omega)]^{1/2} \qquad \text{(IV.8)}$$

where the real refractive index $n_r(\omega)$ and the extinction coefficient $k(\omega)$ are both real and positive numbers. From the above equations it follows that [18]

$$\varepsilon_1 = n_r^2 - k^2 \text{ and } \varepsilon_2 = 2n_r k \qquad \text{(IV.9 a, and b)}$$

and also that

$$n_r(\omega) = \frac{[\varepsilon_1(\omega)^2 + \varepsilon_2(\omega)^2 + \varepsilon_1(\omega)]^{1/2}}{2} \text{ and } n_r(\omega) = \frac{[\varepsilon_1(\omega)^2 + \varepsilon_2(\omega)^2 - \varepsilon_1(\omega)]^{1/2}}{2} \text{ (IV.10 a, and b)}$$

The corresponding variations in the calculated n_r and k for $Al_{0.28}Ga_{0.72}As_{0.97}N_{0.03}$ are shown in Fig. IV.11 over a range of photon energies up to 6 eV, where experimentally the dispersion is normal. Since ε_2 calculated from several located interband transitions may be taken as zero in the transparency region, near and below the lowest direct band gap, we can assume that [18]

$$n(\omega) \approx [\varepsilon_1(\omega)]^{1/2} \qquad \text{(IV.11)}$$

To understand the changes in $n_r(\omega)$ occurring in the SC laser cavity under population inversion resonant frequencies ω_0 need to be considered; the first resonance corresponds to band gap radiation $E_g=\hbar\omega_0$, while for subband gap radiations an increase in ω_0 will cause a shift in the transition energy upwards, which corresponds to quantum transitions between levels [20]. Normal dispersion is associated with a decrease in $n_r(\omega)$ with increase in resonance energy for a given photon energy, which is very useful for SCH [21]. The variations in n_r for GaAs, $Al_{0.28}Ga_{0.72}As$ and $Al_{0.28}Ga_{0.72}As_{0.97}N_{0.03}$ over a range up to 6 eV are shown in Fig. IV.12, where for 1.424 eV as the photon energy, n_r is 3.177 in GaAs and changes from 7.752 in AlGaAsN to 4.269 in Al0.28Ga0.72As. The main peaks in n_r correspond to the interband transitions. The strongest peak for AlGaAsN is related mainly to the E_1 transition of 4.059 eV.

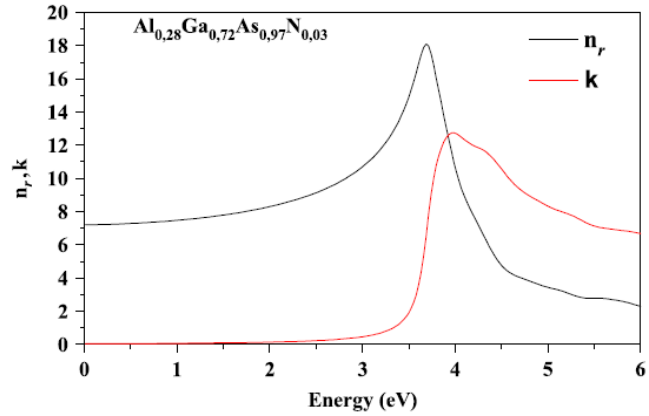

Fig. IV.11. Spectra of refractive index (nr) and extinction coefficient (k) for $Al_{0.28}Ga_{0.72}As_{0.97}N_{0.03}$.

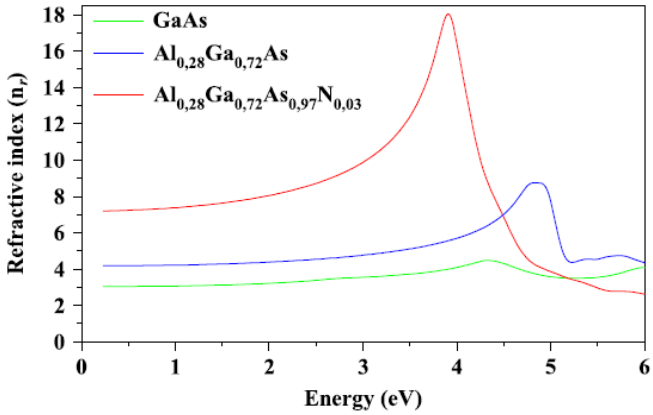

Fig. IV.12. Variation of real part of refractive index (nr) for GaAs, $Al_{0.28}Ga_{0.72}As$ and $Al_{0.28}Ga_{0.72}As_{0.97}N_{0.03}$ over a range of photon energies up to 6 eV.

IV. 11. Reflectivity

The reflection coefficient (R) is among the most important optical constants related to the dielectric function. It characterizes the reflective light energy part at the cleaved facets of the resonant cavity. For normal-incidence the reflectivity is [13,19]

$$R = \frac{(n_r - 1)^2 + k^2}{(n_r + 1)^2 + k^2} \qquad \text{(IV.12)}$$

The facet reflectivity for the $Al_{0.28}Ga_{0.72}As_{0.97}N_{0.03}$ active layer compared with that of the $Al_{0.28}Ga_{0.72}As$ barrier layers have been considered in Fig. IV.13. The main peaks of reflectivity for the barrier layers, 61.2%, 61.9% and 68.9%, are underestimated to those of the active layer, 86.9%, 83.7% and 83.2% at 4.443 (near E_1 transition), 6.208 and 7.211 eV, respectively. One can also see the large effect on the incorporation of N on the facet reflectivity of $Al_{0.28}Ga_{0.72}As_{0.97}N_{0.03}$.

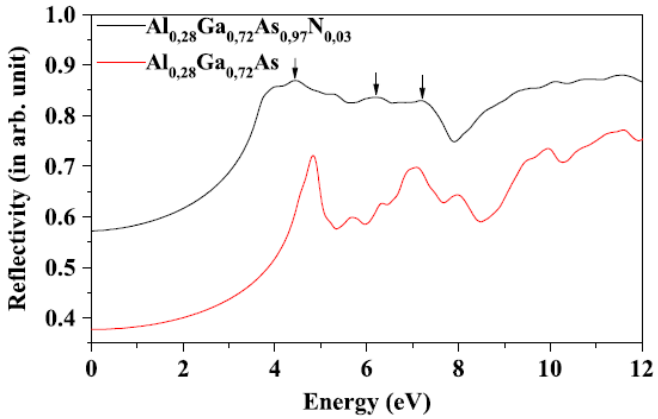

Fig. IV.13. Calculated spectra of normal-incidence reflectivity for $Al_{0.28}Ga_{0.72}As_{0.97}N_{0.03}$ and $Al_{0.28}Ga_{0.72}As$.

IV. 12. Absorption coefficient

The light incident on the AlGaAsN/GaAs QW structure may cause excitation of the ground state electrons from the VB to the CB or from one subband to a higher subband, where the required energy is supplied by the photons and the light is absorbed [22]. The absorption coefficient α(ω) characterizing such a phenomenon, defined as the light energy absorbed in unit length per unit incident energy, depends on both parts of ε(ω) and is given by [13,18]

$$\alpha(\omega) = \frac{4\pi}{\lambda} k(\omega) \qquad \text{(IV.13)}$$

λ is the wavelength of light in the vacuum. Fig. IV.14 shows the absorption in $Al_{0.28}Ga_{0.72}As$ and $Al_{0.28}Ga_{0.72}As_{0.97}N_{0.03}$. A zero absorption coefficient for both alloys is observed for photons possessing energies below the band gap, while oscillations such as 4.024 (≈ E_1), 5.929 and 9.084 eV in the absorption as a function of photon energy for the active layer are

apparent for $\hbar\omega > E_g$, corresponding respectively to the peaks 547.34×10^4, 424.46×10^4 and 429.12×10^4 cm^{-1}.

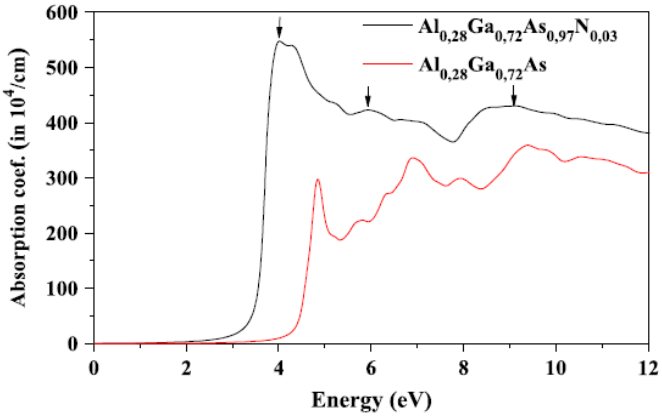

Fig. IV.14. Absorption coefficient (a) of $Al_{0.28}Ga_{0.72}As_{0.97}N_{0.03}$ compared to that of $Al_{0.28}Ga_{0.72}As$.

Part 3: Can the ferromagnetism be observed with doping of nonmagnetic species like nitrogen (N) into the nonmagnetic semiconductor AlGaAs system?

There are currently a large number of observations of ferromagnetism associated with doping of *a priori* nonmagnetic species into nonmagnetic oxide semiconductors. The subject has been given the name of d_0 magnetism to emphasize the fact that the magnetism is probably not coming from partially filled *d* orbitals, but from moments induced in the *p* orbitals of the oxygen band [29].

So, in which way is the physical behavior of AlGaAs:N different than of AlGaAs doped with a metal transition like Mn (i.e., AlGaAs:Mn)?

$Al_xGa_{1-x}As$/GaAs system is potentially of great physical interest and technological importance for many high-speed electronic and optoelectronic devices [30]. However, experiment shows that the radiative performances of arsenides-based optoelectronic devices are strongly sensitive to the density of dislocations, causing the material quality to deteriorate, and yet seems to affect the optoelectronic performances of the nitrides-based layers [14,24]. The diluted N-containing semiconductors (DNS's), such as the AlGaAsN material with a nitrogen (N) content typically less than 5% [31], have attracted considerable interest as the incorporation of even a small amount of N that cause a strong dependence of the lattice parameter on the N content as well as the band gap, and decrease by more than 100 meV per atomic percent of nitrogen [32]. This N-ion- implantation has made the basic properties of DNS's interesting [33], while the III-V-N materials important for long wavelength optoelectronic devices [34] and high efficiency hybrid solar cell applications [35].

Another kind of diluted III-As materials, that shows a great deal of promise due to their potential applications in spintronics, magneto optics and optical fiber networks [36-37], are the diluted magnetic semiconductors (DMS's) in which a transition element, such as Mn, acts both as an acceptor and source of local moments [38]. (Ga,Mn)As for example, the III-V-based-DMS between GaAs and magnetic ion Mn that can be pseudomorphically grown on GaAs, adds a new dimension to the GaAs/(Al,Ga)As heterostructure system by introducing a new degree of freedom associated with magnetic cooperative phenomena and related spin effects [39], can be integrated together with GaAs-based lasers, and is thus a promising material for use in integrated optical isolators [40]. AlGaAsN and AlGaAsMn belonging to DNS's and DMS's may be applied to optoelectronic devices and optical fiber networks, respectively. Our calculations aim for comparing the optical properties of two materials arising from the AlGaAs parent. We have performed a comparative first principle study illustrated by a representative example (x=4/32, y=1/32) between $(Al_xGa_{1-x})_{1-y}Mn_yAs$ and $Al_xGa_{1-x}As_{1-y}N_y$. Despite its electronic properties being strongly affected by inducing small amounts of Mn substitutional atoms in the cationic sublattice of AlGaAs, $(Al_xGa_{1-x})_{1-y}Mn_yAs$ possesses optical properties strictly less than those of $Al_xGa_{1-x}As_{1-y}N_y$, especially its optical conductivity at the peak 1.256 eV. The results indicate that AlGaMnAs may be a good candidate for optoelectronics when exploited in optical fiber networks, and it can still be of great interest because of its promising potential when used for spintronics

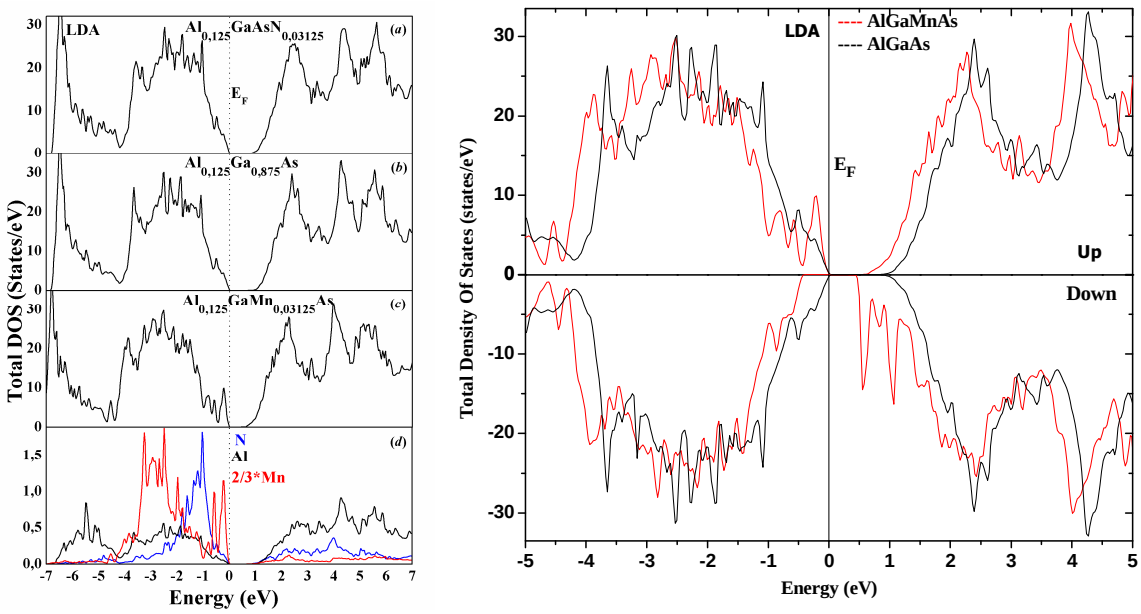

Fig. IV.15 (**Left**) The total DOS of $Al_xGa_{1-x}As$, $Al_xGa_{1-x}As_{1-y}N_y$ and $(Al_xGa_{1-x})_{1-y}Mn_yAs$ for an Al concentration of 12.5 % and a same (Mn or N) content in $Al_xGa_{1-x}As$ of 3.125% (a,b,c). The partial spin-up DOS of Mn, N and Al atoms (d). (**Right**) Total DOS AlGaMnAs compared with that of AlGaAs within the LDA sheme.

From the partial DOS performed within the LDA approach, One can mostly remark (Fig. IV.15 in *bottom* panel) that the (–1.68,–0.65) eV range, near the top of the valence band (VB), for AlGaAsN is dominated by N-contribution (overcome by 2*p* levels) and a weak N-contribution is localized outside this range. The energy zero is taken at the Fermi level E_F. However, for AlGaMnAs, the Mn-contribution (overcome by 3*d* levels) dominates the top of VB by (–0.65, E_F) eV range as shown in Fig. IV.16. We can also point out the Al- states domination over CB and deep levels of VB. The top of AlGaMnAs at VB is also dominated by As 4*p* and Mn 3*d* levels, while a mixture of Ga 4*s* and As 4*p* dominates the bottom of CB. In AlGaAsN, the top of VB arises primarily from the As 4*p* and N 2*p* states, while the bottom of CB is dominated by of a mixture of As 4*p*, Al 3*p* and N 2*s* levels. It should be noted, however, that As 4*p* levels are strongly present over most or all the studied energy range, either for AlGaAsN or AlGaMnAs.

The LDA+U scheme has been used to obtain more realistic energy spectra and help to establish theoretical microscopic origins of ferromagnetic in DMS's [41] such as AlGaMnAs. To illustrate this trend, Fig. IV.16 shows an LDA+U calculation (with U the Hubbard parameter taken to be 0.3 Ry [38]) of total DOS for $Al_{0.125}GaMn_{0.03125}As$ and partial DOS for Mn 3*d* and As 4*p* states. Within the LDA+U scheme, which describe better strong correlations in the Mn *d*-shell, one can see (in *bottom* panels) a weak hybridization between Mn 3*d* and As 4*p* states found for both majority-band and minority-band states.

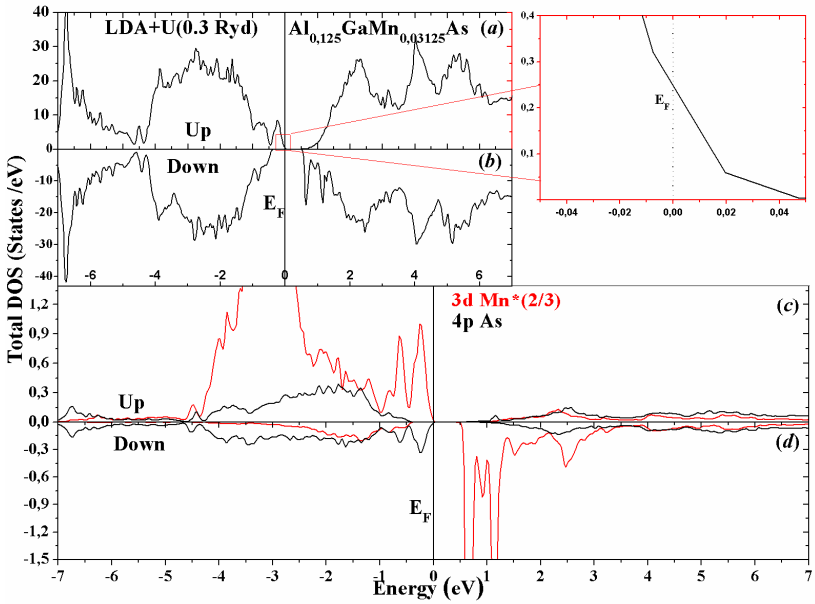

Fig. IV.16 DOSs of AlGaMnAs within LDA+U method (with U=4.08 eV): a weak hybridization between Mn 3*d* and As 4*p* states for both Up and Down-band states can be seen.

Imaginary part ε_2 indicates two inter-band transitions shown in Fig.IV.17; AlGaAsN is characterized by a strongest peak at 3.28 eV, might be strongly dependent on the ionic polarization of the AlGaAsN crystal due to the large electronegativity of N, and a weakest one for AlGaMnAs at 3.25 eV.

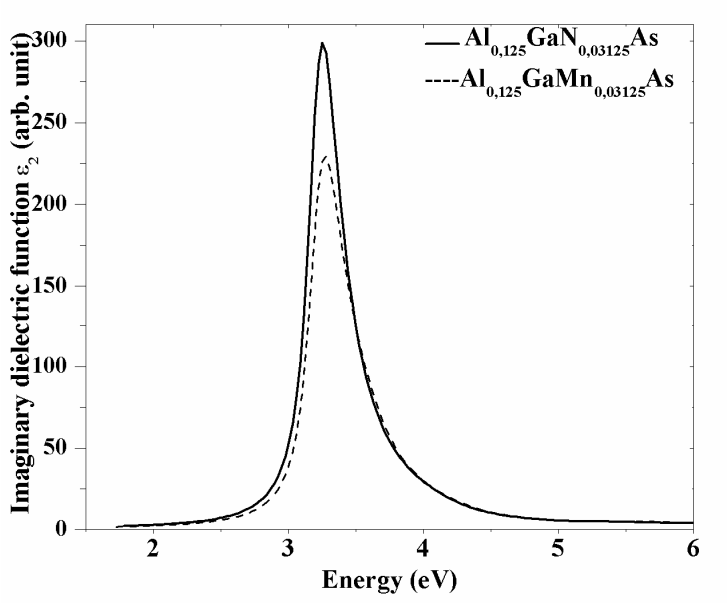

Fig.IV.17 Imaginary part of the dielectric functions of $Al_{0.125}GaAsN_{0.03125}$ and $Al_{0.125}GaMn_{0.03125}As$.

In Fig. IV.18, we show the reflectivity spectra for $Al_{0.125}GaAsN_{0.03125}$ and $Al_{0.125}GaMn_{0.03125}As$ systems. It is interesting that there is an abrupt reduction in the reflectivity spectrum after 20 eV for both systems confirming the occurrence of a collective plasmon resonance.

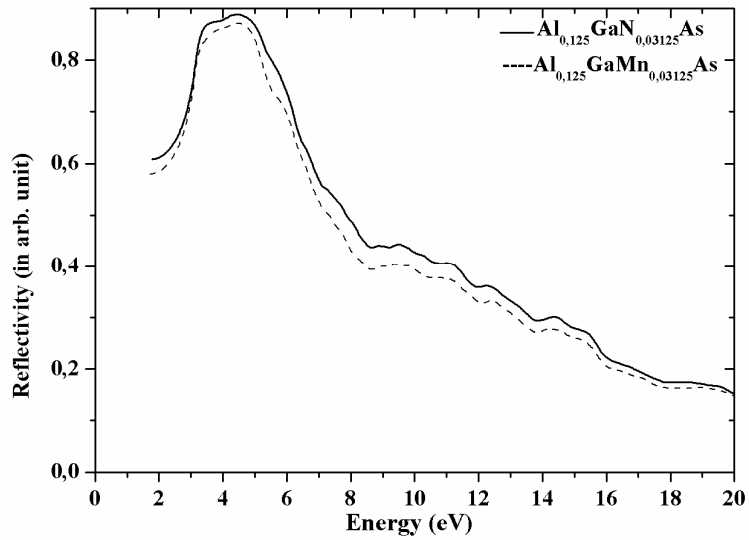

Fig.IV.18 Reflectivities of $Al_{0.125}GaAsN_{0.03125}$ and $Al_{0.125}GaMn_{0.03125}As$.

The calculated refractive index and extinction coefficient are shown in Fig.IV.19. We note that at low energy these systems show high refractive indices, which decrease at higher energies.

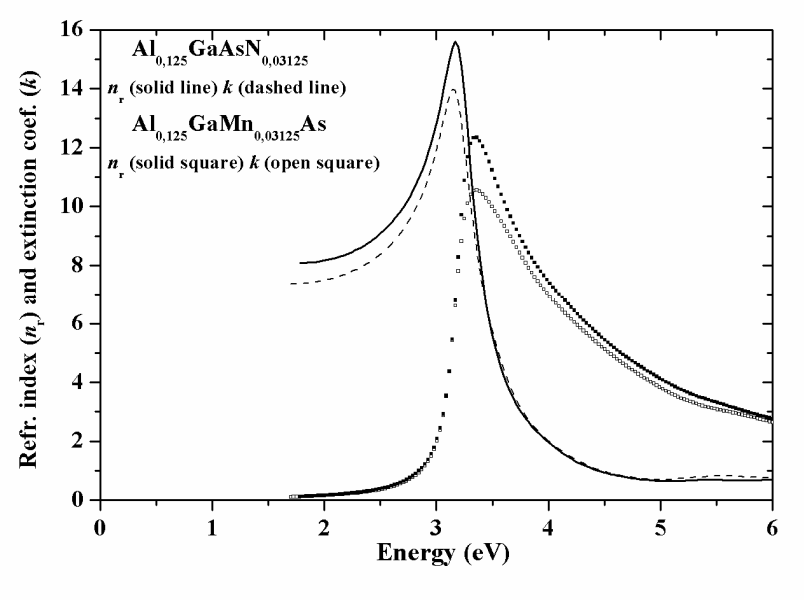

Fig.IV.19 Refractive indexes and extinction coefficients of $Al_{0.125}GaAsN_{0.03125}$ and $Al_{0.125}GaMn_{0.03125}As$.

At low energies between 2.0 to 4.0 eV and at higher energies (at around 11.0 eV), this crystal shows a fast increasing absorption. A strong increase in optical conductivity with increasing the photon energy has been observed for $Al_{0.125}GaAsN_{0.03125}$ compared to $Al_{0.125}GaMn_{0.03125}As$, respectively. Beyond the photon energy of 3.47 eV, the conductivity of AlGaMnAs dominates than of AlGaAsN. The calculated optical conductivity $\sigma(\omega)$ for the investigated systems is shown in Fig. IV.20. The peaks in the optical conductivity spectra are determined by the electric-dipole transitions between the occupied states to the unoccupied states.

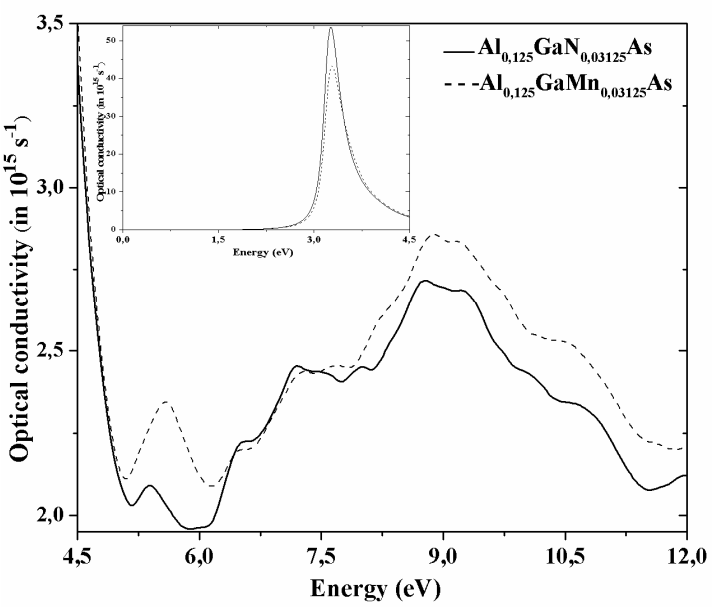

Fig. IV.20 Optical conductivities of $Al_{0.125}GaAsN_{0.03125}$ and $Al_{0.125}GaMn_{0.03125}As$.

The calculated absorption coefficient is shown in Fig. IV.21. At low energies between 2.0 to 4.0 eV and at higher energies (at around 11.0 eV), this crystal shows a fast increasing absorption. A strong increase in optical conductivity with increasing the photon energy has been observed for $Al_{0.125}GaAsN_{0.03125}$ compared to $Al_{0.125}GaMn_{0.03125}As$, respectively. Beyond the photon energy of 3.47 eV, the conductivity of AlGaMnAs dominates than of AlGaAsN.

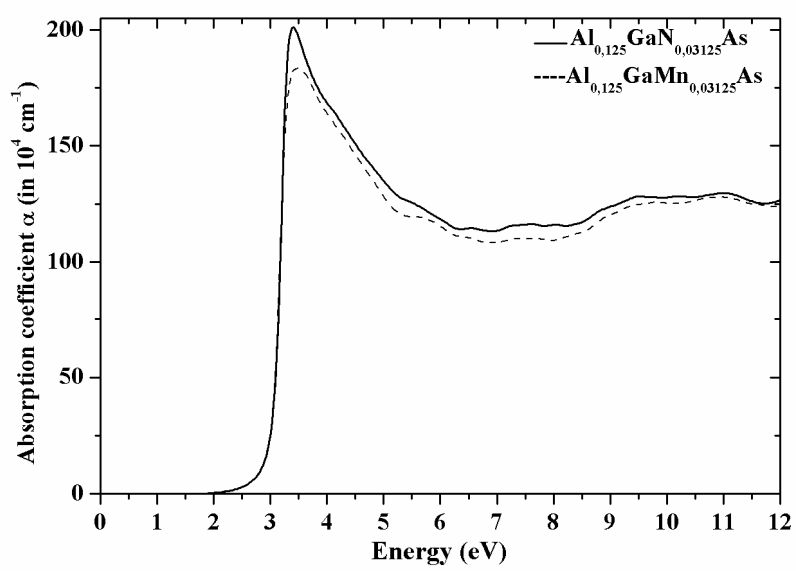

Fig. IV.21 Absorption coefficients of $Al_{0.125}GaAsN_{0.03125}$ and $Al_{0.125}GaMn_{0.03125}As$.

The lowest optical properties of AlGaMnAs compared to those of AlGaAs are mainly due to the non-radiative recombination centers in the GaAs QW while the Mn ions diffusion into the nonmagnetic GaAs QW from the FM layer.

From the intrinsec spin polarization found to be 100% and the large magnetic moment of 4.014 μ_B per Mn -dopant, we can say that a system such as AlGaMnAs may be not only an attractive alternative to MnAs for the realization of integrated optical isolators but also, as a DMS, a good candidate for spintronics. The results indicate that AlGaMnAs may be a good candidate for optoelectronics when exploited in optical fiber networks, and it can still be of great interest because of its promising potential when used for spintronics.
As for the N-doped AlGaAs, we have found that even thought this system is not magnetic like MgO:N, but it may be of great interest for optoelectronic devices.

References of Chap. IV

[1] M. Asada, A. Kameyama, Y. Suematsu, *IEEE J. Quantum Electron.*, **QE-20**, (1984), 745.
[2] Toshihiko Makino, *IEEE J. Quantum Electron.*, **32**, (1996), 493.
[3] N. Sekkal, Initiation au calcul des structures de bandes introduction aux heterostructures semiconductrices, Ecole Normale Supérieure de l'Enseignement Technologique d'Oran (ENSET–ORAN) Département de Physique-Chimie, 1st Ed., 2012.
[4] I. Vurgaftman and J. R. Meyer, Band parameters for nitrogen-containing semiconductors, Journal of Applied Physics Volume 94, Number 6 15 September 2003; I. Vurgaftman, J. R. Meyer and L. R. Ram-Mohan, Band parameters for III–V compound semiconductors and their alloys, Journal of applied physics Volume 89, Number 11 1 June 2001.
[5] Weng W. Chow, Kent D. Choquette, Mary H. Crawford, Kevin L. Lear, G.Ronald Hadley, IEEE Journal of Quantum Electronics 33 (1997) 1810.
[6] C. Yeh, C.H. Wei, A. Zunger, Physical Review B (Rapid Communications) 50 (1994) 2715.
[7] D.P. Munich, R.F. Pierret, Solid-State Electronics 30 (1987) 901.
[8] K.M. Yu, W. Walukiewicz, J. Wu, J.W. Beeman, J.W. Ager III, E.E. Haller, W. Shan, H.P. Xin, C.W. Tu, Applied Physics Letters 90 (2001) 2227.
[9] P. Blaha, K. Schwartz, G.K.H. Madsen, D. Kvasnicka, J. Luitz, An Augmented Plane Wave Plus Local Orbitals Programm for Calculating Crystal Properties, Vienna University of Technology, Austria, 2001 ISBN 3-9501031-1-2.
[10] H.J. Monkhorst, J.D. Pack, Physical Review B 13 (1976) 5188.
[11] W. Shan, W. Walukiewicz, J.W. Ager III, E.E. Haller, J.F. Geisz, D.J. Friedman, J.M. Olson, Sarah R. Kurtz, Journal of Applied Physics 86 (1999) 2349.
[12] S. Procz, M. Fiederle, M. Kunzer, K. Kohler, J. Wagner, Journal of Applied Physics

103 (2008) 073103-1.

[13] S.M. Sze, Physics of Semiconductor Devices, 2nd ed., WIE Willey, New York, 1981.

[14] W. Lu, R.P. Campion, C.T. Foxon, E.C. Larkins, Journal of Crystal Growth 312 (2010) 1029.

[15] K. Kim, A. Zunger, Physical Review Letters 86 (2001) 2609.

[16] A. Hashimoto, T. Kitano, K. Takahashi, H. Kawanishi, A. Patane, C.T. Foxon, A. Yamamoto, Physica Status Solidi B 228 (2001) 283.

[17] A. Vytcheslav, P. Elyukhin, P. Lyudmila, Crystal Growth & Design 4 (2004) 337.

[18] Sadao Adachi, Physical Properties of III–V Semiconductor Compounds, John Wiley & Sons, New York, 1992.

[19] Emmanuel Rosencher, Borge Vinter, Optoelectronics, English Edition, Cambridge University Press, United Kingdom, 2004.

[20] W.A. Fedak, J.J. Prentis, American Journal of Physics 70 (2002) 332.

[21] D.E. Aspnes, S.M. Kelso, R.A. Logan, R. Bhat, Journal of Applied Physics 60 (1986) 754.

[22] B.R. Nag, Physics of Quantum Well Devices, Kluwer Academic, Calcutta, 2000.

[23] Peter J. Klar, Prog. Solid State Chem., 31, (2003), 301.

[24] [2] H. Mathieu, H. Fanet, Physics of Semiconductors and electronic components, 6th Ed., Dunod, Paris (2009)

[25] Sadao Adachi, Optical Constants of Crystalline and Amorphous Semiconductors, Kluwer Academic, Boston, 1999.

[26] Y. Juan, E. Kaxiras, Physical Review B 48 (1993) 14944.

[27] M.L. Cohen, Physical Review B 32 (1985) 7988.

[28] H.C. Casey Jr., M.B. Panish, Heterostructure Lasers, Academic Press, New York, 1978.

[29] Bo Gu, Nejat Bulut, Timothy Ziman, and Sadamichi Maekawa, Possible d_0 ferromagnetism in MgO doped with nitrogen, PHYSICAL REVIEW B **79**, 024407 (2009).

[30] S. Adachi, Optical properties of $Al_xGa_{1-x}As$ alloys, Phys. Rev. B **38** (1988) 12345

[31] K. M. Yu, W. Walukiewicz, J. Wu, J. W. Beeman, J. W. Ager III, E. E. Haller, W. Shan, H. P. Xin, C. W. Tu, Formation of diluted III-V Nitride thin films by N ion implantation, Appl. Phys. Lett. **90** (2001) 2227

[32] M. Weyers, M. Sato, H. Ando, Red shift of Photoluminescence and Absorption in Dilute GaAsN Alloys Layers, J. Appl. Phys. **31** (1992) L853; M. Kondow, K. Uomi, K. Hosomi, T. Mozume, Gas-Source Molecular Beam Epitaxy of GaN_xAs_{1-x} Using a N Radical as the N Source, Jpn. J. Appl. Phys., **33** (1994) L1056

[33] D.N. Talwar, Assessment of microscopic lattice structures in dilute (AlGaIn)NAs laser materials by local mode spectroscopy and numerical simulations, J. Appl. Phys. **99** (2006) 123505

[34] M. Kondow, T. Kitatani, S. Nakatsuka, M. C. Larson, K. Nakahara, Y. Yazawa, M. Okai, K. Uomi, GaInNAs: a novel material for long-wavelength semiconductor lasers, IEEE J. Sel. Areas Commun. **3** (1997) 719

[35] S. R. Kurtz, A. A. Allerman, E. D. Jones, J. M. Gee, J. J. Banas, B. E. Hammons, InGaAsN solar cells with 1.0 eV band gap, lattice matched to GaAs, Appl. Phys. Lett. **74** (1999) 729

[36] R. Q. Wu, G. W. Peng, L. Liu, Y. P. Feng, Z. G. Huang, Q. Y. Wu, Cu-doped GaN: A dilute magnetic semiconductor from first-principles study, Appl. Phys. Lett. **89** (2006) 062505; T. Hayashi, Y.Hashimoto, S. Katsumoto, Y. Iye, Effect of low-temperature annealing on transport and magnetism of diluted magnetic semiconductor (Ga,Mn)As, Appl. Phys. Lett. **78** (2001) 1691

[37] T. Kuroiwa, T. Yasuda, F. Matsukura, A. Shen, Y. Ohno, Y. Segawa, H. Ohno, Faraday rotation of ferromagnetic (Ga, Mn)As, Electron. Lett. **34**, (1998) 190;

[38] T. Jungwirth, Jairo Sinova, J. Masek, J. Kucera, A. H. Mac Donald, Theory of ferromagnetic (III,Mn)V semiconductors, J. Mod. Phys. **78** (2006) 809

[39] H. Ohno, F. Matsukura, T. Omiya, and N. Akiba, Spin-dependent tunneling and properties of ferromagnetic Ga,Mn.As, J. Appl. Phys. **85**, 4277 (1999)

[40] H.Ohno, F. Matsukura, Y.Ohno, General Report Semiconductor Spin Electronics, JSAP International **5** (2002) 4

[41] J. H. Park, S. K. Kwon, B. I. Min, Electronic structures of III–V based ferromagnetic semiconductors: half-metallic phase, Physica B: Cond. Matt. **281-282** (2000) 703

Conclusion and Outlook

The Optoelectronic components from the technological nitrided GaAs spinneret (simple, efficient and of low cost) are used to implement an emission wavelength strategic and privileged by the modern optical fibers. Our contribution focuses on the study of the AlGaAsN/GaAs quantum wells used in long-wavelengths VCSELs and photovoltaic cells.

The objective of this work, motivated by our curiosity to discover more about the AlGaAsN promoter material, is to study its electronic and optical properties.

The aim of this work, motivated by obtaining lasers operating at the wavelength of 1,3 μm on GaAs substrate and suitable window layers for solar cells, was to study the optical properties of the $Al_xGa_{1-x}As_{1-y}N_y$ SC alloys with low nitrogen (N) content. In particular, it's suitable to precise the role that plays N on the emission characteristics of these alloys.

A first study is to understand the effects of nitrogen incorporation on the nitrides of the III-Vs, where we reported (using the anti-crossing band model) that the fundamental energy gap decreases and the effective mass increase when the rate of nitrogen incorporated increases.

The second part focuses on the study of the dilute III-As-N alloys applied in LW-VCSELs and spin VCSELs, and solar cells. About substituting N by a transition element, like Mn, it was observed that the resulting alloy AlGaAsMn maybe a candidate for integrated optical isolators and spintronics, but contrary to what one might think, the incorporation of N in AlGaAs give rise no magnetic effects such is the case of MgO:N, although AlGaAsN remains a good candidate for optoelectronics.

Theoretical tools represented by the FP- LAPW method and the Wien2K code are given in the third part. The linearized augmented plane wave (LAPW) method is among the most accurate methods for performing electronic structure calculations for crystals. It is based on the density functional theory for the treatment of exchange and correlation, using here the local spin density approximation (LSDA).

The fourth part of this thesis focuses on the results and discussions, where first the analytical expressions derived for the quantized energy levels have been show to provide not only an efficient way of computing the optical transition wavelength between these quantized levels of electrons and holes in QWs but also a convenient way of designing the $Al_xGa_{1-x}N_yAs_{1-y}$ QW lasers for which the analytical approach is expected to show its significant advantage for tuning the emission wavelength in the near infra-red range until 1.3 μm.

Based on the near perfect match between AlGaAs and GaAs and that the choice of varying N content (up to 4%) allows one to control electronicand optical properties of the III-AsN materials, an efficient ab initio calculation using the FP-LAPW method has been presented to

study the optical properties of a predicted $Al_xGa_{1-x}As_{1-y}N_y$ SCH laser. We can assume that the BAC model may provide an efficient approach of estimating the band gap shifts with the LDA approximation when using the scissors operation to calculate the optical properties. The band structures of $Al_xGa_{1-x}As$ and $Al_xGa_{1-x}As_{1-y}N_y$ alloys (with $x \leq 0.375$ and $y \approx 0.03$) show a direct gap, which is of great interest for optical transitions. The bonding charge strongly displaced towards the N atom in AlGaAsN and the presence of the N states in all bands of the partial DOS of this material proves the powerful effect that produces the incorporation of N in AlGaAs. For AlGaAsN the strongest peak in refractive index at 4.059 eV and the main peak in reflectivity of 87% at 4.443 eV are related mainly to the E_1 transition and may be also due to the N+ implantation in AlGaAs. The observed peaks in absorption coefficient such as $\approx 5.5 \times 10^6$ cm^{-1},which appears beyond the band gap and near the E_1 transition, are expected to show a significant interest in the design of QW solar cell heterostructures on a wide range of wavelengths. Finally, we can say that AlGaAsN may not only be an attractive alternative to AlGaAs for the realization of devices operating by inter-subband transition but also an efficient way of computing the dielectric function-related parameters.

Appendix

(Important Terms and Effects in Optoelectronics and Photonics)

Absorption coefficient α characterizes the loss of **photons** as light propagates along a certain direction in a medium. It is the fractional change in the intensity of light per unit distance along the propagation direction, that is,

$$\alpha = -\frac{\delta I}{I \delta x}$$

where I is the intensity of the radiation. The absorption coefficient depends on the photon energy or wavelength λ. Absorption coefficient α is a material property. Most of the photon **absorption** (63%) occurs over a distance 1/α and 1/α is called the **penetration depth** δ.

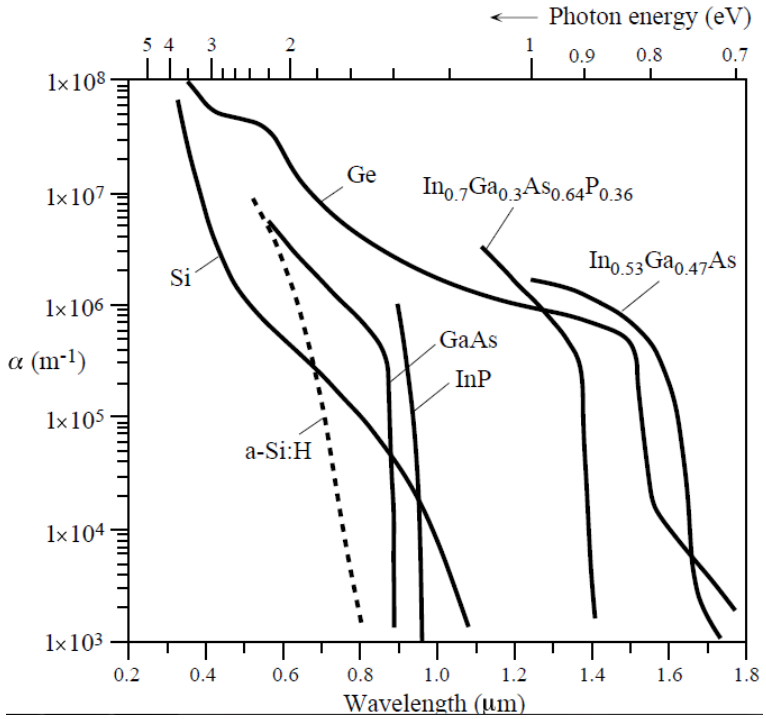

Absorption coefficient (α) vs. wavelength (λ) for various semiconductors.

Absorption is the loss in the power of an electromagnetic radiation that is traveling in a medium. The loss is due to the conversion of light energy to other forms of energy, *e.g.* lattice vibrations (heat) during the polarization of the molecules of the medium, local vibrations of impurity ions, excitation of electrons from the valence band to the conduction band, *etc*.

Active region is the region in a medium where direct electron hole pair (EHP) recombination takes place. For LEDs it is the region where most EHP recombination takes place. In the laser diode it's the region where stimulated emission exceeds spontaneous emission and absorption. It is the region where coherent emission dominates.

Antireflection (AR) coating is a thin dielectric layer coated on an optical device or component to reduce the reflection of light and increase the transmitted light intensity.

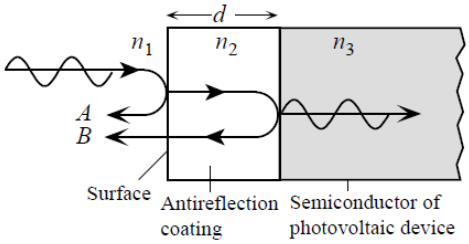

Illustration of how an antireflection coating reduces the reflected light intensity.

Buried double heterostructure laser diode is a double heterostructure semiconductor laser device that has its active region "buried" within the device in such a way that it is surrounded by low refractive index materials rendering the active region as a waveguide.

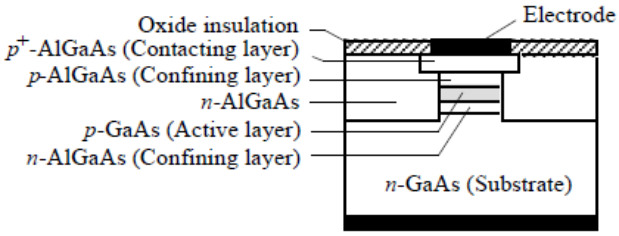

Schematic illustration of the cross sectional structure of a buried heterostructure laser diode.

Bragg wavelength is a particular wavelength λ_B of electromagnetic radiation that satisfies the **Bragg diffraction condition**,

$$q\frac{\lambda_B}{n} = 2\Lambda \sin\theta$$

where Λ is the periodicity of the diffracting structure, n is the refractive index of the medium diffracting the **waves** and θ is the diffraction angle, and q is an integer (1,2,..), so that the electromagnetic radiation becomes diffracted.

Carrier confinement is the restriction of injected charge carriers to a small volume to increase the carrier concentration. The restriction of injected carriers is achieved by using a **heterojunction** so that there is a step change in the **conduction band** edge (ΔE_c) or a step change in the **valence band** edge (ΔE_v).

Chemical vapor deposition (CVD) is a chemical process by which reaction between gaseous reactants results in products that are deposited as solid.

Chromatic dispersion is due to the **dispersion** of a traveling pulse of light along an **optical fiber** as a result of the wavelength dependence of the propagation characteristics and waveguide properties but excluding multimode dispersion. Chromatic dispersion arises as a result of the range of wavelengths in the emission **spectrum** of the **emitter** (*e.g.* LED or **laser**

diode) that are coupled into the fiber. It is the combination of **material dispersion** and **waveguide dispersion**.

Cladding is the **dielectric** layer that surrounds the dielectric core of an **optical waveguide**.

Coherent radiation (or light) consists of **waves** that have the same wavelength and always have the same phase difference with respect to each other at all times.

Complex refractive index characterizes the propagation of a light wave in a medium in which there is a loss of energy, that is, the electromagnetic wave experiences attenuation, due to various loss mechanisms such as the generation of phonons (lattice waves), photogeneration, free carrier absorption, scattering, etc. If N is the complex refractive index, then $N = n - jK$, where the real part n, the refractive index, represents the effect of the medium on the phase velocity, and the imaginary part, K, called the extinction coefficient, represent the attenuation suffered by the wave as it travels along a well-defined propagation direction.

Confining layer is a layer with a wider bandgap than the active layer, and adjacent to it, to confine the injected **minority carriers** to the active layer.

Core is the central region of an **optical fiber** that has a higher **refractive index** than the outer region. Most of the light propagates through the core region of a fiber.

Cryptography: (*cryptology*; from, "hidden, secret"; and "writing", or "study", respectively) is the practice and study of techniques for secure communication in the presence of third parties (called adversaries). More generally, it is about constructing and analyzing protocols that overcome the influence of adversaries and which are related to various aspects in information security such as data confidentiality, data integrity, and authentication. Modern cryptography intersects the disciplines of mathematics, computer science, and electrical engineering. Applications of cryptography include ATM cards, computer passwords, and electronic commerce.

Distributed Bragg reflector (DBR) laser diode has one of the optical cavity reflectors as a mirror that has been designed like a reflection type **diffraction grating**; it has a periodic corrugated structure.

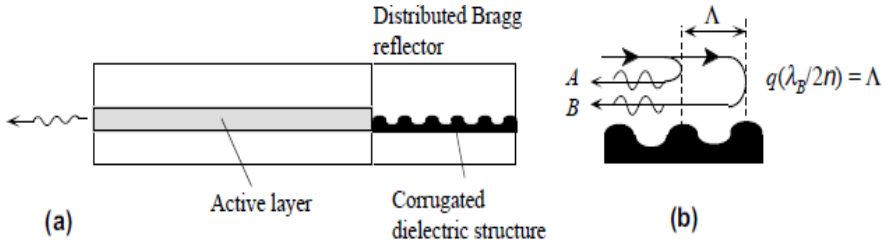

(a) Distributed Bragg reflection (DBR) laser principle. (b) Partially reflected waves at the corrugations can only constitute a reflected wave when the wavelength satisfies the Bragg condition.

Dry etching refers to the removal of material, typically a masked pattern of semiconductor material, by exposing the material to a bombardment of ions (usually a plasma of reactive gases such as fluorocarbons, oxygen, chlorine, boron trichloride; sometimes with addition of nitrogen, argon, helium and other gases) that dislodge portions of the material from the exposed surface. Unlike with many (but not all, see isotropic etching) of the wet chemical etchants used in wet etching, the dry etching process typically etches directionally or anisotropically.

Electromagnetic (EM) wave is a traveling wave in which the electric field and magnetic field oscillations are at perpendicular to each other and also to the direction of propagation. It is a solution of Maxwell's wave equation subject to appropriate boundary conditions. One very simple example is a plane polarized electromagnetic wave that has harmonic electric and magnetic field variations with time and space. Such a wave, if of infinite extent, would be a monochromatic EM wave. Suppose that **E** (say E_x) is the electric field and **B** (say B_y) is the magnetic field at one instant at one location (at a particular z). If **k** is the **wavevector**, then **E**, **B** and **k** are all perpendicular in a linear **dielectric** medium (optically isotropic).

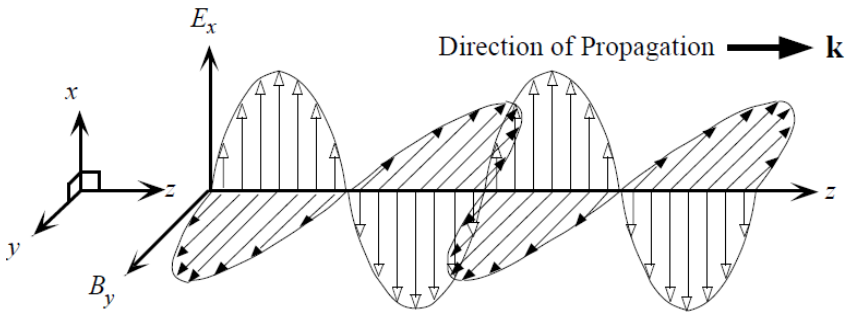

An electromagnetic wave is a travelling wave which has time varying electric and magnetic fields which are perpendicular to each other and the direction of propagation, z.

Infrared (IR) is radiation with wavelengths that are longer than 700 nm but shorter than 1 mm. Infrared radiation was discovered by *William Herschel* (1738 - 1822) in 1800 in the **spectrum** of the Sun.

Lasing conditions are the conditions for obtaining **continuous wave** lasing emissions from a laser device consisting of a pumped medium with an **optical gain** within an **optical resonator**

structure, that is within an optical cavity with end reflectors. The optical gain of the medium is must just overcome the losses in the medium and also the losses from the end reflectors (*i.e.* radiation escaping from the cavity). The net round-trip gain must be unity and the phase change must be a multiple of 2π; otherwise the **electromagnetic wave** cannot replicate itself. The corresponding optical gain of the medium is the threshold optical gain g_{th}.

Light emitting diode (LED) is a semiconductor diode which emits incoherent radiation. LEDs operate on the principle of **spontaneous emission** resulting from electron hole pair injection and *direct* **recombination** under forward bias. Consider what happens when a p-n_+ junction is forward biased. As soon as a forward bias V is applied across this **junction**, this voltage drops across the depletion region since this is the most resistive part of the device.

Luminescence, in general terms, is the emission of light as a result of an excited electron transiting down to the ground energy level. In a **semiconductor**, this would correspond to the **recombination** of an electron and a hole; the excited electron is the **conduction band** (CB) electron and its ground state corresponds to a hole in the **valence band** (VB) . In contrast, light emitted from an ordinary light bulb is due to the heating of the metal filament. The emission of radiation from a heated object is called **incandescence**. In luminescence, emission of radiation requires the initial excitation of electrons. If the electron excitation is due to photon **absorption**, then the process is identified as *photoluminescence*. The direct electron–hole recombination mechanism generally occurs very quickly.

Metalorganic vapour phase epitaxy (**MOVPE**), also known as **organometallic vapour phase epitaxy (OMVPE)** or **metalorganic chemical vapour deposition (MOCVD)** , is an arranged chemical vapour deposition method. It is a highly complex process for growing crystalline layers to create complex semiconductor multilayer structures. In contrast to molecular beam epitaxy (MBE) the growth of crystals is by chemical reaction and not physical deposition. This takes place not in a vacuum, but from the gas phase at moderate pressures (2 to 100 kPa). As such, this technique is preferred for the formation of devices incorporating thermodynamically metastable alloys, and it has become a major process in the manufacture of optoelectronics.

Multiple quantum well (MQW) lasers have the structure of alternating ultrathin layers of wide and narrow bandgap **semiconductors**. The smaller bandgap layers are the active layers

where electron confinement and lasing transition take place whereas the wider bandgap layers are the barrier layers.

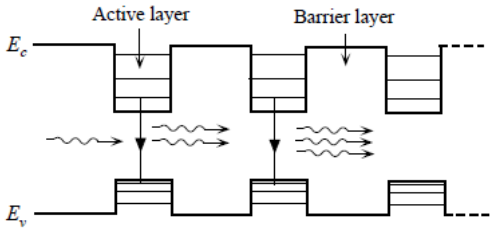

A multiple quantum well (MQW) structure. Electrons are injected by the forward current into active layers which are quantum wells.

Photocatalysis in chemistry, is the acceleration of a photoreaction in the presence of a catalyst. In catalysed photolysis, light is absorbed by an adsorbed substrate. In photogenerated catalysis, the photocatalytic activity (PCA) depends on the ability of the catalyst to create electron–hole pairs, which generate free radicals (hydroxyl radicals: •OH) able to undergo secondary reactions. Its practical application was made possible by the discovery of water electrolysis by means of titanium dioxide. The commercially used process is called the advanced oxidation process (AOP). There are several ways the AOP can be carried out; these may (but do not necessarily) involve TiO_2 or even the use of UV light. Generally the defining factor is the production and use of the hydroxyl radical. **Optical isolator** allows light to pass in one direction and not in the opposite direction.